REPORT 1041

EQUATIONS AND CHARTS FOR THE RAPID ESTIMATION OF HINGE-MOMENT AND EFFECTIVENESS PARAMETERS FOR TRAILING-EDGE CONTROLS HAVING LEADING AND TRAILING EDGES SWEPT AHEAD OF THE MACH LINES [1]

By Kennith L. Goin

SUMMARY

Existing conical-flow solutions have been used to calculate the hinge-moment and effectiveness parameters of trailing-edge controls having leading and trailing edges swept ahead of the Mach lines and having streamwise root and tip chords. Equations and detailed charts are presented for the rapid estimation of these parameters. Also included is an approximate method by which these parameters may be corrected for airfoil-section thickness.

Deflected controls are assumed to be located either at the wing tip or far enough inboard to prevent the outermost Mach lines from the controls from crossing the wing tip. For either of these locations, the innermost Mach lines are assumed not to cross the wing root chord. The method for determining control hinge moment resulting from wing angle-of-attack loading is valid for wing plan forms having the leading edges swept ahead of the Mach lines and having streamwise tips. The only additional restrictions are that the controls must not be influenced by the tip conical flow from the opposite wing panel or by the interaction of the wing-root Mach cone with the wing tip.

INTRODUCTION

Linearized theory, though neglecting viscosity and second-order effects existing in practice, is the most practical method now available for estimating the characteristics of control surfaces at supersonic speeds. A general application of this theory to control surfaces having edges swept either ahead of or behind the Mach lines is presented in reference 1. (Edges swept ahead of or behind the Mach lines are subsequently referred to as supersonic or subsonic edges.) Conical-flow solutions for various deflected control configurations are presented in reference 2. Such solutions were used in reference 3 to evaluate the characteristics of a restricted family of trailing-edge control surfaces.

In the present report a general analysis based on existing conical-flow solutions has been made which will apply to a broad range of trailing-edge control configurations having supersonic edges and will provide for a comprehensive coverage of control location, aspect ratio, taper ratio, and sweep. Equations and detailed charts are presented from which lift, pitching-moment, rolling-moment, and hinge-moment coefficients due to control deflection and hinge-moment coefficient due to wing angle of attack, as predicted by linearized theory, may be determined in an estimated 5 percent of the time required without the use of such equations and charts. Also included is an approximate method by which these hinge-moment and effectiveness parameters may be corrected for airfoil-section thickness.

The equations and charts presented are applicable to control-surface plan forms that vary throughout the range in which the leading and trailing edges are supersonic and the root and tip chords are in a streamwise direction. Deflected controls are assumed to be located either at the wing tip or far enough inboard to prevent the outermost Mach lines from the controls from crossing the wing tip. For either of these locations, the innermost Mach lines are assumed not to cross the wing root chord. The method for calculating the hinge-moment coefficient due to wing angle of attack is valid for wing plan forms having straight supersonic edges and streamwise tips. This method is restricted only in that the controls must not lie in a region influenced by the tip conical flow from the opposite wing panel or by the interaction of the wing-root Mach cone with the wing tip.

SYMBOLS

M	free-stream Mach number
$\beta=\sqrt{M^2-1}$	
C_1, C_2	functions of Mach number used in calculating two-dimensional-flow characteristics
Λ	angle of sweep of wing leading edge, positive when swept back
Λ_{HL}	angle of sweep of control hinge line, positive when swept back
Λ_{TE}	angle of sweep of wing trailing edge, positive when swept back
b_f	span of control surface
c_{f_r}	root chord of control surface
c_{f_t}	tip chord of control surface
λ_f	control-surface taper ratio (c_{f_t}/c_{f_r})
S_f	area of control surface
A_f	aspect ratio of control surface (b_f^2/S_f)
$A_f'=\beta A_f$	
M_a	area moment of control surface about hinge axis

[1] Supersedes NACA TN 2221, "Equations and Charts for the Rapid Estimation of Hinge-Moment and Effectiveness Parameters for Trailing-Edge Controls Having Leading and Trailing Edges Swept Ahead of the Mach Lines" by Kennith L. Goin, 1950.

S_L area of a loaded region

S_{L_0} area of part of deflected control surface lying in two-dimensional-flow region less area lying in region of overlap of conical-flow fields

m_0 moment of S_{L_0} about hinge axis

l_0 moment of S_{L_0} about control root chord

$\bar{x}$ distance of center of loading from control hinge axis measured normal to hinge axis

$\bar{y}$ spanwise distance of center of loading from control root chord

θ slope of airfoil-section contour

$t/2c$ one-half airfoil-thickness ratio measured in plane normal to control hinge axis

$(t/c)_{max}$ maximum airfoil-thickness ratio measured in plane normal to control hinge axis

x/c chordwise position measured in plane normal to control hinge axis

x_h/c chordwise location of control hinge axis measured in plane normal to control hinge axis

$(t/2c)'$, $(x/c)'$ dimensions measured in plane normal to wing leading edge

x_f distance of leading edge of control root chord behind wing axis of pitch

y_f distance of root chord of control from root chord of wing

b wing span

c_r wing root chord

c_t wing tip chord

$\bar{c}$ mean aerodynamic chord of wing

S area of semispan wing

$g=\dfrac{\tan \Lambda}{\beta}$

$a=\dfrac{\tan \Lambda_{HL}}{\beta}$

$d=\dfrac{\tan \Lambda_{TE}}{\beta}$

α wing angle of attack, degrees

δ angle of control-surface deflection measured in streamwise direction, degrees

q free-stream dynamic pressure

$C_{L'}=\dfrac{\text{Lift induced by deflected control}}{qS_f}$

$C_{l'}=\dfrac{\text{Moment about control root chord induced by deflected control}}{qb_fS_f}$

$C_{m'}=\dfrac{\text{Moment about hinge axis induced by deflected control}}{2qM_a}$

$C_h=\dfrac{\text{Hinge moment}}{2qM_a}$

$C_L=\dfrac{\text{Lift induced by deflected control}}{qS}$

$C_l=\dfrac{\text{Rolling moment about wing root chord}}{2qbS}$

$C_m=\dfrac{\text{Pitching moment about wing axis of pitch}}{qS\bar{c}}$

F_1 thickness correction factor for C_{L_δ}' and C_{l_δ}'

F_2 thickness correction factor for C_{h_δ} and C_{m_δ}'

F_3 thickness correction factor for C_{h_α}

Δp difference between local pressure and stream static pressure

C_p pressure coefficient $(\Delta p/q)$

C_{p_0} two-dimensional pressure coefficient $\left(\dfrac{2\delta}{57.3\beta\sqrt{1-a^2}}\right)$ or $\left(\dfrac{2\alpha}{57.3\beta\sqrt{1-g^2}}\right)$.

P' local pressure ratio (C_p/C_{p_0})

P average value of pressure ratio P' over conical-flow region $\left(\dfrac{\int P'dS_L}{S_L}\right)$

τ angle denoting arbitrary position of ray in conical-flow field

$\tau'=\tau+\Lambda_{TE}$

$t=\beta \tan \tau$

$t'=\beta \tan \tau'$

$r=\dfrac{1}{t}$

n, r' nondimensional coordinates used in integration of wing root and tip conical pressures

η angle of sweep of line intersecting conical-flow regions of wing at angle of attack

Subscripts:

δ, α denote partial derivative of force and moment coefficients with respect to δ or α

cp denotes center-of-pressure ray location

Superscript:

$*$ indicates that parameters P, PS_L, $PS_L\bar{x}$, $PS_L\bar{y}$, t_{cp}', and r_{cp} refer to loss of loading from two-dimensional value rather than to actual loading

ANALYSIS

CHARACTERISTICS DUE TO DEFLECTION OF CONTROL SURFACES

Scope.—Existing solutions of the linearized equations of fluid motion have been used as a basis for calculating the characteristics due to deflection of trailing-edge control surfaces on wings in steady flight at supersonic speeds. These solutions, as presented in reference 2, are applicable to configurations for which the leading and trailing edges of the control are supersonic and the root and tip chords are streamwise. Two control-surface locations are considered.

The control is assumed to be located either at the wing tip or far enough inboard to prevent the outermost Mach line from the control from crossing the wing tip. For either of these locations, the innermost Mach lines are assumed not to cross the wing root chord. For these locations, deflected control-surface characteristics are functions only of Mach number and control-surface plan form. (The parameter C_{h_1} depends on control-surface location only when the control is located inboard from the wing tip and lies in a region influenced either by the interaction of the control-tip Mach cone with the wing tip or by the reflection from the wing root chord of the innermost control Mach line.) If the limitations previously mentioned are considered, the analysis is valid for all controls except those located at the wing tip and having the inboard conical-flow regions intersecting the tip. In such cases, the conical pressures on the control, as given in reference 2, are not applicable in the region influenced by the interaction of the Mach cone with the wing tip. Necessary corrections for this region can be determined by the method described in reference 4. Such corrections are not considered in the present report because of the prohibitive amount of computation involved. Results not including these corrections are presented, however, because they should be very useful as an indication of trends and should in many cases closely approximate the corrected result.

Method.—In order to determine control-surface characteristics, the two-dimensional region and the triangular segments of the conical-flow regions (fig. 1) are considered independently. The characteristics are obtained by summing the products of pressure ratio and nondimensional-area and moment-arm parameters for all parts (table I). The nature of conical flow is such that the pressure is constant along any ray from the origin of the flow field. Any infinitesimal triangle having the origin of the flow field as an apex, therefore, has its center of pressure located at two-thirds of the distance from the apex to the base. It follows that the summation of the loading of such infinitesimal triangles results in a finite triangle having its center of pressure lying on a line parallel to the base and located at two-thirds of the distance from the apex to the base. The center-of-pressure location and, consequently, the desired moment arms can therefore be determined from the location of the ray on which the center of pressure lies. General equations for the average pressure ratio and center-of-pressure ray location for each conical segment (tables II (a) and II (b)) were obtained by integrating the pressure equations of reference 2. (See appendix A.) Table II(c) presents equations for the nondimensional-area and moment-arm parameters (in terms of center-of-pressure ray location) for each conical segment. Equations pertaining to the two-dimensional region were obtained by treating this region as a simple geometric area and are also included in table II(c). Results obtained by evaluating the general equations of table II when they become indeterminate at taper ratios of 1.0 are presented in table III.

For regions in which the two conical-flow fields overlap, the method of superposition must be used wherein the losses in pressure ratio from the two-dimensional value ($P'=1.0$) in the two conical-flow regions are additive; that is,

$$P'=1.0-(1.0-P_{mc_1}')-(1.0-P_{mc_2}')$$

$$=-1.0+P_{mc_1}'+P_{mc_2}'$$

(Subscripts mc_1 and mc_2 refer to inboard and outboard conical-flow regions, respectively.) The net effects of the pressure distribution in this region are obtained by adding the effects of the two conical-flow regions as though the flow regions did not overlap and by subtracting the effects of a two-dimensional pressure distribution. This subtraction is accomplished by use of the equations for the two-dimensional region (tables II (c) and III (b)). In calculating control hinge moments it was convenient to calculate the effects of regions I_c and II_c or III (fig. 1) and then to subtract the effects of the parts of these regions lying off the control. For controls located at the wing tip and having the inboard Mach cone intersecting the tip, a similar procedure was also used to reduce to zero the lift, pitching moment, and rolling moment contributed by the triangular part of the inboard conical-flow region lying beyond the tip. As previously mentioned for this case, a rigid application of linearized theory would require a correction, as described in reference 4, to the loading assumed in the region influenced by the interaction of the root Mach cone with the free edge. It should be pointed out that the areas influenced by such interactions become appreciable for extreme conditions and approximate results for such configurations should be used with caution.

HINGE MOMENT DUE TO WING ANGLE-OF-ATTACK CHANGE

Scope.—Conical-flow solutions for swept wings at supersonic speeds, as presented in reference 5, are used as a basis for the analysis. These solutions are applicable to wing plan forms having straight supersonic edges and streamwise tips.

As in the analysis for deflected control surfaces, only control surfaces having supersonic edges and streamwise root and tip chords are considered. The only restrictions regarding control location are that the control must not lie in a region influenced by the tip conical flow from the opposite wing panel or by the interaction of the wing-root Mach cone with the wing tip.

Method.—The method consists essentially of determining the hinge-moment parameter $PS_L\bar{x}$ for the flap by assuming two-dimensional loading and then subtracting the losses

resulting from the wing-root and wing-tip concial flows. The conical-flow losses are obtained by dividing the conical regions into a series of triangular segments, each having its apex at the origin of the Mach cone, and by summing the hinge-moment parameters $(PS_L\bar{x})^*$ for these segments as illustrated in figure 2. In determining $(PS_L\bar{x})^*$ for the triangular segments, integrations of the loading are necessary for obtaining P^* and $\bar{x}$. As has been previously explained for this type of conical-flow segment, it is sufficient to determine P^* and t_{cp} because the moment arm $\bar{x}$ can be determined from t_{cp}. The method for obtaining P^* and t_{cp} is illustrated in figure 3 and involves integrating the pressure losses along the bases of the segments. From integrations of the pressure losses between 0 and n_1 (or 0 and r_1'), values of P^* and n_{cp} (or r_{cp}') are obtained. Values of P^* and values of t_{cp}, corresponding to n_{cp} (or r_{cp}'), obtained in this manner are applicable to the triangular segment bounded by the Mach line, the ray $\tau=\tau_1$, and the section intersecting the Mach cone. Results have been obtained by numerical integration using Simpson's rule (reference 6) except in regions where the slopes of the pressure curves become infinite (fig. 3). In these regions, integrating coefficients, as presented in reference 7, have been used. Forms by which the integrations were made are presented in tables IV to VII. The upper parts of these forms are used for computing the pressure distributions $(1-P')$ along the sections intersecting the Mach cones (fig. 3). In the lower part of the form, the areas and area moments about n (or r')$=0$ of the curves of $1-P'$ plotted against n (or r') are determined and are used to obtain P^* and t_{cp} for the corresponding triangular segments. Tables IV to VII can be used directly for calculating the loading distribution for intermediate cases or cases not included in the present report.

METHOD FOR APPROXIMATELY CORRECTING RESULTS OBTAINED FROM USE OF LINEARIZED THEORY FOR AIRFOIL-SECTION THICKNESS

Scope.—The method for approximately correcting the theoretical results for airfoil-section thickness is based on the assumption that, at any chordwise position on an airfoil having finite thickness, the ratio of conical to two-dimensional pressure is the same as that predicted by linearized theory for an infinitely thin flat plate. (This method is a variation of the method presented in reference 8.) The method can be logically applied only to configurations having similar sections at all spanwise positions affected. The method is expected to give most accurate results at moderate and high Mach numbers for thin controls located inboard from the wing tip and having relatively large areas over which the flow is two-dimensional.

Method.—On the basis of the preceding assumption, the method requires the determination of the following three factors:

$$F_1=\frac{C_L'(\text{Two-dimensional with thickness})}{C_L'(\text{Two-dimensional flat plate})}=\frac{C_l'(\text{Two-dimensional with thickness})}{C_l'(\text{Two-dimensional flat plate})} \quad (1)$$

$$F_2=\frac{C_m'(\text{Two-dimensional with thickness})}{C_m'(\text{Two-dimensional flat plate})}=\frac{C_h(\text{Two-dimensional with thickness})}{C_h(\text{Two-dimensional flat plate})} \quad (2)$$

$$F_3=\frac{C_h(\text{Two-dimensional with thickness})}{C_h(\text{Two-dimensional flat plate})} \quad (3)$$

(The coefficients in equations (1) and (2) are for deflected controls, and the coefficients in equation (3) are those resulting from wing angle-of-attack loading.) Corrected values of C_{L_δ}', C_{l_δ}', C_{m_δ}', C_{h_δ}, and C_{h_α} are obtained by multiplying the results obtained by use of the linearized theory for three-dimensional flat plates by the appropriate factors.

The factors are determined, as described in appendix B, by using the Busemann second-order approximation to determine the coefficients for sections having thickness. This approximation gives results which are generally in good agreement with results obtained by use of the more involved exact theories. The theory is not considered accurate, however, at Mach numbers for which the shocks become detached or at Mach numbers below about 1.3 (reference 9). For the general group of airfoil sections that are symmetrical about the chord plane, equations for the correction factors as derived in appendix B are:

$$F_1=\frac{1}{\left(1-\frac{x_h}{c}\right)}\int_{x_h/c}^{1.0}\left(1+2\frac{C_2}{C_1}\frac{d\frac{t}{2c}}{d\frac{x}{c}}\right)d\frac{x}{c} \quad (4)$$

$$F_2=\frac{2}{\left(1-\frac{x_h}{c}\right)^2}\int_{x_h/c}^{1.0}\left(\frac{x}{c}-\frac{x_h}{c}\right)\left(1+2\frac{C_2}{C_1}\frac{d\frac{t}{2c}}{d\frac{x}{c}}\right)d\frac{x}{c} \quad (5)$$

$$F_3=\frac{2}{\left(1-\frac{x_h}{c}\right)^2}\int_{x_h/c}^{1.0}\left(\frac{x}{c}-\frac{x_h}{c}\right)\left[1+2\frac{C_2}{C_1}\frac{d\left(\frac{t}{2c}\right)'}{d\left(\frac{x}{c}\right)'}\right]d\frac{x}{c} \quad (6)$$

CHARTS

PRESENTATION

Aside from the restrictions regarding location, the characteristics of deflected control surfaces are functions only of control plan form and Mach number. The effects of plan form and Mach number are determined from solutions to equations (tables I to III) involving the variables $\frac{\tan\Lambda_{HL}}{\beta}$, $\frac{\tan\Lambda_{TE}}{\beta}$, and λ_f. (For untapered controls the variables are $\frac{\tan\Lambda_{HL}}{\beta}$ and βA_f.) Figure 4 presents $\beta C_{L_\delta}'$, $\beta C_{l_\delta}'$, $\beta C_{m_\delta}'$, and βC_{h_δ} as functions of these variables for controls located at the wing tip. Each chart of figure 4 presents the characteristics of a series of plan forms having a fixed hinge-line sweep angle (if the Mach number is considered to be fixed)

and varying trailing-edge sweep angles and taper ratios. The solid-line curves present the effects of varying taper ratio for plan forms having fixed hinge line and trailing-edge sweep angles. The characteristics of controls having constant aspect ratios are indicated in the charts for βC_{h_δ} by dashed lines. Constant-aspect-ratio curves are not included in the charts for the other characteristics because, in many cases, they would be quite confusing. If desired, such curves can be drawn by simply determining the taper ratio at which the curve will intersect each of the curves of constant d from the following relation:

$$\lambda_f=\frac{2-A_f'(a-d)}{2+A_f'(a-d)}$$

For inversely tapered controls, the parameter $1/\lambda_f$ is used as a coordinate to avoid elongation of the curves. Calculations were made at values of λ_f and $\frac{1}{\lambda_f}=0$, 0.20, 0.40, 0.60, 0.80, and 0.95 and at values of $A_f'=0.8$, 2.0, 4.0, 6.0, 8.0, and 10.0 for untapered controls. Calculated results not included in the charts are presented in table VIII. The results not included in the charts are mainly for configurations having values of $\frac{\tan \Lambda_{TE}}{\beta}$ near $|1.0|$ and, consequently, having extremely large areas of induced loading on the wing. Results for such configurations are of little practical value because if these large areas are to lie entirely on the wing, as has been assumed, the wing must have a very large span or the control must have a very small chord.

Charts presenting the characteristics of deflected controls located inboard from the wing tip are presented in figures 5 and 6. These charts vary somewhat from those for controls located at the wing tip. Equations for $\beta C_{L_\delta}'$ and $\beta C_{m_\delta}'$ were simplified and found to be dependent only on $\frac{\tan \Lambda_{HL}}{\beta}$ and $\frac{\tan \Lambda_{TE}}{\beta}$. These equations, with results in chart form, are presented in figure 5. Charts for βC_{h_δ} and $\beta C_{l_\delta}'$ (fig. 6) are presented only for normal taper ratios because the characteristics of inversely tapered controls can be obtained by entering the charts at $\frac{-\tan \Lambda_{HL}}{\beta}$, $\frac{-\tan \Lambda_{TE}}{\beta}$, and $1/\lambda_f$.

The computing form for C_{h_α} is presented in table IX and is self-explanatory. Supplementary charts for determining the loading distribution (P^* and t_{cp}) for the various triangular segments of the conical-flow regions are presented in figures 7 to 10. It should be pointed out that figures 8 and 10 can easily be used for determining the spanwise and chordwise loading of the wings considered in this report and will therefore be of value in making loads analyses.

USE

In order to use the charts for determining the characteristics of deflected controls, values of $\frac{\tan \Lambda_{HL}}{\beta}$, $\frac{\tan \Lambda_{TE}}{\beta}$, and λ_f for the configuration being considered must be determined. These values are then used for entry into the charts, figures 4 or 5 and 6, depending on control location. The coefficients obtained from the charts have been made nondimensional by use of control geometric parameters. For determining the coefficients based on the usual wing parameters, the following equations are given (approximate thickness correction factors are included but can be neglected by letting the factors equal 1.0):

$$(C_{L_\delta})_c=F_1 C_{L_\delta}'\frac{S_f}{S} \tag{7}$$

$$(C_{l_\delta})_c=\frac{(C_{L_\delta})_c}{2b}\left(y_f+b_f\frac{C_{l_\delta}'}{C_{L_\delta}'}\right) \tag{8}$$

$$(C_{m_\delta})_c=\frac{(C_{L_\delta})_c}{\bar{c}}\left(\frac{F_2 C_{m_\delta}'}{F_1 C_{L_\delta}'}\frac{2M_a}{S_f}\sqrt{1+\beta^2 a^2}-\beta a b_f\frac{C_{l_\delta}'}{C_{L_\delta}'}-x_f\right) \tag{9}$$

$$(C_{h_\delta})_c=F_2 C_{h_\delta} \tag{10}$$

(The subscript c indicates that the approximate thickness correction factors have been included.)

For determining the control hinge moment due to wing angle of attack, preliminary calculations are first made on the computing form of table IX. Results of these computations indicate positions in the charts (figs. 7 to 10) from which P^* and t_{cp} are to be obtained. Values from the charts are then inserted in table IX and the operations indicated in the computing form are completed. The approximate thickness correction factor can be applied by use of the following equation:

$$(C_{h_\alpha})_c=F_3 C_{h_\alpha} \tag{11}$$

ILLUSTRATIVE EXAMPLE

As an example of the use of the charts, the control-surface characteristics are determined for the configuration shown in figure 11. The wing is assumed to have 5-percent-thick symmetrical parabolic sections in planes normal to the control hinge line.

Lift and pitching-moment coefficients are obtained by entering the charts of figure 5 at values of $\frac{\tan \Lambda_{HL}}{\beta}=0.40$ and $\frac{\tan \Lambda_{TE}}{\beta}=0.35$. Hinge-moment and rolling-moment coefficients are obtained by entering the charts of figure 6 (g) at values of $\frac{\tan \Lambda_{TE}}{\beta}=0.35$ and $\lambda_f=0.713$. Coefficients obtained from the charts are $\beta C_{L_\delta}'=0.0748$, $\beta C_{m_\delta}'=-0.0365$, $\beta C_{l_\delta}'=0.0372$, and $\beta C_{h_\delta}=-0.0345$. The calculation of C_{h_α} for the example is presented in table IX. Preliminary calculations are made in table IX (a) and in column (1) of table IX (b). Values of n and r' calculated in column (1) are used to enter the charts (figs. 7 to 10). Values of P^* and t_{cp} obtained from the charts are inserted in columns (2) and (3) of table IX (b) and the computations are completed. The theoretical value of C_{h_α} is -0.0194.

The equation for the section contour in a plane normal to the control hinge axis is

$$\frac{t}{2c}=2\left(\frac{t}{c}\right)_{max}\left[\frac{x}{c}-\left(\frac{x}{c}\right)^2\right] \tag{12}$$

The slope in this plane at any point along the airfoil is

$$\frac{d\frac{t}{2c}}{d\frac{x}{c}}=2\left(\frac{t}{c}\right)_{max}\left(1-2\frac{x}{c}\right) \tag{13}$$

Substitution of equation (13) in equations (4) and (5) yields the following equations for F_1 and F_2:

$$F_1=1-4\frac{C_2}{C_1}\left(\frac{t}{c}\right)_{max}\frac{x_h}{c} \tag{14}$$

$$F_2=1-\frac{4}{3}\frac{C_2}{C_1}\left(\frac{t}{c}\right)_{max}\left(1+2\frac{x_h}{c}\right) \tag{15}$$

For determining F_3, the equation for the section contour in a plane normal to the wing leading edge is written as

$$\left(\frac{t}{2c}\right)'=\frac{2\left(\frac{t}{c}\right)_{max}}{\cos\left(\Lambda-\Lambda_{HL}\right)}\left[\frac{\left(\frac{x}{c}\right)'-\left(\frac{x}{c}\right)'^2}{1+K\left(\frac{x}{c}\right)'}\right] \tag{16}$$

where

$$K=\tan\left(\Lambda-\Lambda_{HL}\right)\tan\left(\Lambda-\Lambda_{TE}\right)$$

The slope of the airfoil contour in this plane is

$$\frac{d\left(\frac{t}{2c}\right)'}{d\left(\frac{x}{c}\right)'}=\frac{2\left(\frac{t}{c}\right)_{max}}{\cos\left(\Lambda-\Lambda_{HL}\right)}\left\{\frac{1-2\left(\frac{x}{c}\right)'-K\left(\frac{x}{c}\right)'^2}{\left[1+K\left(\frac{x}{c}\right)'\right]^2}\right\} \tag{17a}$$

or in terms of x/c

$$\frac{d\left(\frac{t}{2c}\right)'}{d\left(\frac{x}{c}\right)'}=\frac{2\left(\frac{t}{c}\right)_{max}}{\cos\left(\Lambda-\Lambda_{HL}\right)}\left[1-2\frac{x}{c}+\frac{K}{1+K}\left(\frac{x}{c}\right)^2\right] \tag{17b}$$

Substitution of equation (17b) in equation (6) yields the following equation for F_3:

$$F_3=1-\frac{2C_2\left(\frac{t}{c}\right)_{max}}{3C_1(1+K)\cos\left(\Lambda-\Lambda_{HL}\right)}\left[2\left(1+2\frac{x_h}{c}\right)-K\left(1-\frac{x_h}{c}\right)^2\right] \tag{18}$$

From equations (14), (15), and (18), the following correction factors are obtained for the sample configuration: $F_1=0.8077$, $F_2=0.7889$, and $F_3=0.7355$. It is of interest to note that these values indicate appreciable losses in loading due to airfoil-section thickness, and it might be pointed out that greater losses would be obtained for thicker airfoil sections.

The coefficients obtained from the charts and the preceding correction factors are then substituted in equations (4) to (8). The results obtained are

$$(C_{L_\delta})_c=0.00411$$

$$(C_{m_\delta})_c=-0.00318$$

$$(C_{l_\delta})_c=0.000619$$

$$(C_{h_\delta})_c=-0.0182$$

$$(C_{h_\alpha})_c=-0.0143$$

LANGLEY AERONAUTICAL LABORATORY,
NATIONAL ADVISORY COMMITTEE FOR AERONAUTICS,
LANGLEY FIELD, VA., *September 8, 1950.*

APPENDIX A

METHOD OF INTEGRATING PRESSURES OVER CONICAL REGIONS OF DEFLECTED CONTROLS

The pressure distributions in the conical-flow regions shown in figure 12 are given in reference 2. With suitable changes in notation these are:

For region I,

$$P'=\frac{1}{\pi}\cos^{-1}\frac{a-t}{1-at} \tag{A1}$$

For region III,

$$P'=\frac{1}{\pi}\cos^{-1}\frac{1-(2+a)t}{1+at} \tag{A2}$$

Because the flow is conical in regions I and III, integrations of the pressures along the trailing edge within these regions are representative of integrations over corresponding triangular segments having the Mach cone origin as apexes. For such integrations, a coordinate for distance along the trailing edge must be introduced. The nondimensional coordinate chosen was $t'=\beta\cdot\tan\tau'$ (fig. 12 and reference 2). The integrations required for determining average pressure ratio and center-of-pressure ray location for any segment are

$$P=\frac{\int_{t_1'}^{t_2'}P'\,dt'}{\int_{t_1'}^{t_2'}dt'} \tag{A3}$$

and

$$t_{cp}'=\frac{\int_{t_1'}^{t_2'}t'P'\,dt'}{\int_{t_1'}^{t_2'}P'\,dt'} \tag{A4}$$

(Subscripts 1 and 2 indicate values of t' corresponding to the end points of the part of t' over which integrations were made.)

A Mach number of $\sqrt{2}$ was assumed for convenience ($\beta=1$) in making the integrations of equations (A3) and (A4). This assumption is valid because any case of Mach number greater than 1 can readily be reduced to an equivalent case at $M=\sqrt{2}$ by an affine transformation corresponding to the Prandtl-Glauert transformation for the subsonic case (reference 5). An example of this transformation is shown in figure 13. The equivalent plan form is obtained by dividing all streamwise dimensions by β and leaving lateral dimensions unchanged; consequently, values of a, d, and t (for equivalent points) are the same. From equations (A1) and (A2), it can readily be seen that values of P' for equivalent points are the same. It follows that summation of P' over equivalent regions results in equal values of P and t_{cp}. It is apparent from figure 13, however, that values of t_{cp}' are different. This difference is of no consequence because values of t_{cp} for the equivalent wing (obtained from t_{cp}' and geometric relations) are the same as values of t_{cp} for the initial wing.

The procedures followed in the integrations of equations (A3) and (A4) are the same for regions I and III and are only shown for region I. If the Mach number is assumed to equal $\sqrt{2}$, where $\beta=1$, equation (A1) may be written in terms of t' as follows:

$$P'=\frac{1}{\pi}\cos^{-1}\frac{(a+d)-(1-ad)t'}{(1+ad)-(a-d)t'}$$

If y is substituted for $\cos\pi P'$, equations (A3) and (A4) become

$$P=\frac{\dfrac{-(1-a^2)(1+d^2)}{\pi}\displaystyle\int_{y_1}^{y_2}\frac{\cos^{-1}y}{[(1-ad)-(a-d)y]^2}\,dy}{-(1-a^2)(1+d^2)\displaystyle\int_{y_1}^{y_2}\frac{dy}{[(1-ad)-(a-d)y]^2}} \tag{A5}$$

$$t_{cp}'=\frac{\dfrac{-(1-a^2)(1+d^2)}{\pi}\displaystyle\int_{y_1}^{y_2}\frac{(a+d)-(1+ad)y}{[(1-ad)-(a-d)y]^3}\cos^{-1}y\,dy}{\dfrac{-(1-a^2)(1+d^2)}{\pi}\displaystyle\int_{y_1}^{y_2}\frac{\cos^{-1}y}{[(1-ad)-(a-d)y]^2}\,dy} \tag{A6}$$

Integration by parts was then employed in the solutions of equations (A5) and (A6).

For cases in which the conical-flow region overlaps the opposite parting line, the average pressure loss and center-of-pressure ray location are required for regions I_a and I_b (fig. 1). Equations (A3) and (A4) may be used in obtaining the solutions for region I_a by a slight modification requiring no additional integration. Thus,

$$P^*=\frac{\int_{t_1'}^{t_2'}(1-P')\,dt'}{\int_{t_1'}^{t_2'}dt'}=1-\frac{\int_{t_1'}^{t_2'}P'\,dt'}{\int_{t_1'}^{t_2'}dt'} \tag{A7}$$

$$t_{cp}'=\frac{\int_{t_1'}^{t_2'}t'(1-P')\,dt'}{\int_{t_1'}^{t_2'}(1-P')\,dt'}=\frac{\left[\dfrac{t'^2}{2}\right]_{t_1'}^{t_2'}-\int_{t_1'}^{t_2'}t'P'\,dt'}{\left[t'\right]_{t_1'}^{t_2'}-\int_{t_1'}^{t_2'}P'\,dt'} \tag{A8}$$

In obtaining the solutions for region I_b (fig. 1), essentially the same procedure as previously outlined was used. The parameter $r=\frac{1}{t}$ was used to represent distance along the parting line nondimensionally. Values of P^* and r_{cp} were obtained by making integrations similar to those in equations (A7) and (A8) (before simplifications).

Results of integrations over all regions shown in figure 1 are presented in tables II (a) and II (b). Results of evaluating these equations at taper ratios of 1.0, where they become indeterminate, are presented in table III (a).

APPENDIX B

METHOD FOR DETERMINING THICKNESS CORRECTION FACTORS

The pressure coefficient at any point on a two-dimensional surface as given by the Busemann second-order approximation (reference 8, with suitable changes in notation) is

$$C_p = C_1(\delta+\theta)+C_2(\delta+\theta)^2 \tag{B1}$$

(The angle δ is considered positive when calculating C_p for lower surface and negative when calculating C_p for upper surface. Throughout appendix B, δ is considered to be in radians.) The constants C_1 and C_2 are functions only of Mach number. Equations for these constants and tabulated values are presented in reference 10.

The lifting pressure coefficient at any chordwise position is simply the difference between the pressure coefficients on the lower and upper surfaces. The net lift coefficient is obtained by integrating the local lifting pressure coefficients between the hinge line $\left(\frac{x}{c}=\frac{x_h}{c}\right)$ and the trailing edge $\left(\frac{x}{c}=1.0\right)$. (See fig. 14.) Thus,

$$C_{L'_{\text{thickness }(\delta)}} = \frac{1}{1-\frac{x_h}{c}}\int_{x_h/c}^{1.0}[(C_p)_L-(C_p)_U]\,d\,\frac{x}{c} \tag{B2}$$

(The subscripts L and U denote lower and upper surfaces.) Similarly, the hinge-moment coefficient is obtained by integrating the products of local lifting pressure coefficient and moment arm between the hinge line and the trailing edge. Thus,

$$C_{h_{\text{thickness }(\delta)}} = \frac{-1}{\left(1-\frac{x_h}{c}\right)^2}\int_{x_h/c}^{1.0}\left(\frac{x}{c}-\frac{x_h}{c}\right)[(C_p)_L-(C_p)_U]\,d\,\frac{x}{c} \tag{B3}$$

An application of sweepback theory, as explained in reference 10, must be used for determining $C_{p_L}-C_{p_U}$. It is important to note that, for deflected controls, this theory requires the use of the Mach number component and the airfoil section in a plane normal to the control hinge axis. Values of C_L' and C_h thus obtained are based on the dynamic-pressure component normal to the hinge line and the deflection angle measured in a plane normal to the hinge line. Values of C_L' and C_h for a two-dimensional flat-plate control, based on the same q and δ, are obtained by considering the Mach number normal to the hinge line in determining values of C_1. Equations for these coefficients are

$$C_{L'_{\text{flat plate}}} = 2C_1\delta \tag{B4}$$

$$C_{h_{\text{flat plate}}} = -C_1\delta \tag{B5}$$

The following correction factors are then determined by dividing equations (B2) and (B3) by equations (B4) and (B5), respectively:

$$F_1 = \frac{1}{2C_1\delta\left(1-\frac{x_h}{c}\right)}\int_{x_h/c}^{1.0}[(C_p)_L-(C_p)_U]\,d\,\frac{x}{c} \tag{B6}$$

$$F_2 = \frac{1}{C_1\delta\left(1-\frac{x_h}{c}\right)^2}\int_{x_h/c}^{1.0}\left(\frac{x}{c}-\frac{x_h}{c}\right)[(C_p)_L-(C_p)_U]\,d\,\frac{x}{c} \tag{B7}$$

If the sections are assumed to be symmetrical about the chord plane, equations (B6) and (B7) can be simplified because

$$(C_p)_L-(C_p)_U = 2\delta\left(C_1+2C_2\frac{d\,\frac{t}{2c}}{d\,\frac{x}{c}}\right) \tag{B8}$$

Equations (B6) and (B7) then become

$$F_1 = \frac{1}{1-\frac{x_h}{c}}\int_{x_h/c}^{1.0}\left(1+2\,\frac{C_2}{C_1}\frac{d\,\frac{t}{2c}}{d\,\frac{x}{c}}\right)d\,\frac{x}{c} \tag{B9}$$

$$F_2 = \frac{2}{\left(1-\frac{x_h}{c}\right)^2}\int_{x_h/c}^{1.0}\left(\frac{x}{c}-\frac{x_h}{c}\right)\left(1+2\,\frac{C_2}{C_1}\frac{d\,\frac{t}{2c}}{d\,\frac{x}{c}}\right)d\,\frac{x}{c} \tag{B10}$$

The equation for F_3, may be written as equation (B7) for F_2 (substituting α for δ)

$$F_3 = \frac{1}{C_1\alpha\left(1-\frac{x_h}{c}\right)^2}\int_{x_h/c}^{1.0}\left(\frac{x}{c}-\frac{x_h}{c}\right)[(C_p)_L-(C_p)_U]\,d\,\frac{x}{c} \tag{B11}$$

In this case, however, the airfoil section and Mach number component in a plane normal to the wing leading edge must be used in determining values of C_1 and $(C_p)_L-(C_p)_U$.

For symmetrical sections, the equation for F_3 may be simplified in the same manner as the equivalent equation for F_2. Thus,

$$F_3 = \frac{2}{\left(1-\frac{x_h}{c}\right)^2}\int_{x_h/c}^{1.0}\left(\frac{x}{c}-\frac{x_h}{c}\right)\left[1+2\,\frac{C_2}{C_1}\frac{d\left(\frac{t}{2c}\right)'}{d\left(\frac{x}{c}\right)'}\right]d\,\frac{x}{c} \tag{B12}$$

Equation (B12) will in some cases become somewhat involved because $\frac{d(t/c)'}{d(x/c)'}$ must be determined from the equation for the airfoil section in a plane normal to the wing leading edge and must then be written in terms of x/c (unless the surfaces are plane). It should be pointed out that suitable approximations for most symmetrical biconvex airfoils (which in general require involved expressions for defining the contour) may be obtained by assuming the sections to have parabolic contours. General equations for the thickness correction factors for symmetrical sections having parabolic contours have been derived in the illustrative example of the present report.

REFERENCES

1. Frick, Charles W., Jr.: Application of the Linearized Theory of Supersonic Flow to the Estimation of Control-Surface Characteristics. NACA TN 1554, 1948.
2. Lagerstrom, P. A., and Graham, Martha E.: Linearized Theory of Supersonic Control Surfaces. Rep. No. SM–13060, Douglas Aircraft Co., Inc., July 24, 1947.
3. Kainer, Julian H., and Marte, Jack E.: Theoretical Supersonic Characteristics of Inboard Trailing-Edge Flaps Having Arbitrary Sweep and Taper. Mach Lines behind Flap Leading and Trailing Edges. NACA TN 2205, 1950.
4. Cohen, Doris: The Theoretical Lift of Flat Swept-Back Wings at Supersonic Speeds. NACA TN 1555, 1948.
5. Lagerstrom, P. A., Wall, D., and Graham, M. E.: Formulas in Three-Dimensional Wing Theory. Rep. No. SM–11901, Douglas Aircraft Co., Inc., July 8, 1946.
6. Sokolnikoff, Ivan S., and Sokolnikoff, Elizabeth S.: Higher Mathematics for Engineers and Physicists. Second ed., McGraw-Hill Book Co., Inc., 1941.
7. Lock C. N. H., and Knowler, A. E.: Integrating Coefficients for Airscrew Analysis. R. & M. No. 2043, British A.R.C., 1941.
8. Bonney, E. Arthur: Aerodynamic Characteristics of Rectangular Wings at Supersonic Speeds. Jour. Aero. Sci., vol. 14, no. 2, Feb. 1947, pp. 110–116.
9. Laitone, Edmund V.: Exact and Approximate Solutions of Two-Dimensional Oblique Shock Flow. Jour. Aero. Sci., vol. 14, no. 1, Jan. 1947, pp. 25–41.
10. The Staff of the Ames 1- by 3-Foot Supersonic Wind-Tunnel Section: Notes and Tables for Use in the Analysis of Supersonic Flow. NACA TN 1428, 1947.

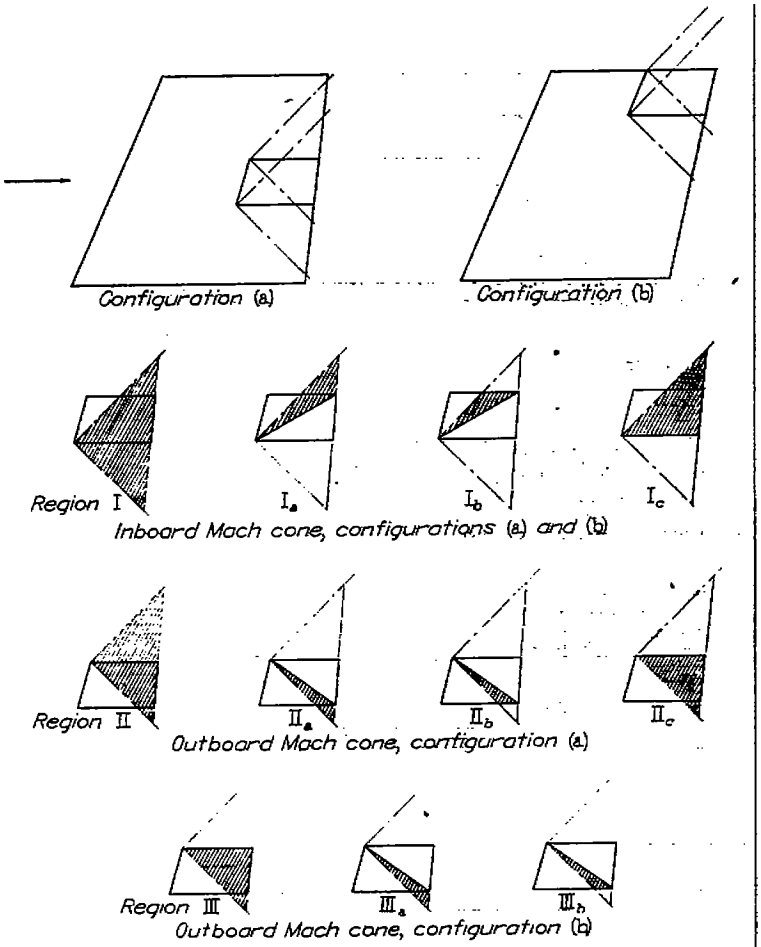

FIGURE 1.—Conical-flow regions for which solutions were obtained in the calculation of deflected control characteristics.

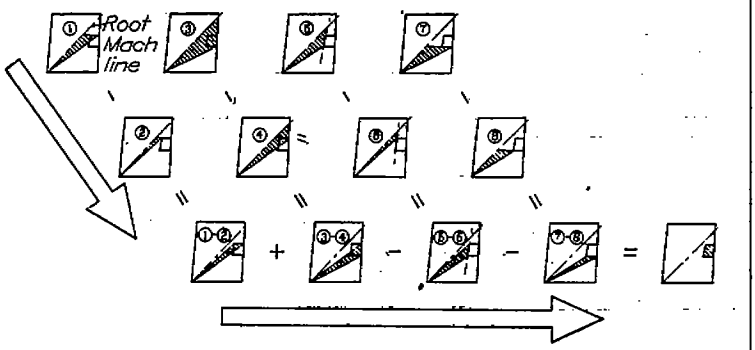

FIGURE 2.—Procedure followed in summing $(PS_L\bar{z})^*$ of conical-flow regions for calculation of C_{h_a}. (Encircled numbers correspond to regions as designated in computing form for C_{h_a}.)

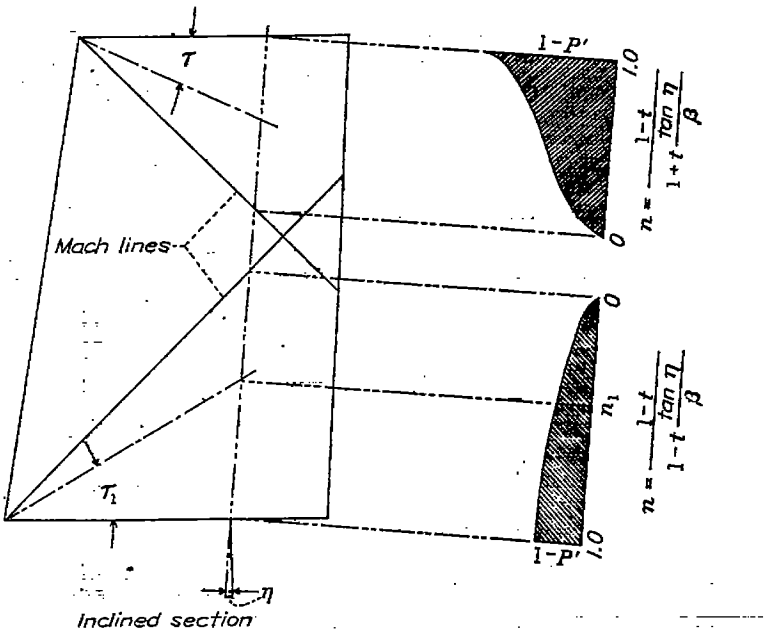

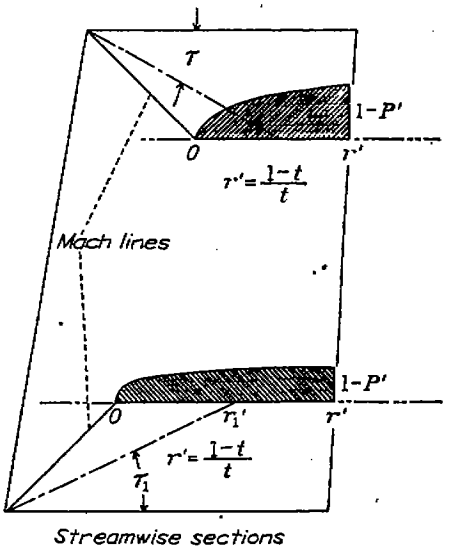

FIGURE 3.—Illustration of method by which P^* and t_{c_2} for triangular segments of the wing-root and wing-tip Mach cones are obtained for use in determining C_{h_a}.

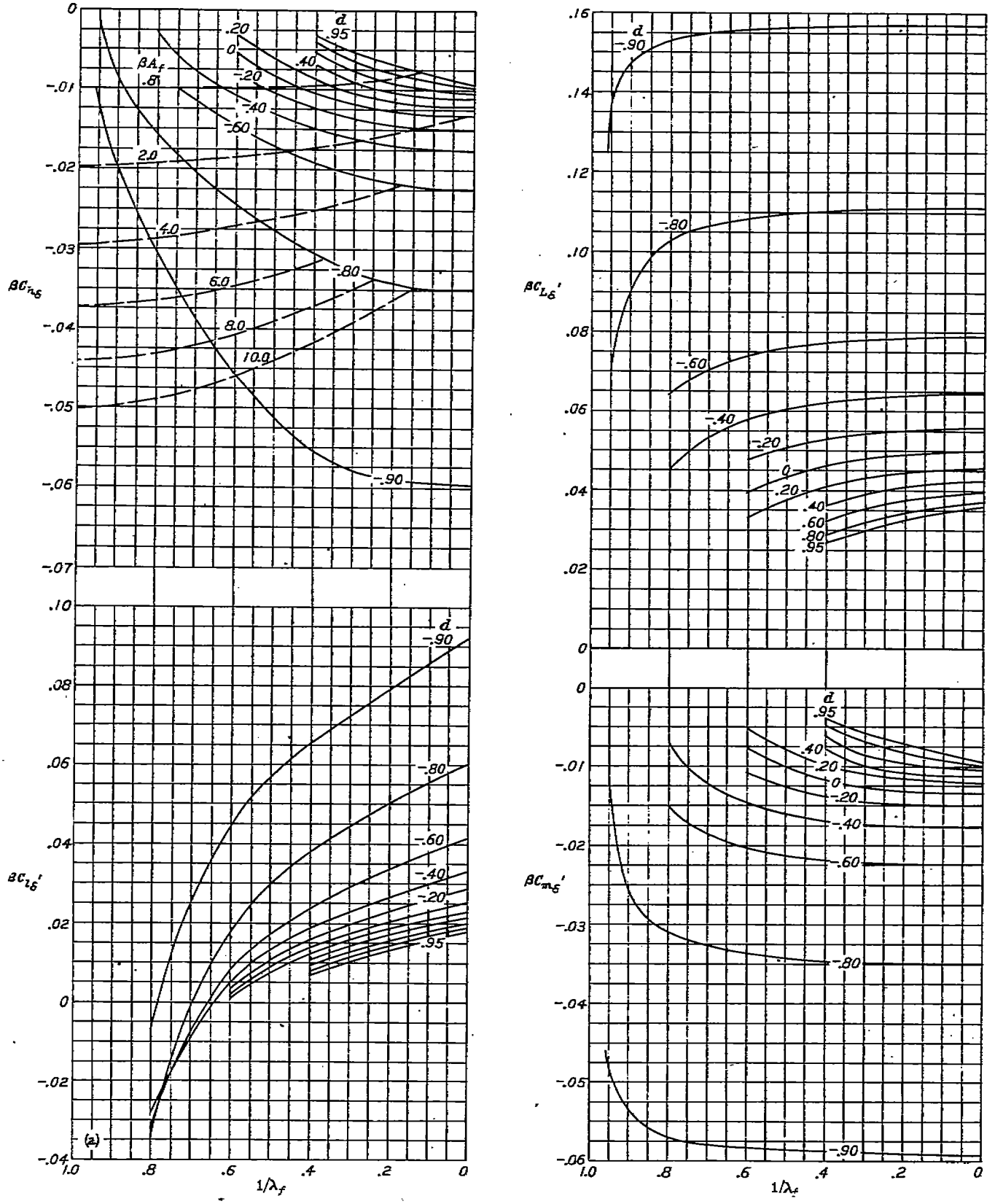

(a) $\frac{\tan \Lambda_{EL}}{\beta} = -0.95$.

FIGURE 4.—Characteristics of deflected trailing-edge controls located at the wing tip. Results for values of $\lambda_f \geq \frac{1-\epsilon}{1-d}$ have been obtained by use of an approximation and should be used with caution.

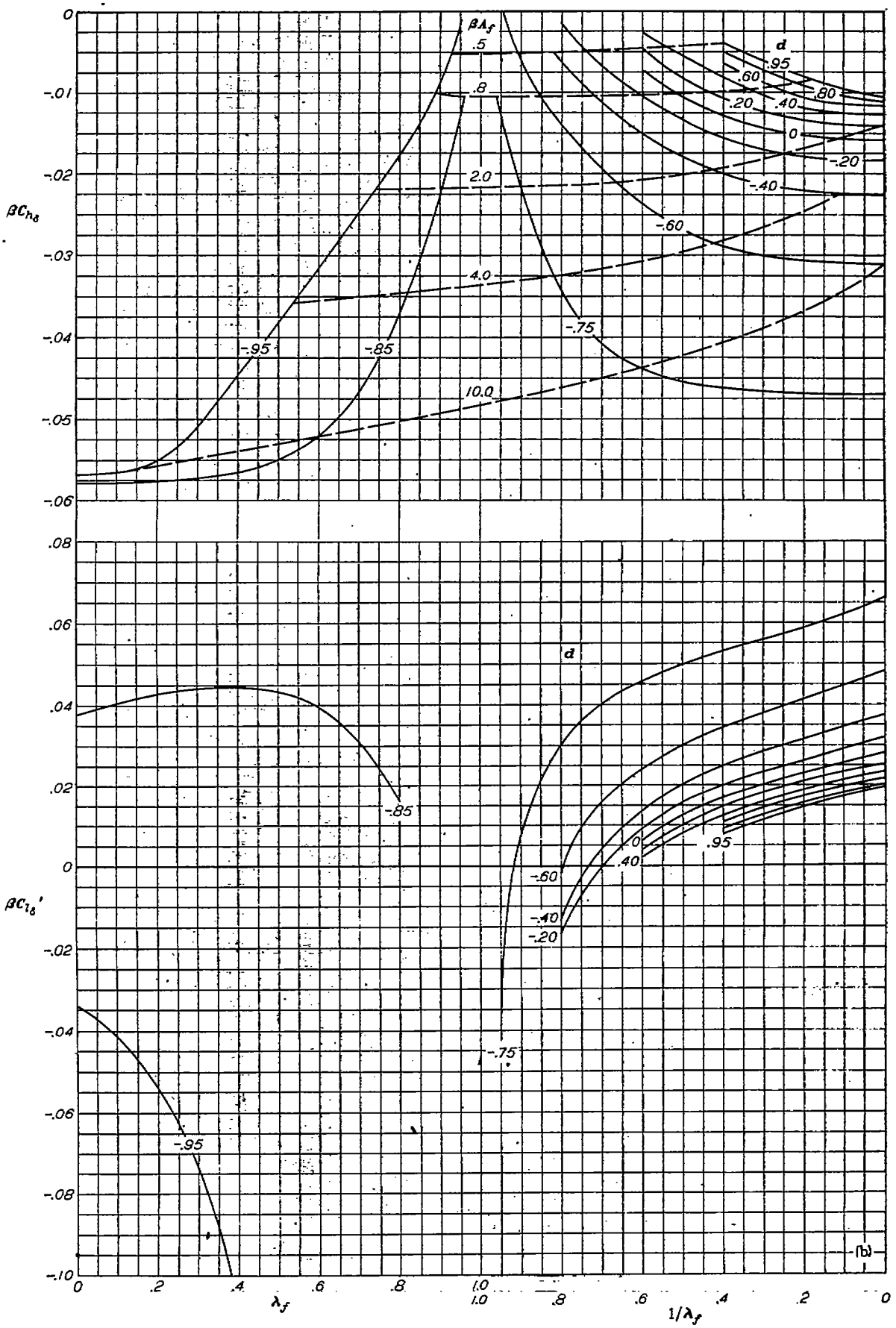

(b) $\frac{\tan \Lambda_{HL}}{\beta} = -0.80$.

FIGURE 4.—Continued.

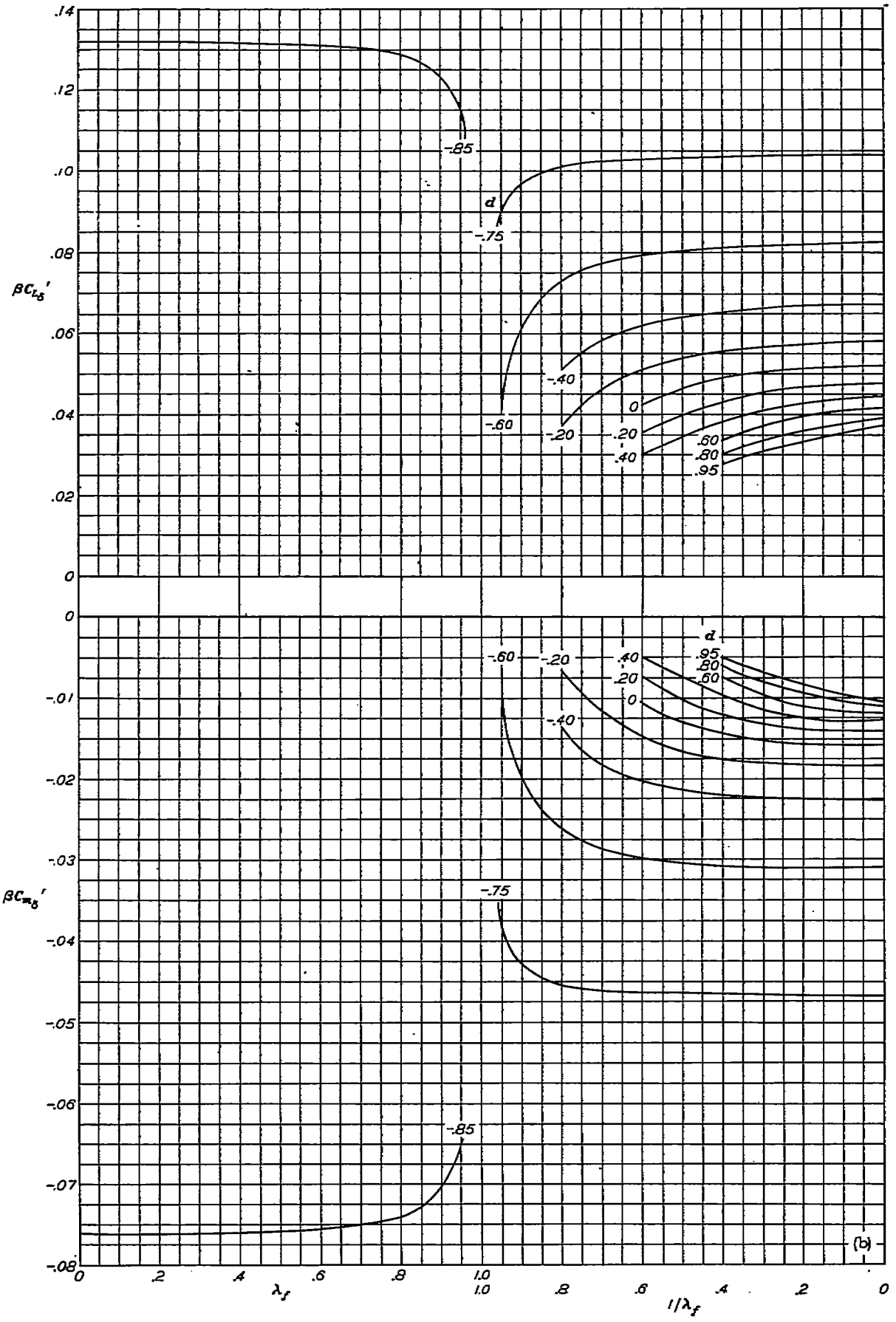

(b) Concluded.

FIGURE 4.—Continued.

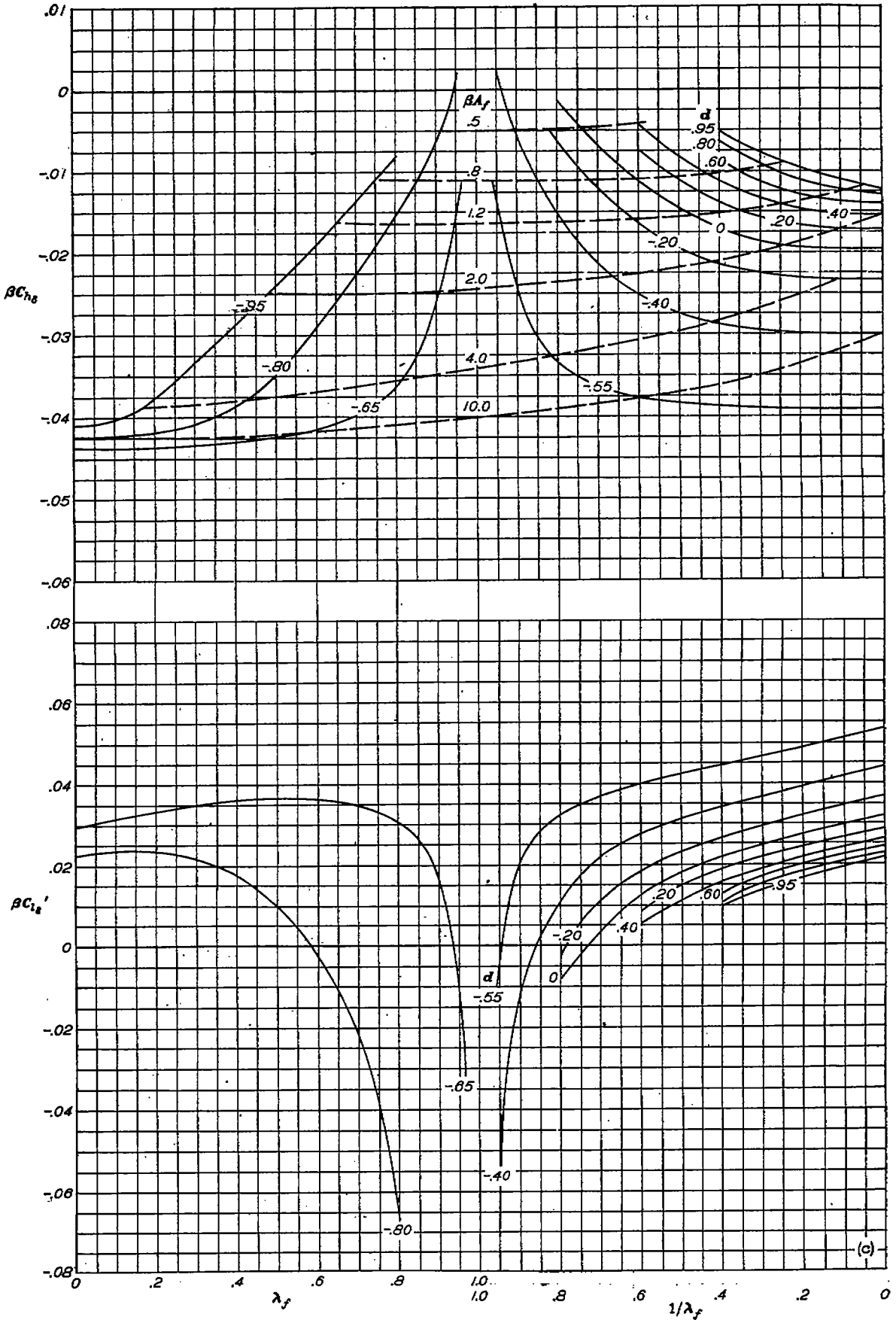

(c) $\frac{\tan \Lambda_{HL}}{\beta} = -0.60$.

FIGURE 4.—Continued.

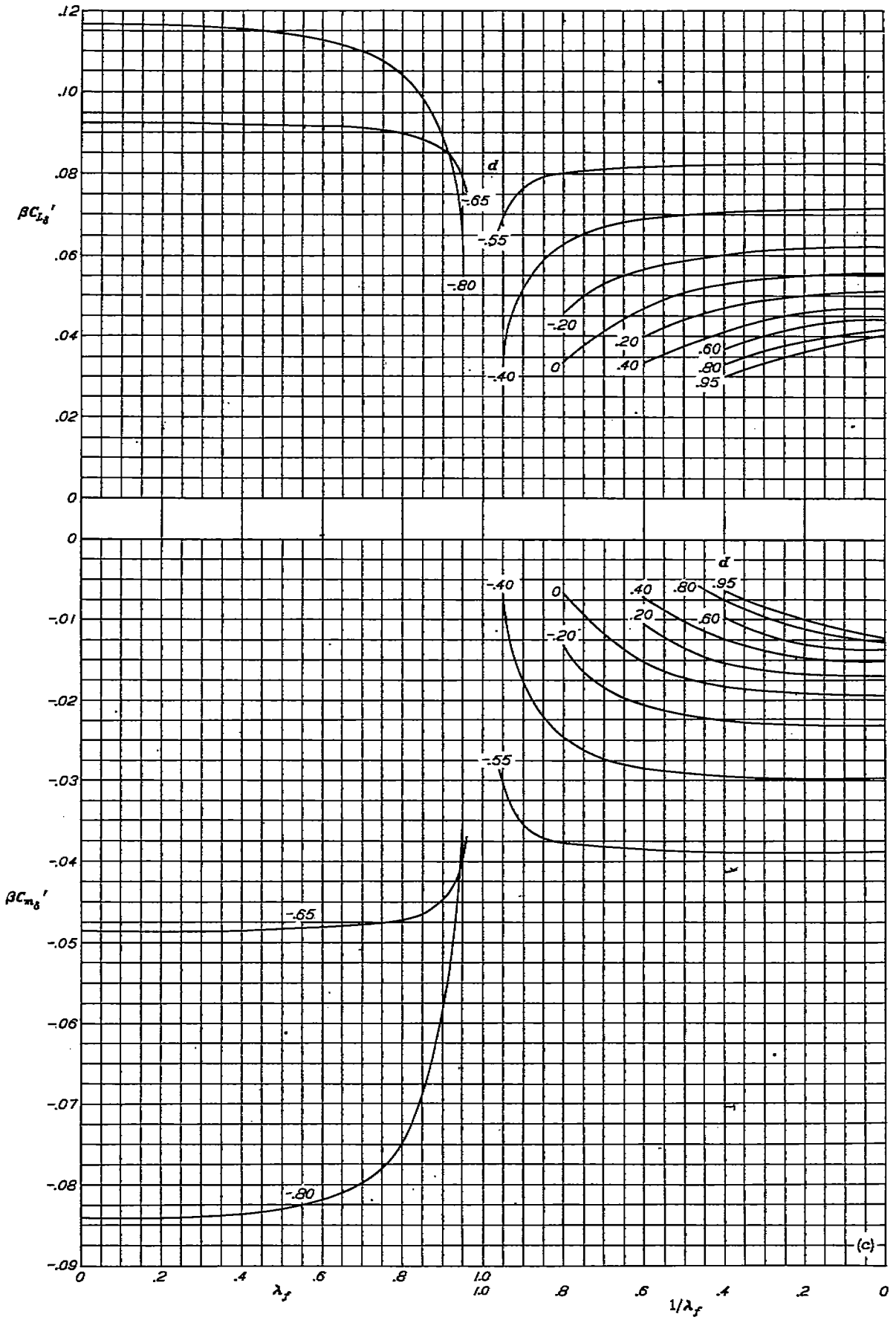

(c) Concluded.

FIGURE 4.—Continued.

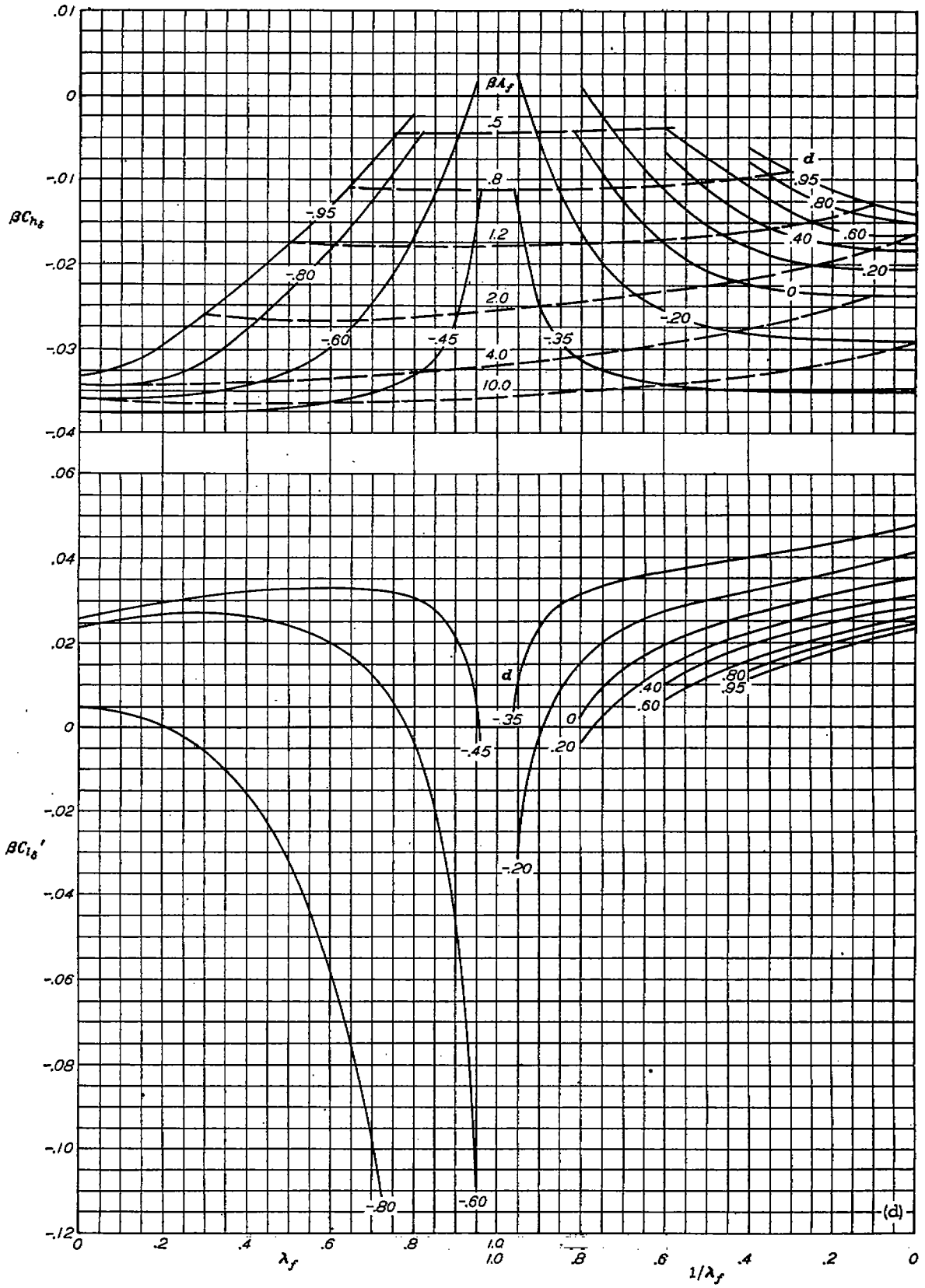

(d) $\frac{\tan \Lambda_{HL}}{\beta} = -0.40$.

FIGURE 4.—Continued.

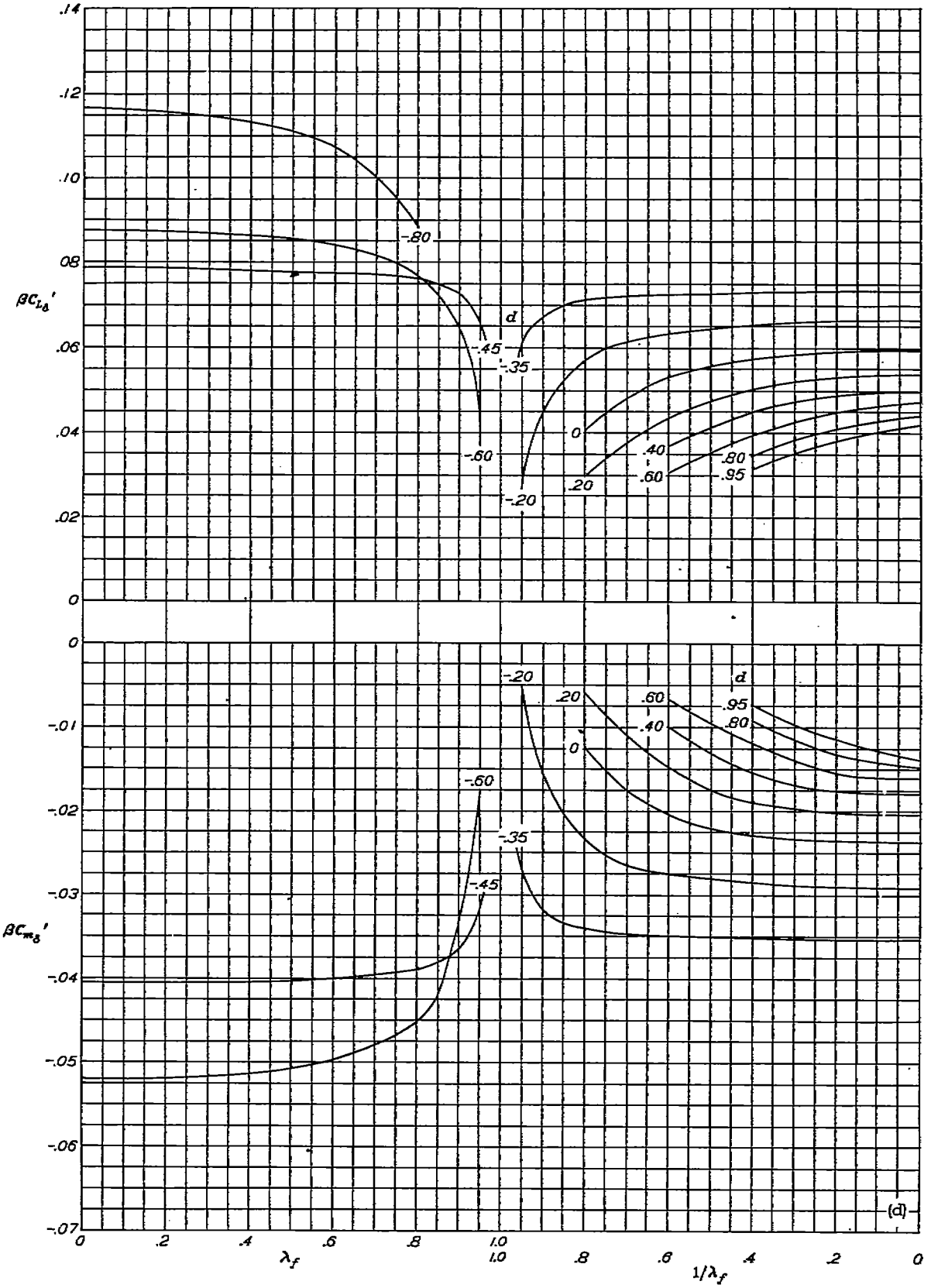

(d) Concluded.

FIGURE 4.—Continued.

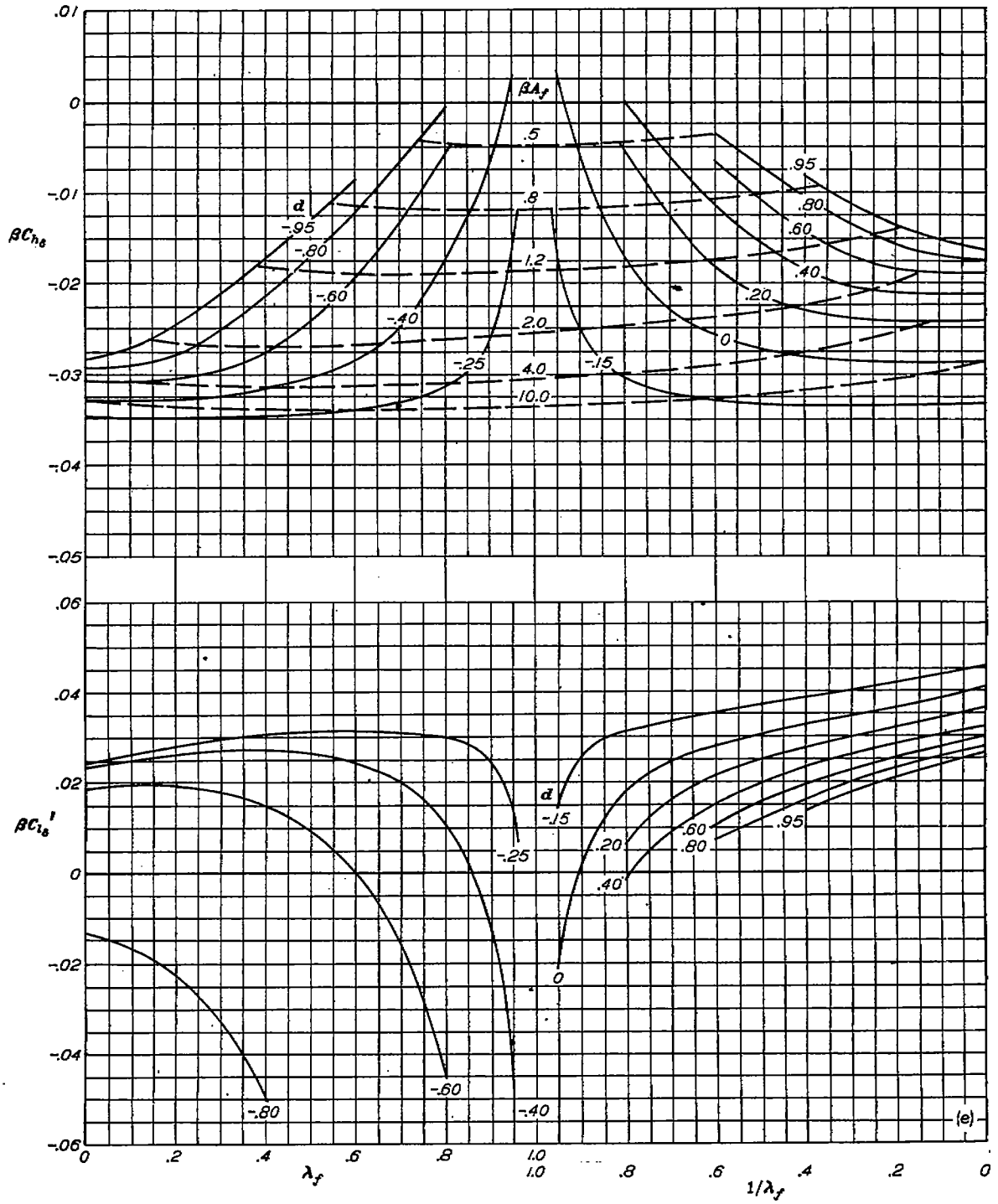

(e)] $\frac{\tan \Lambda_{HL}}{\beta} = -0.20$.

FIGURE 4.—Continued.

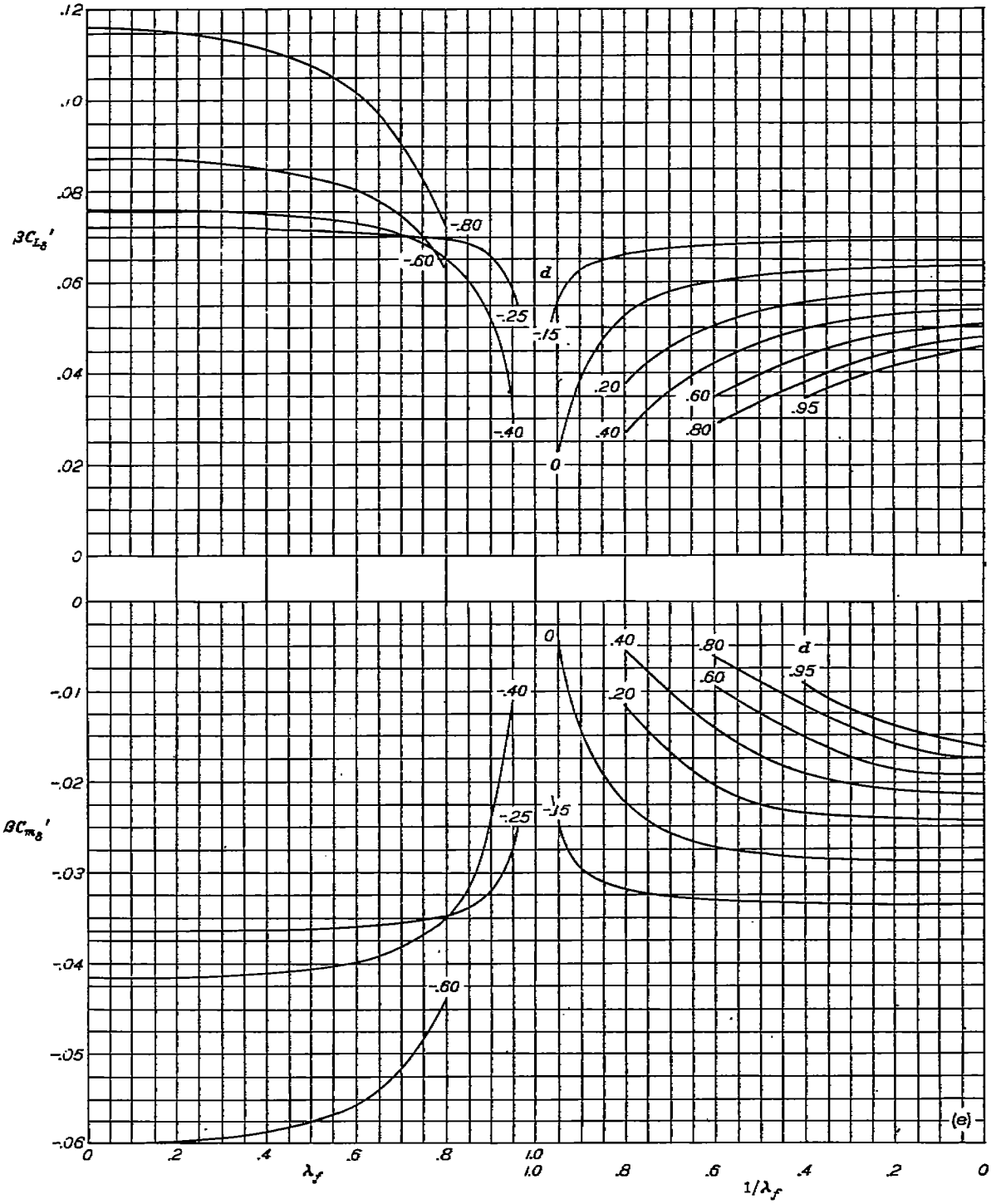

(e) Concluded.

FIGURE 4.—Continued.

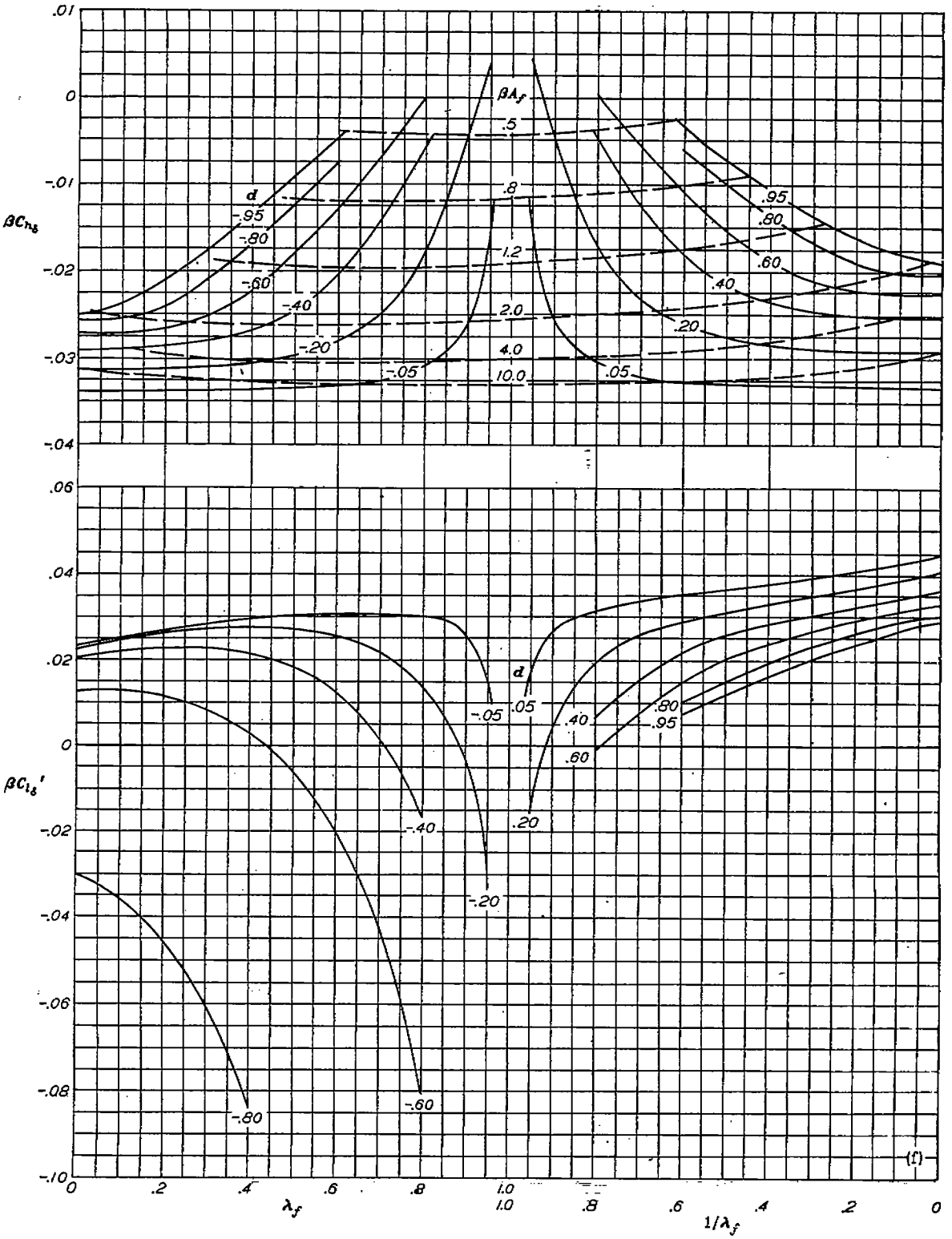

(f) $\frac{\tan \Lambda_{HL}}{\beta}=0$.

FIGURE 4.—Continued.

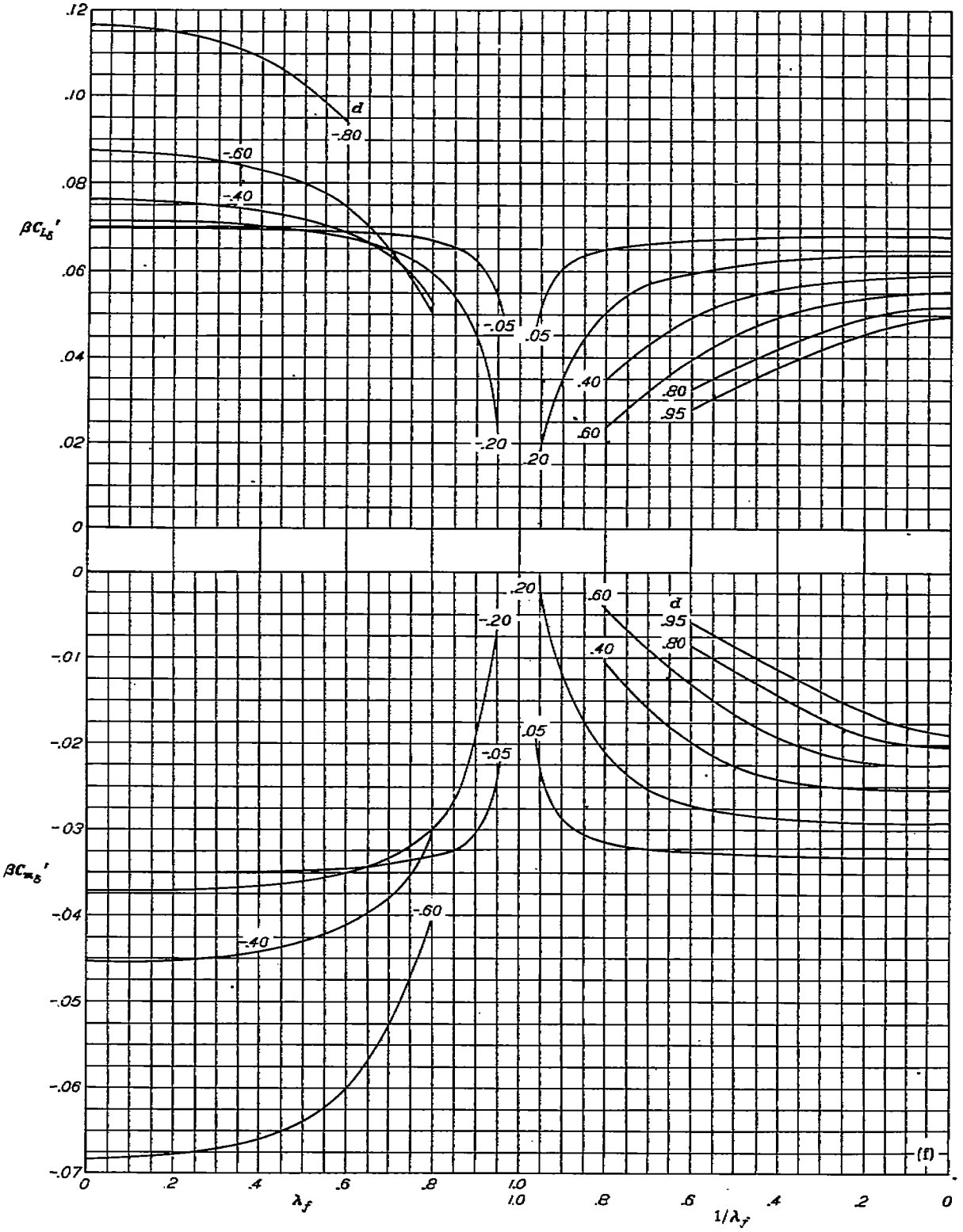

(f) Concluded.

FIGURE 4.—Continued.

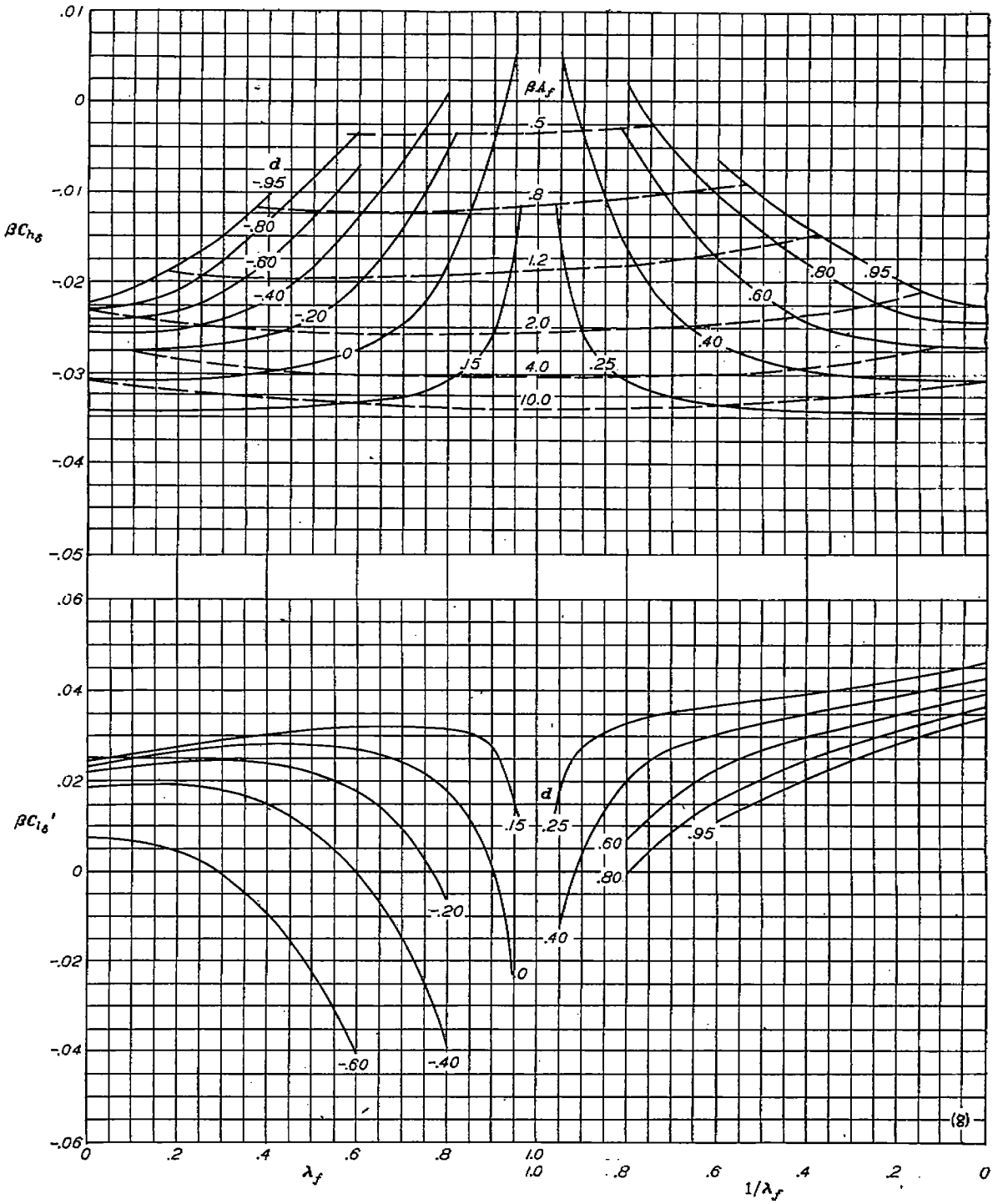

(g) $\frac{\tan \Lambda_{HL}}{\beta}=0.20$.

FIGURE 4.—Continued.

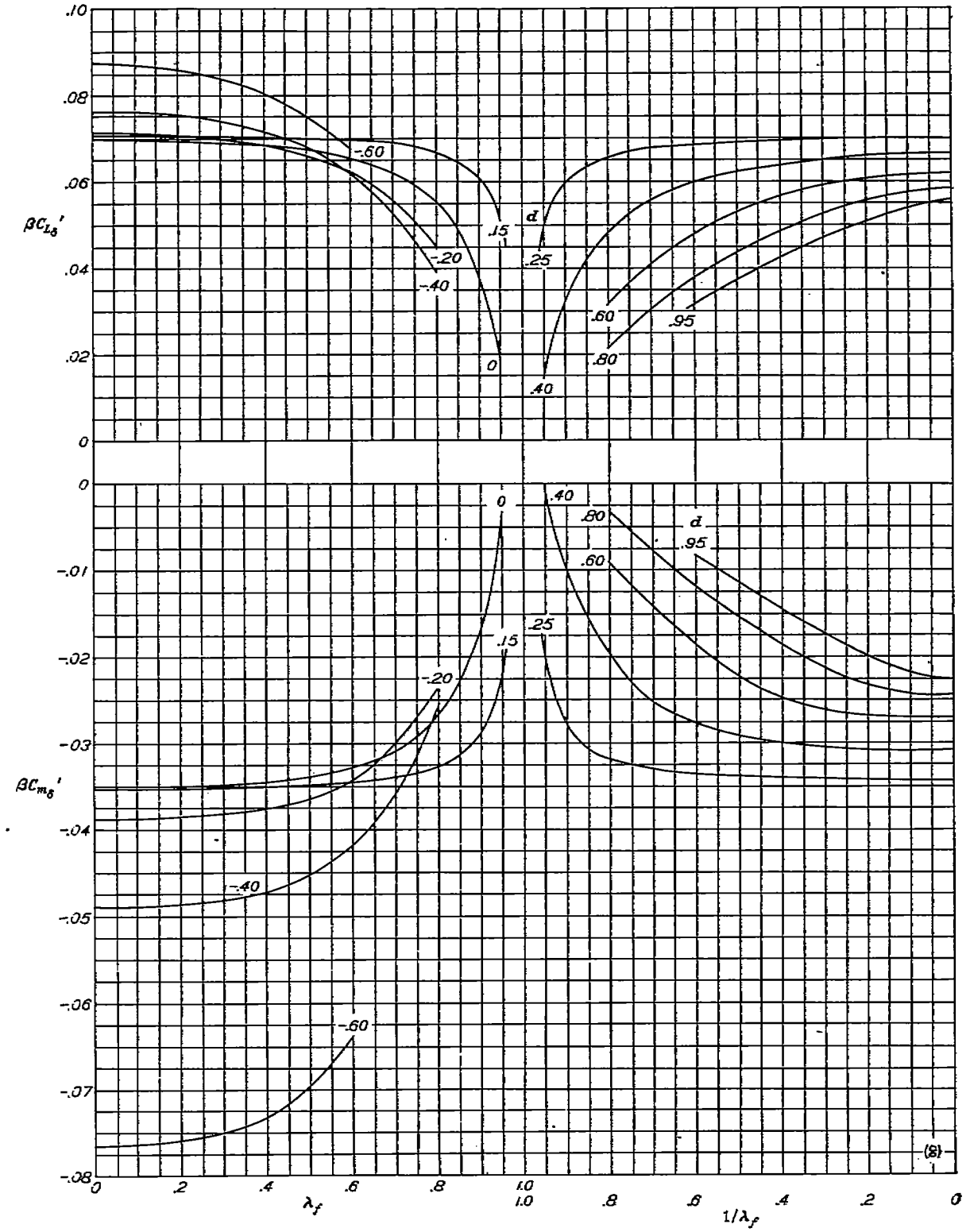

(g) Concluded.

FIGURE 4.—Continued.

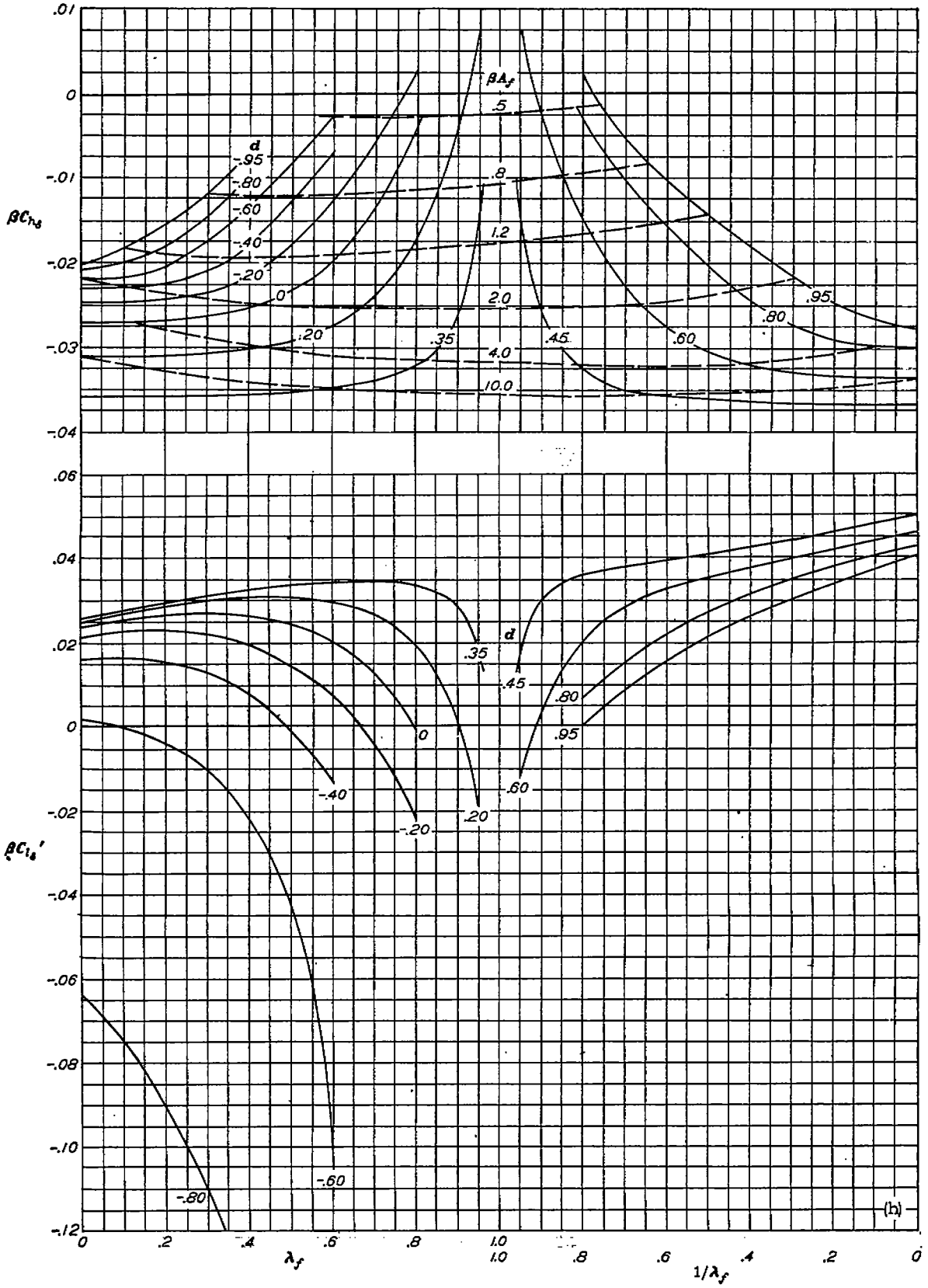

(h) $\frac{\tan \Lambda_{HL}}{\beta} = 0.40$.

FIGURE 4.—Continued.

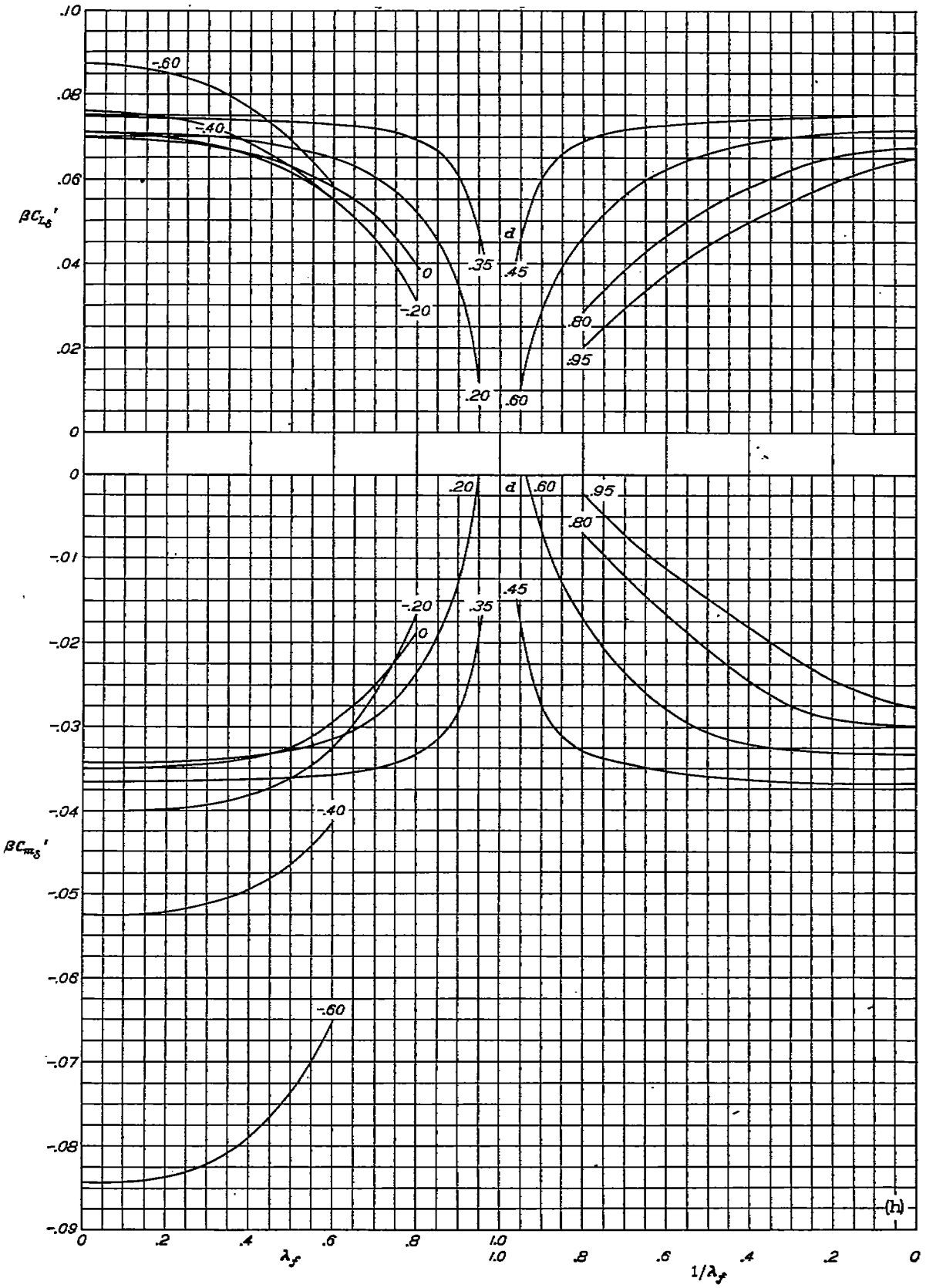

(h) Concluded.

FIGURE 4.—Continued.

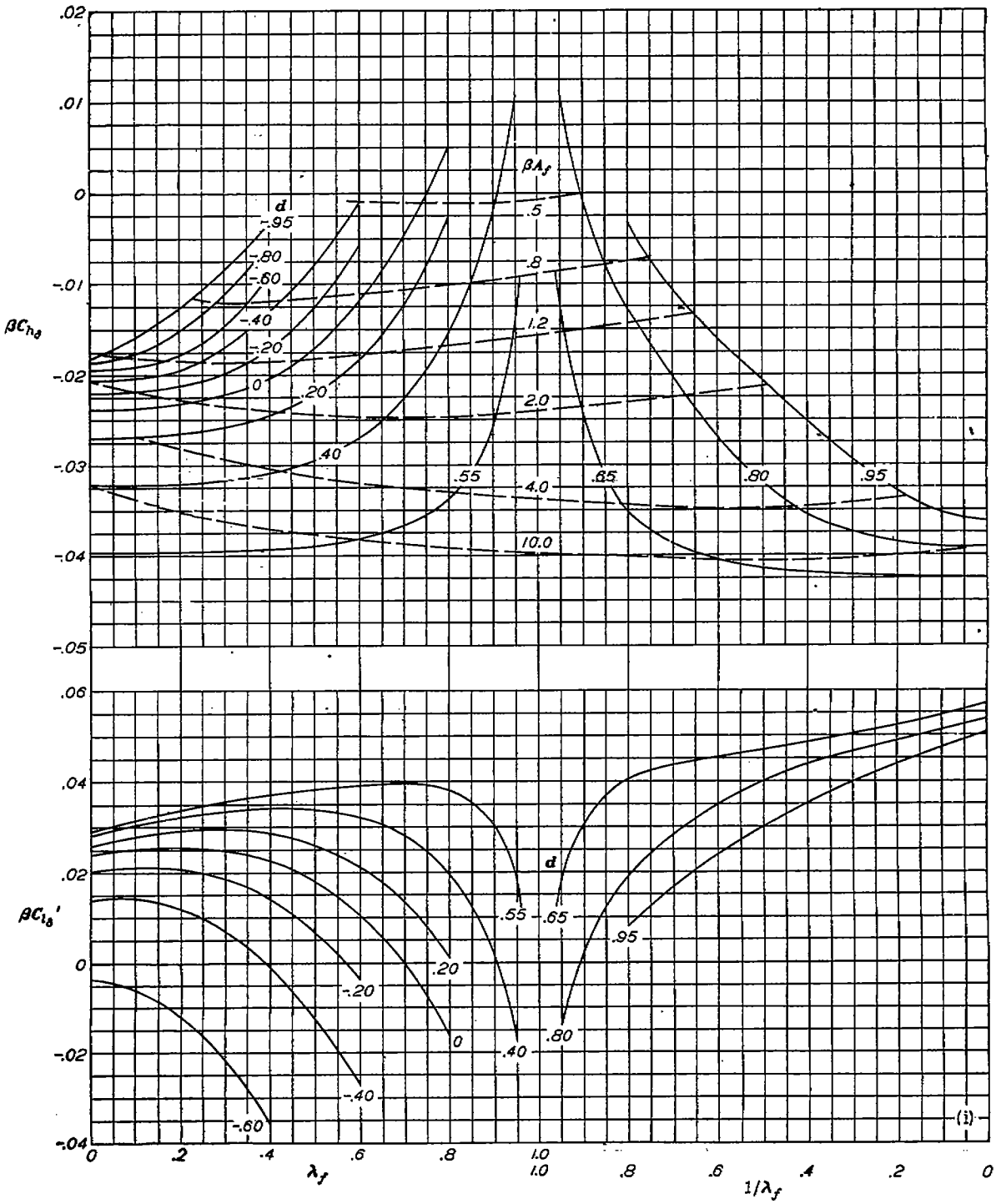

(i) $\frac{\tan \Lambda_{HL}}{\beta} = 0.60$.

FIGURE 4.—Continued.

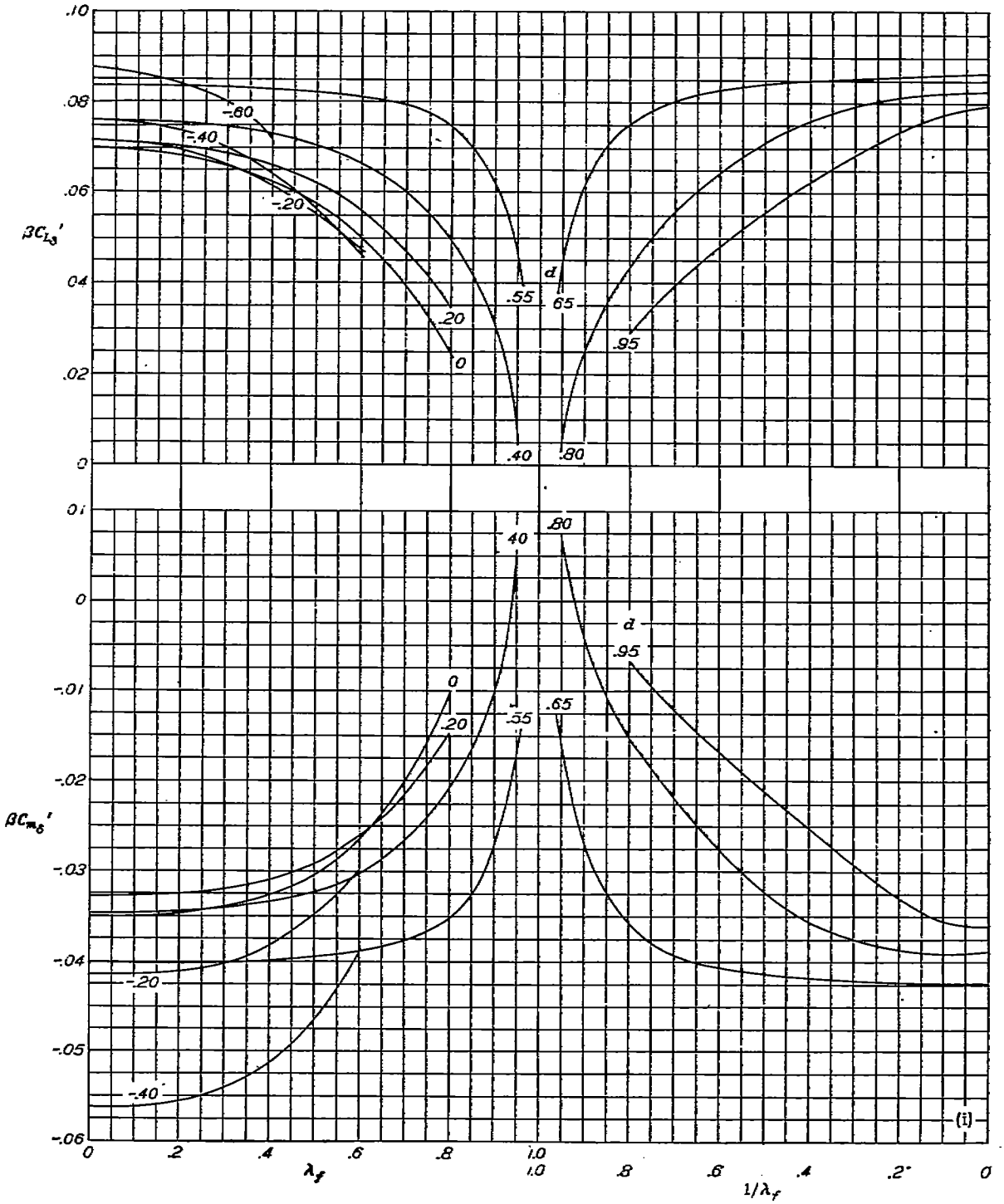

(i) Concluded.

FIGURE 4.—Continued.

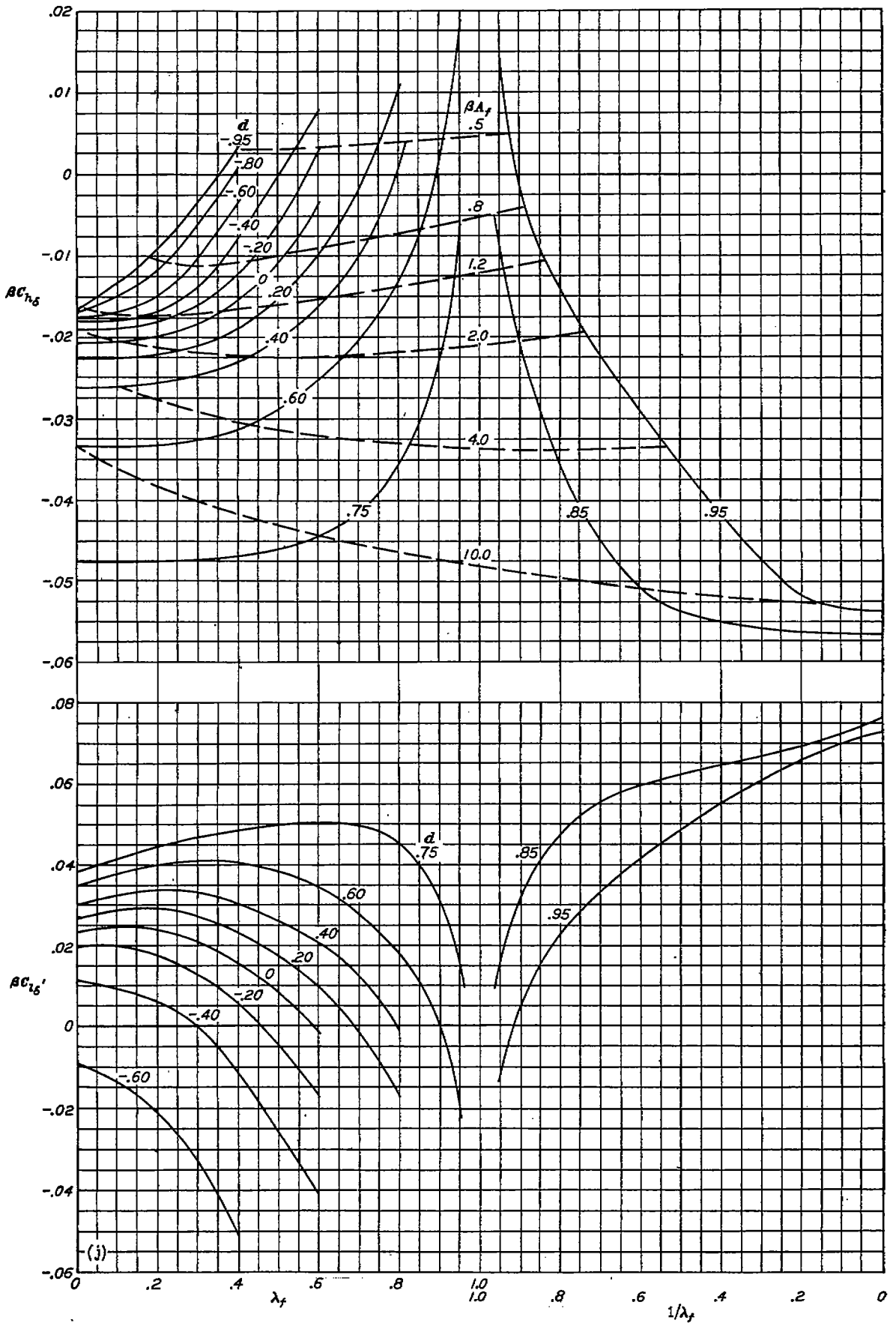

(j) $\frac{\tan \Lambda_{HL}}{\beta}$=0.80.

FIGURE 4.—Continued.

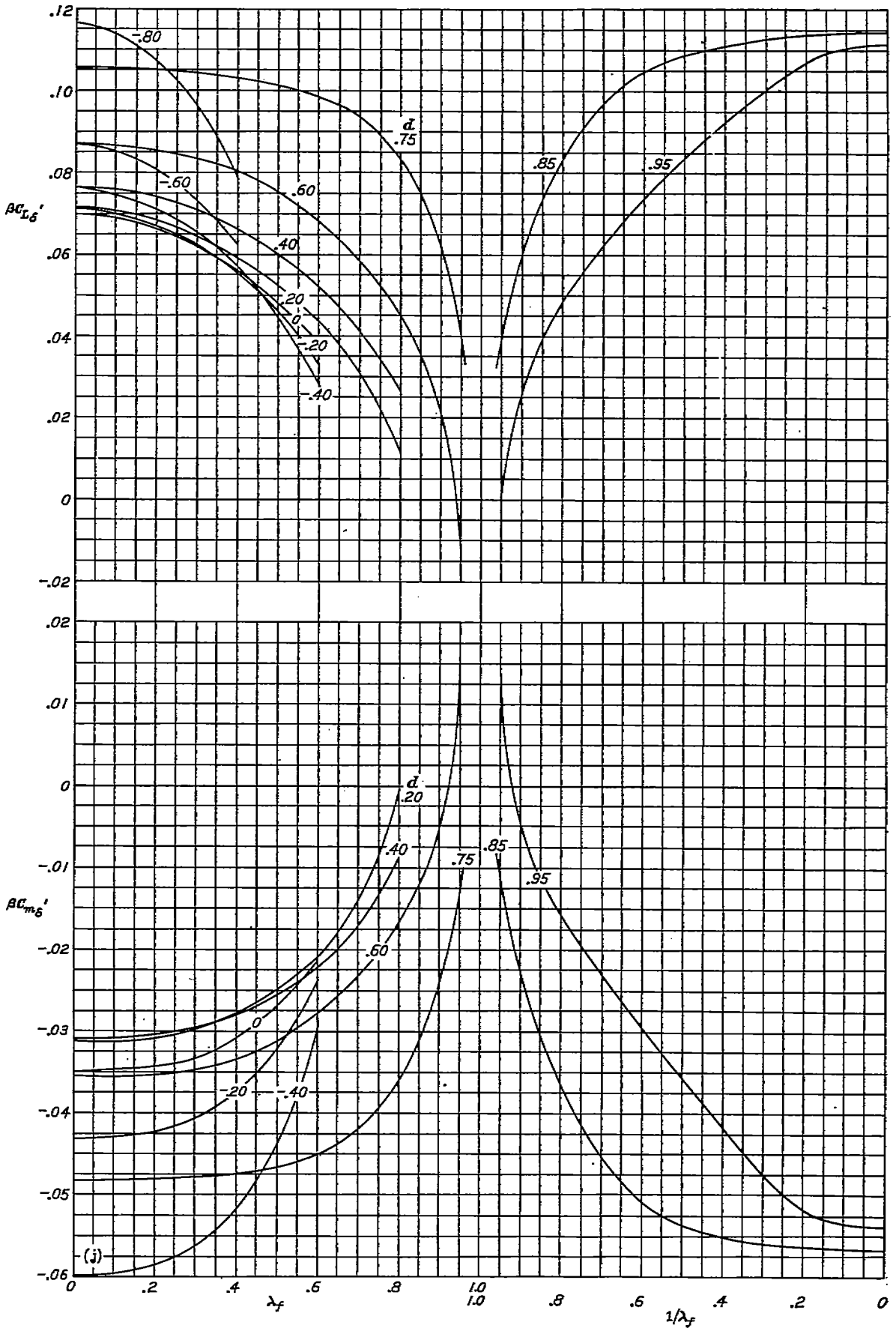

(j) Concluded.

FIGURE 4.—Continued.

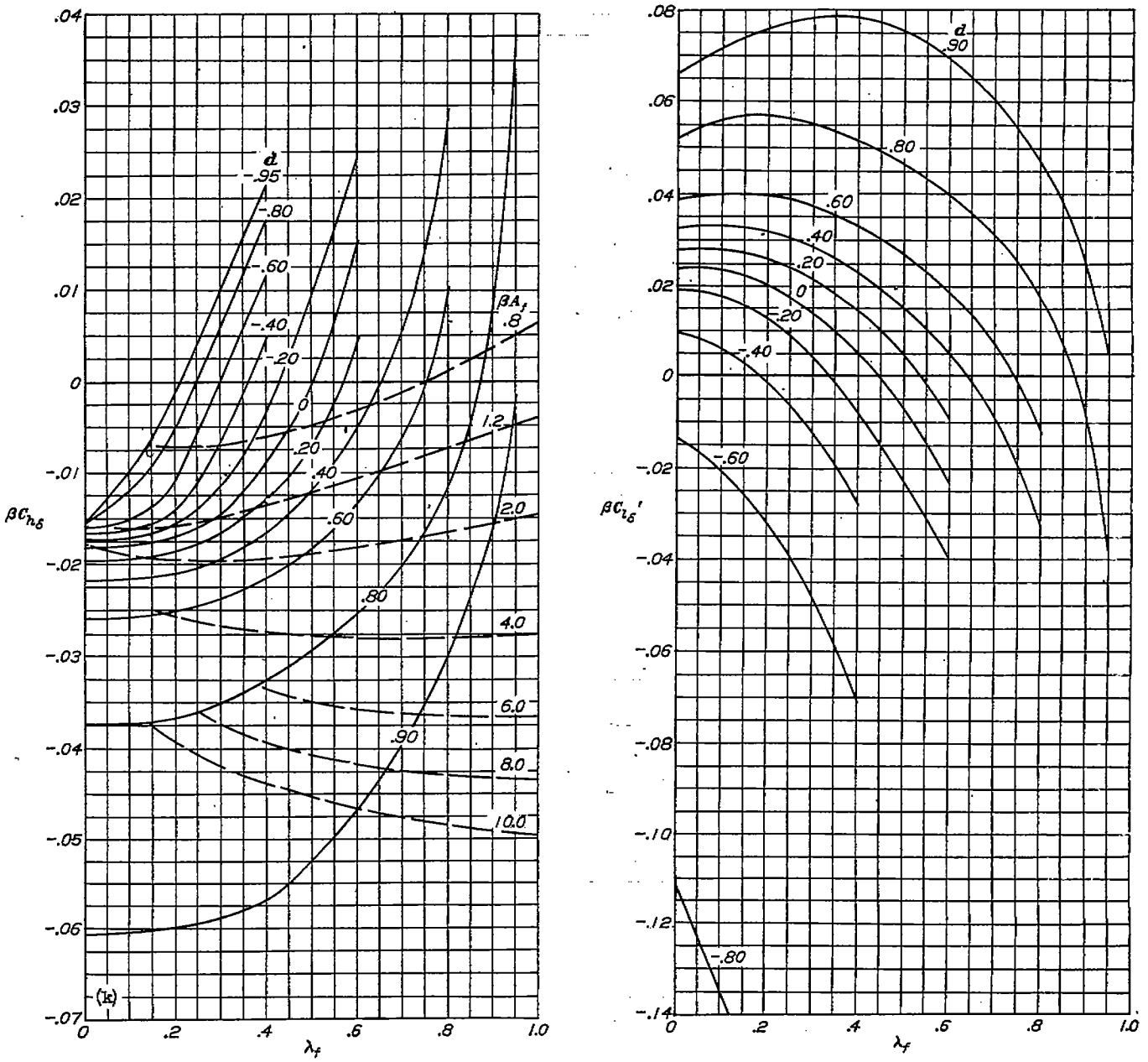

(k) $\frac{\tan \Lambda_{HL}}{\beta}=0.95$.

FIGURE 4.—Continued.

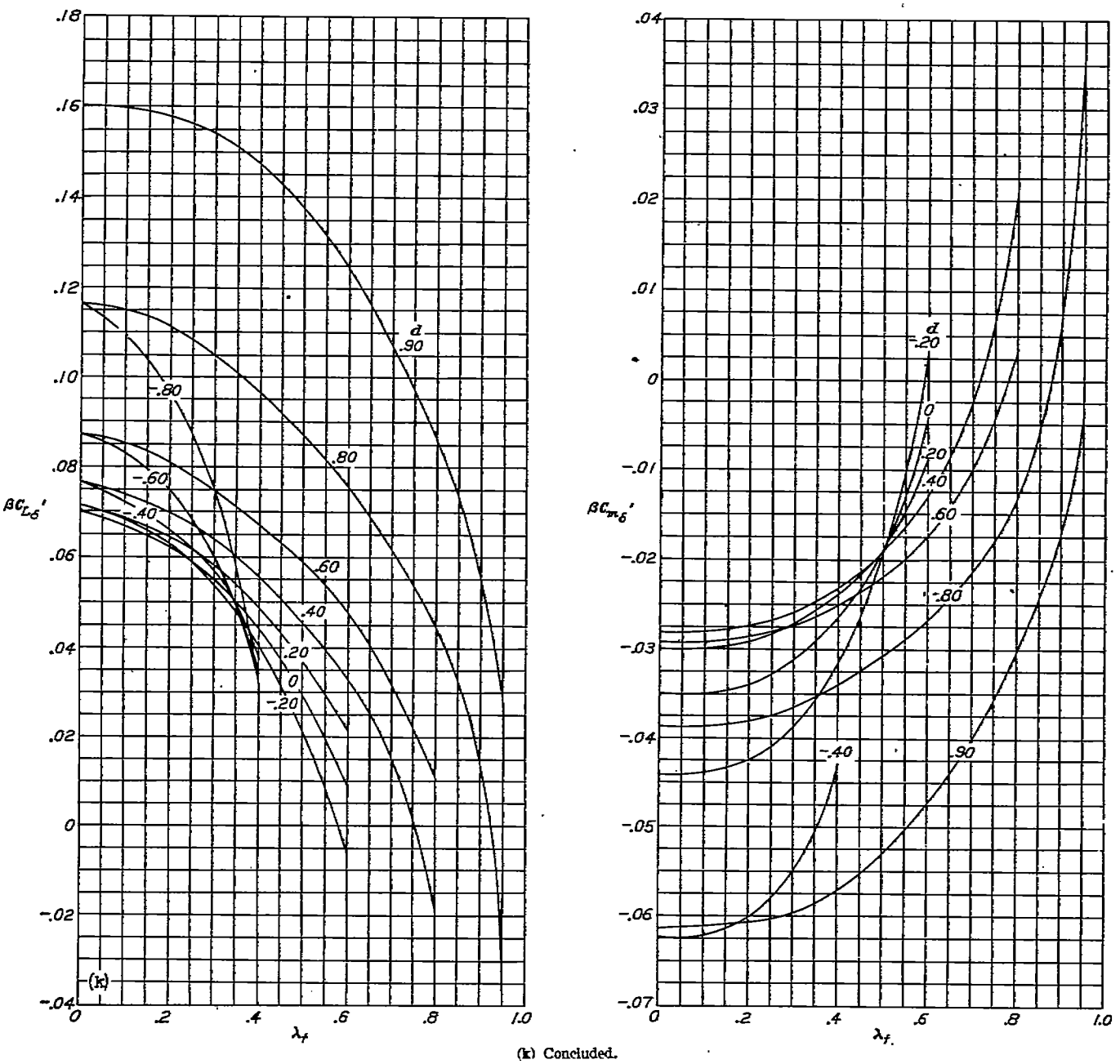

(k) Concluded.

FIGURE 4.—Concluded.

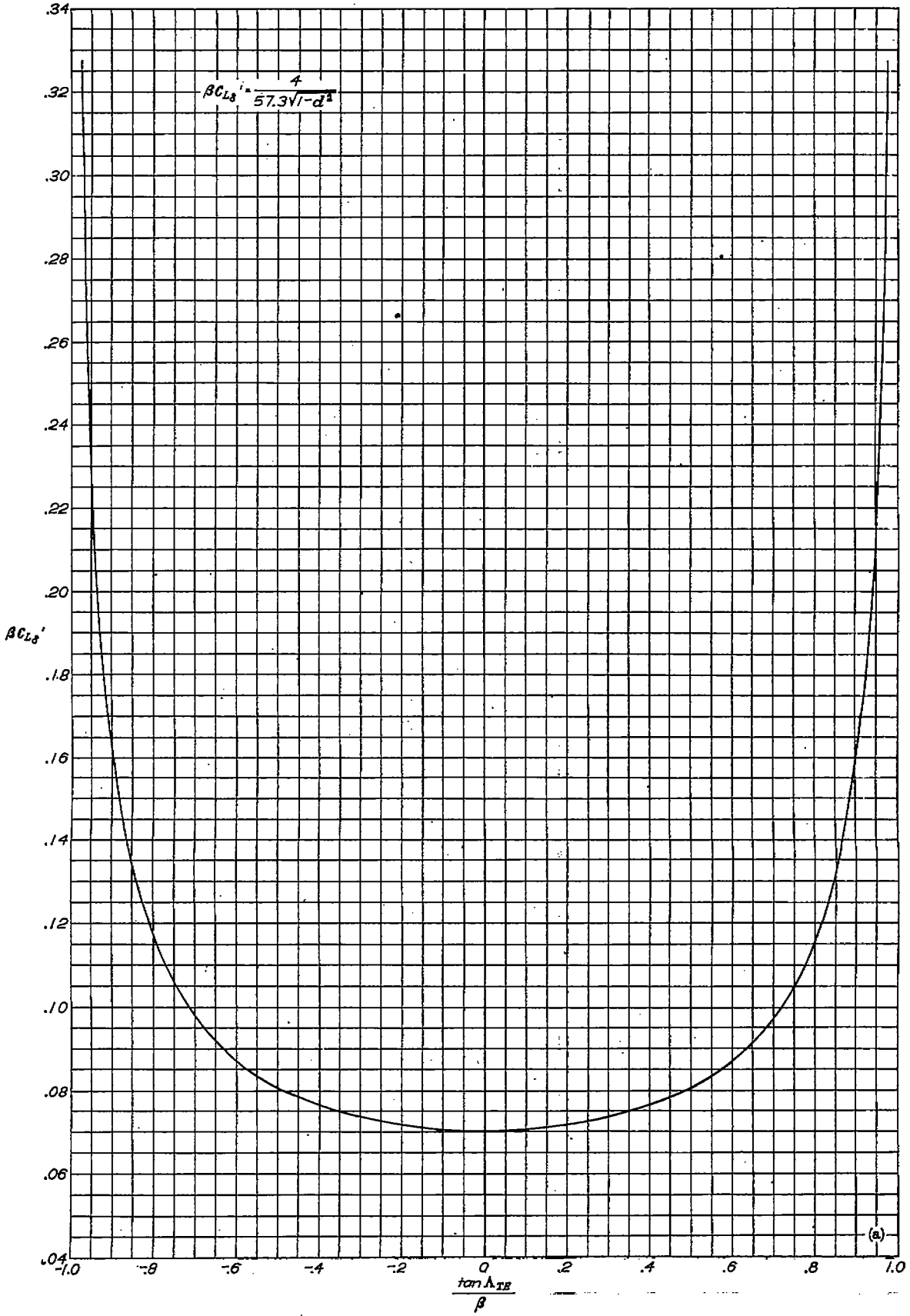

(a) Lift coefficient.

FIGURE 5.—Lift and pitching-moment parameters for deflected trailing-edge flaps located inboard from wing tip.

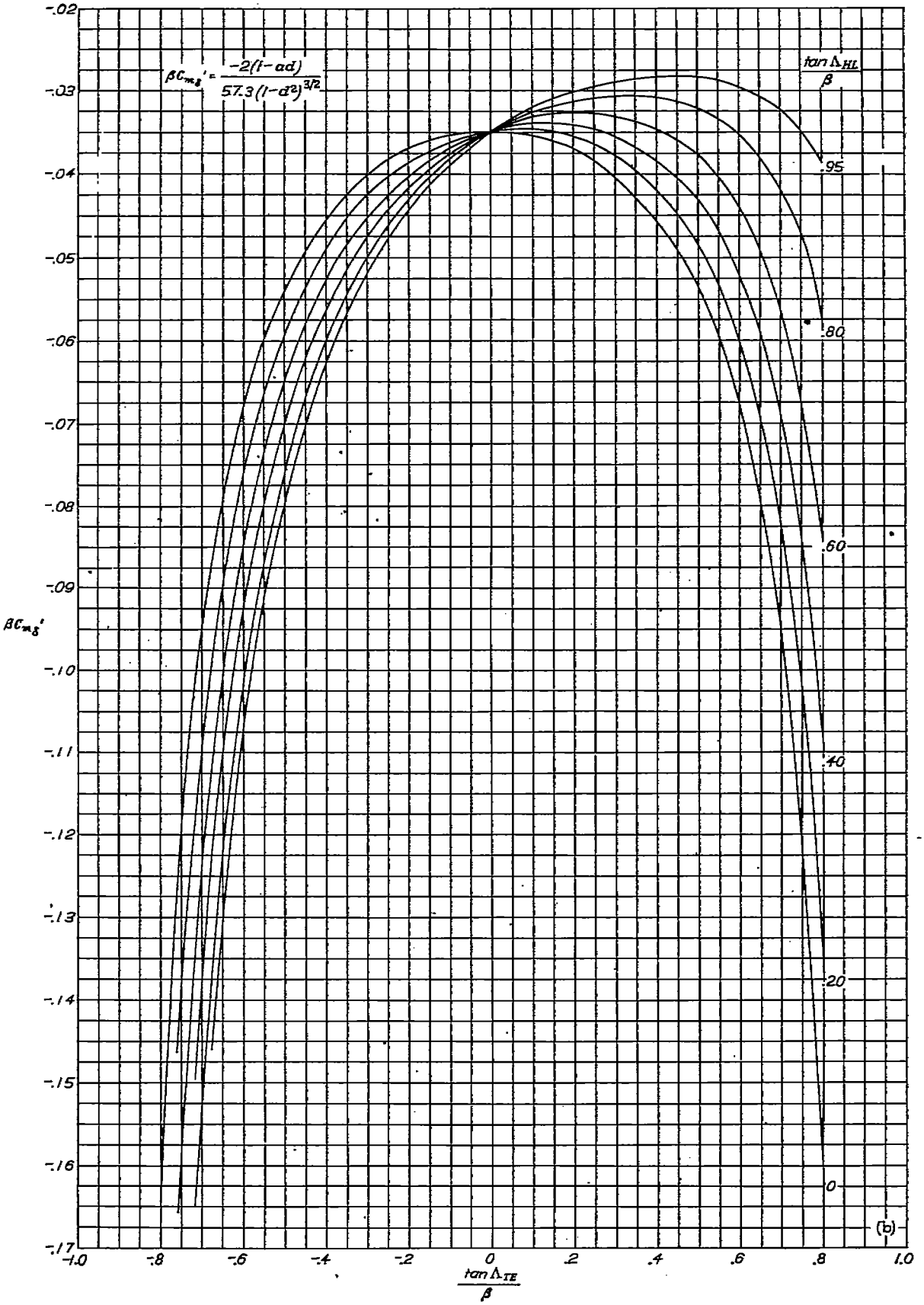

(b) Pitching-moment coefficient.

FIGURE 5.—Concluded.

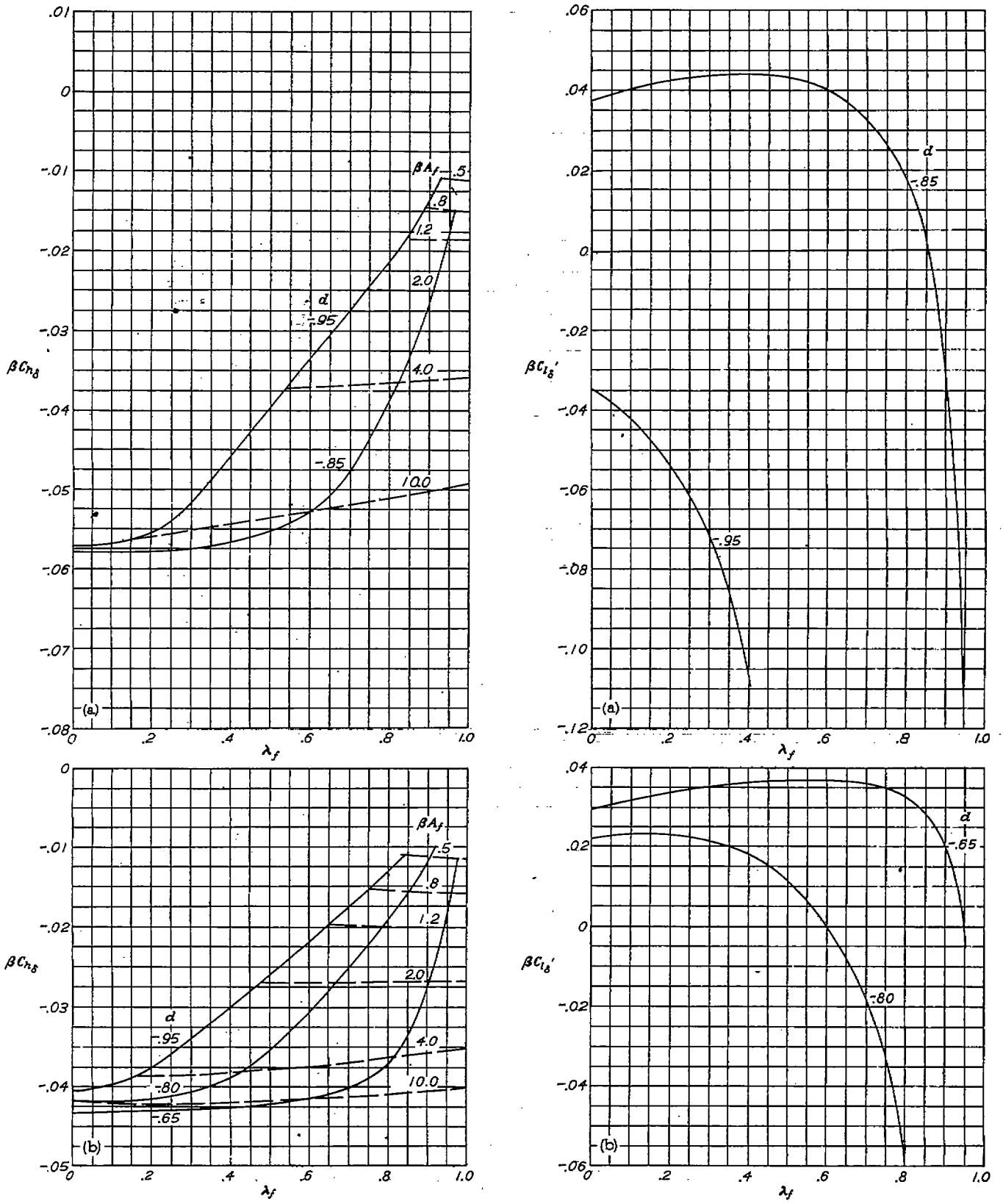

(a) $\frac{\tan \Lambda_{HL}}{\beta} = -0.30$.

(b) $\frac{\tan \Lambda_{HL}}{\beta} = -0.60$.

FIGURE 6.—Hinge-moment and rolling-moment parameters for control surfaces located inboard from wing tip.

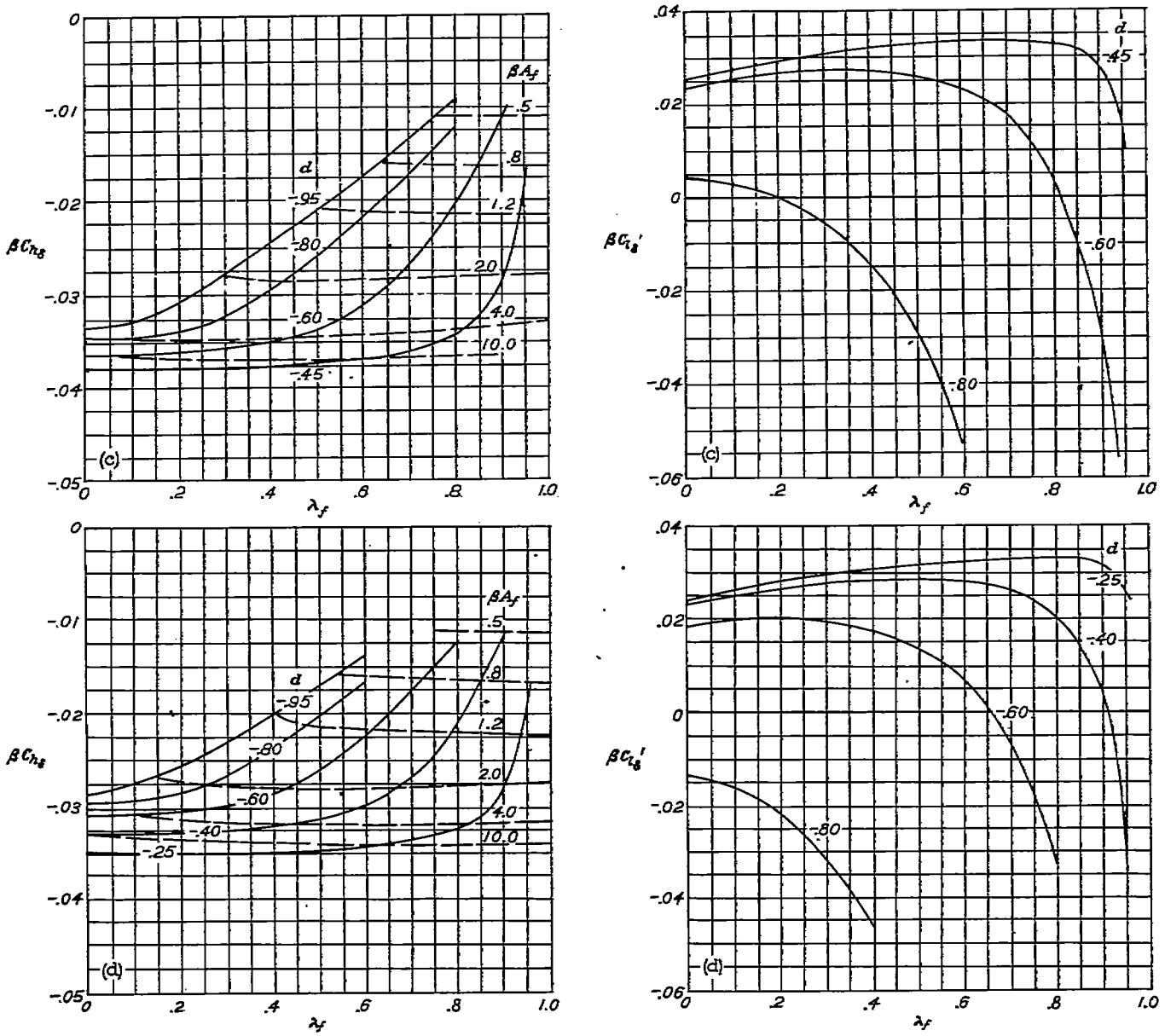

(c) $\frac{\tan \Lambda_{HL}}{\beta} = -0.40$.

(d) $\frac{\tan \Lambda_{HL}}{\beta} = -0.20$.

FIGURE 6.—Continued.

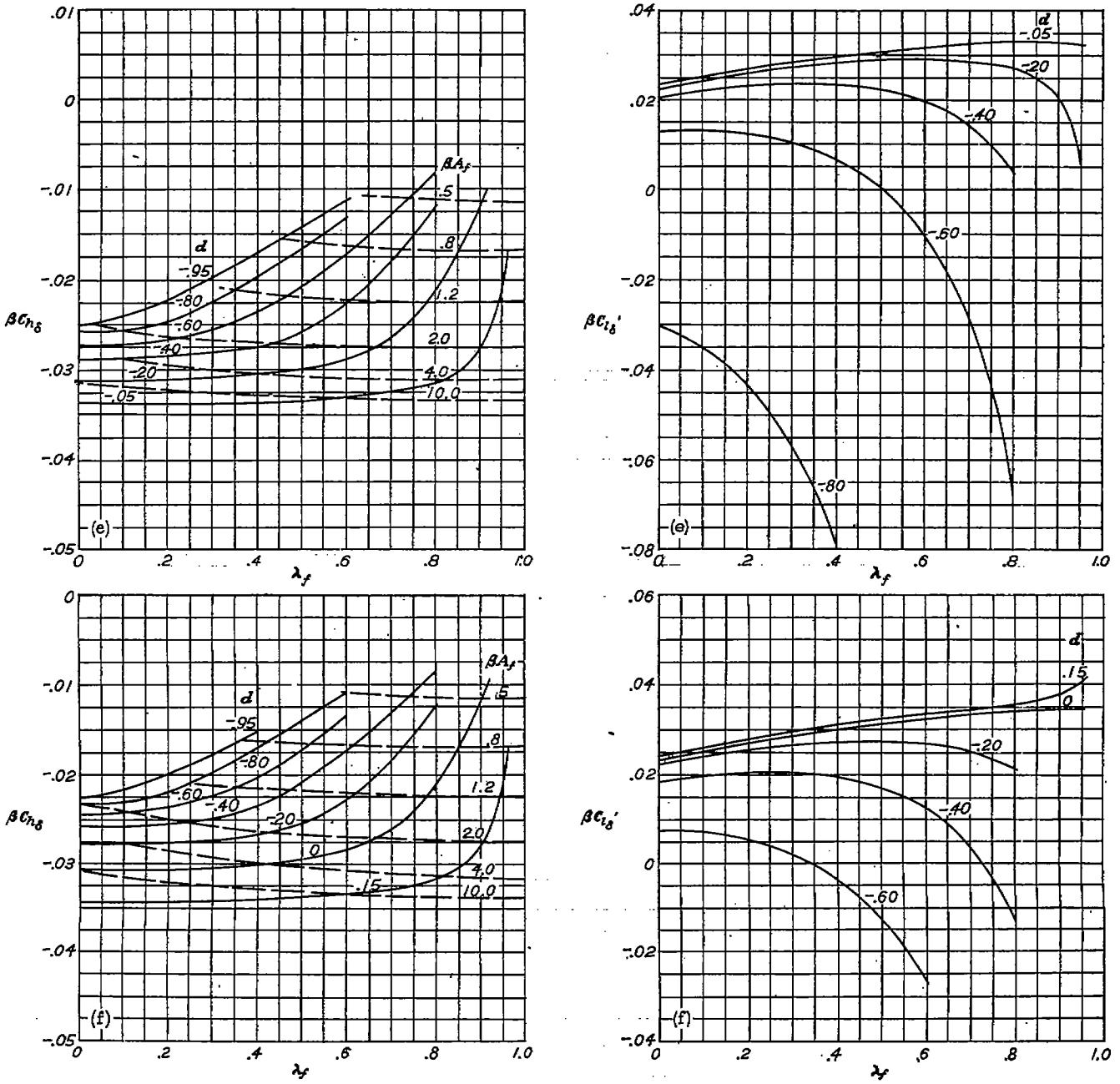

(e) $\frac{\tan \Lambda_{HL}}{\beta}=0.$

(f) $\frac{\tan \Lambda_{HL}}{\beta}=0.20.$

FIGURE 6.—Continued.

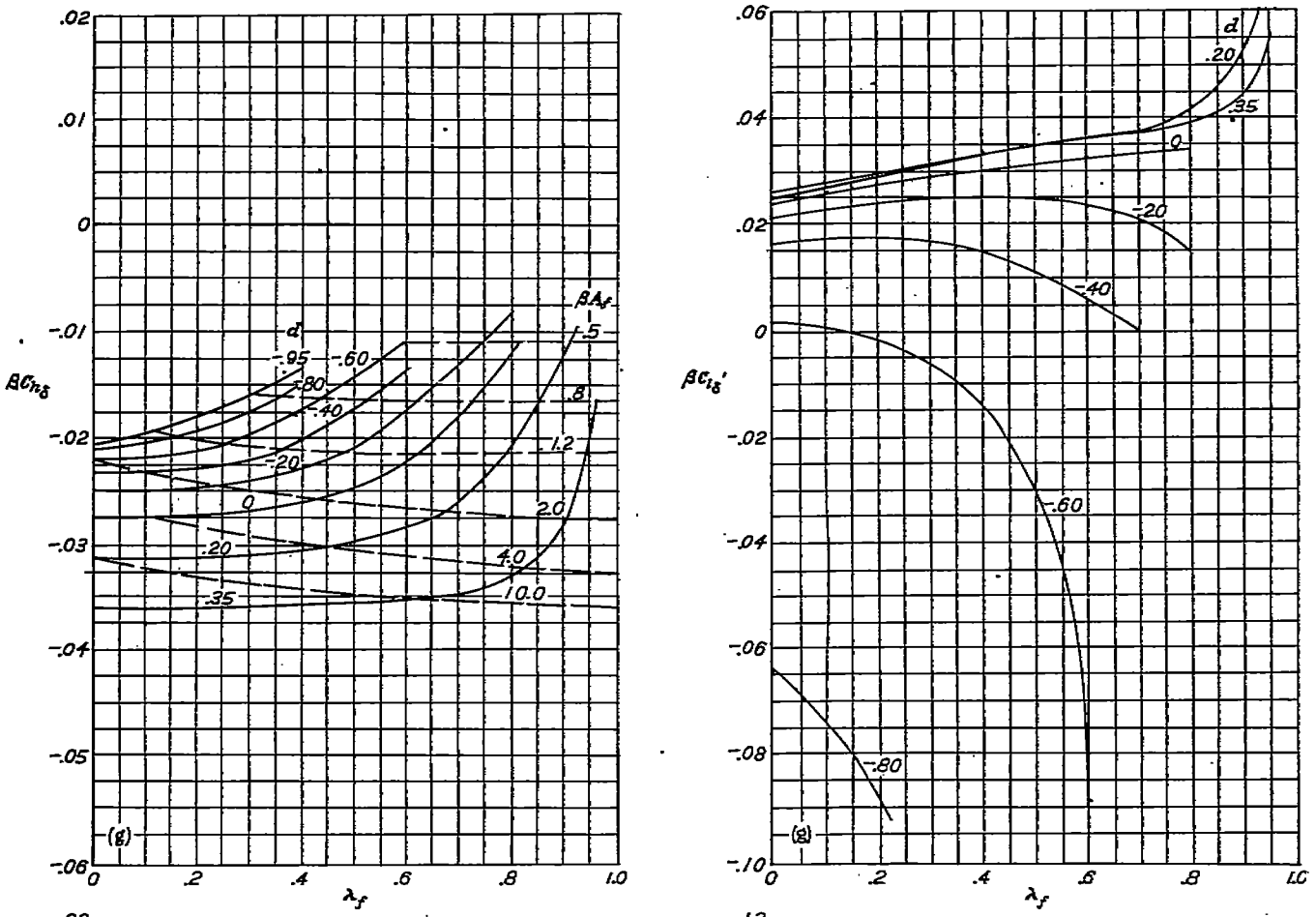

(g) $\frac{\tan \Lambda_{HL}}{\beta}=0.40$.

(h) $\frac{\tan \Lambda_{HL}}{\beta}=0.60$.

FIGURE 6.—Continued.

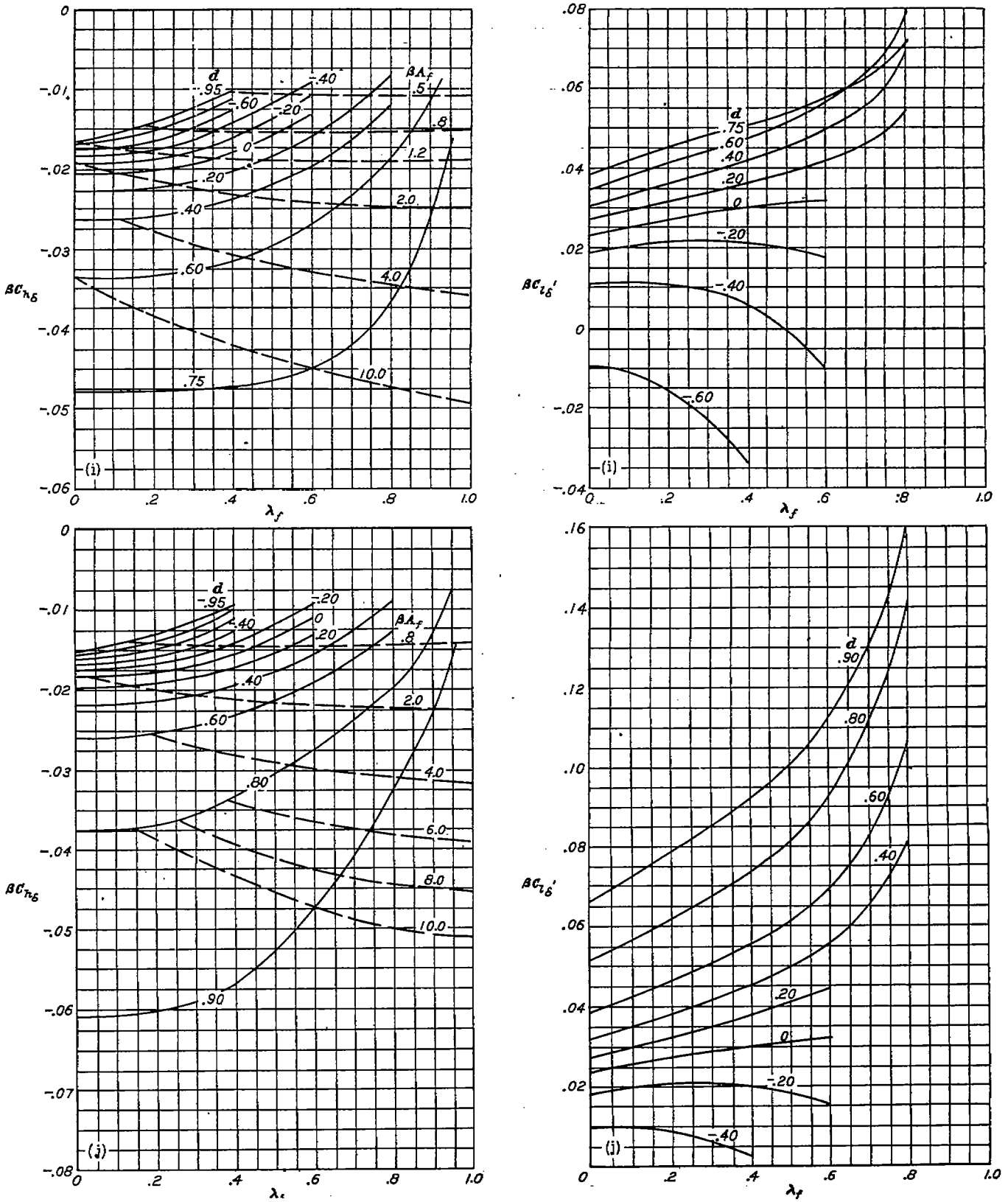

(i) $\frac{\tan \Lambda_{HL}}{\beta}$=0.80.

(j) $\frac{\tan \Lambda_{HL}}{\beta}$=0.95.

FIGURE 6.—Concluded.

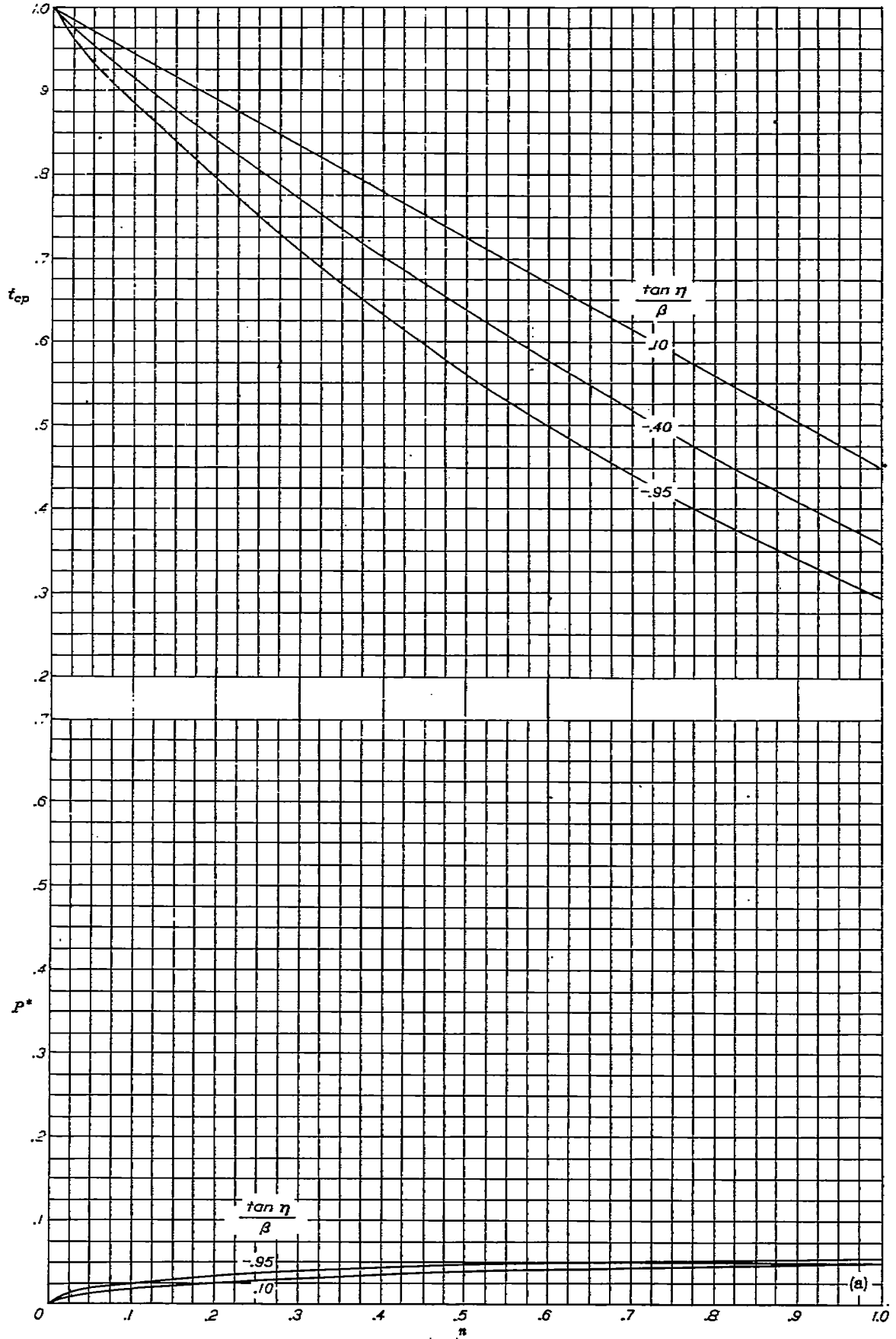

(a) $\frac{\tan \Lambda}{\beta}=0.10$.

FIGURE 7.—Loading distribution along inclined sections intersecting the wing-root Mach cone.

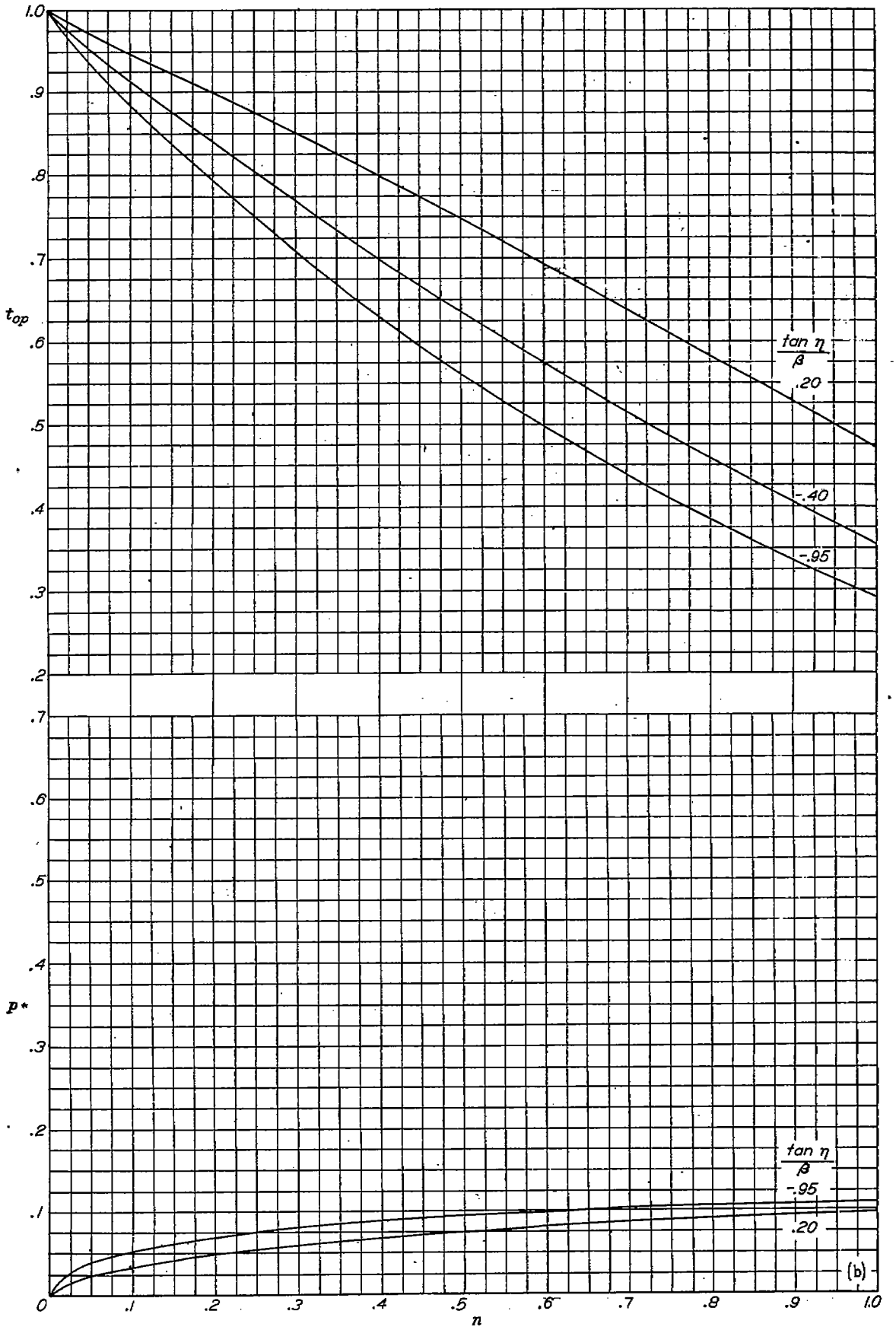

(b) $\frac{\tan \Lambda}{\beta}=0.20$.

FIGURE 7.—Continued.

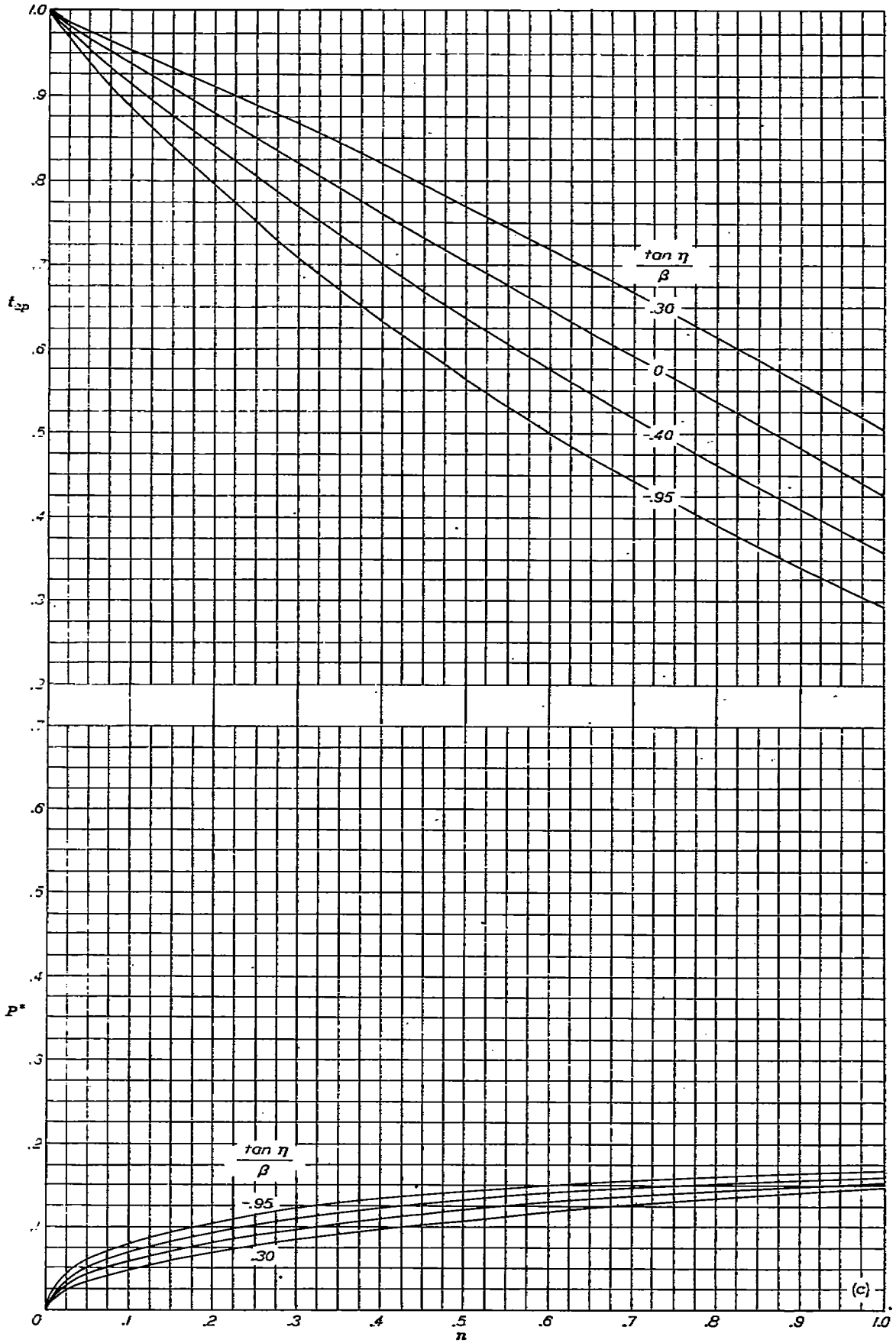

(c) $\frac{\tan \Lambda}{\beta}$=0.30.

FIGURE 7.—Continued.

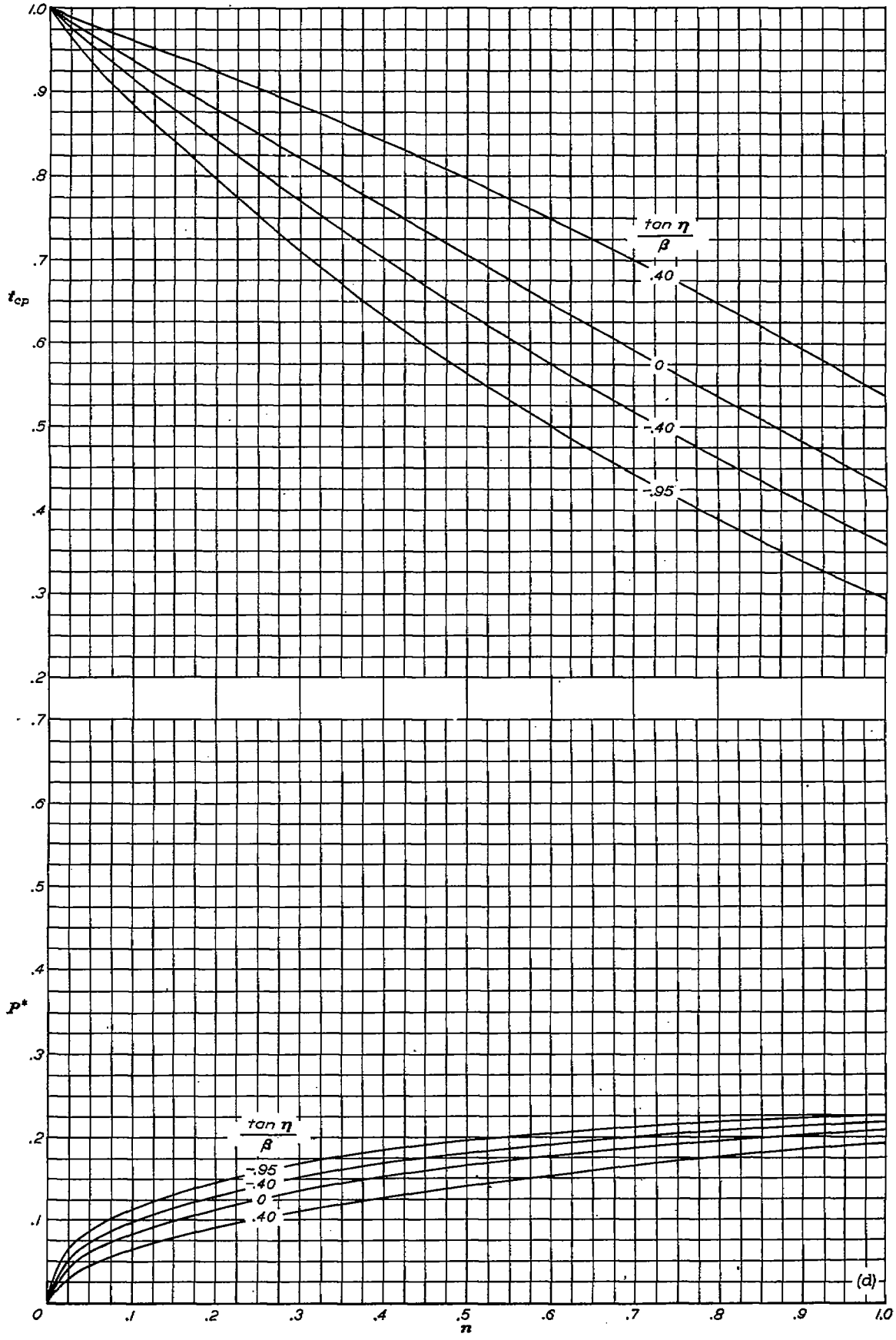

(d) $\frac{\tan \Lambda}{\beta}=0.40$.

FIGURE 7.—Continued.

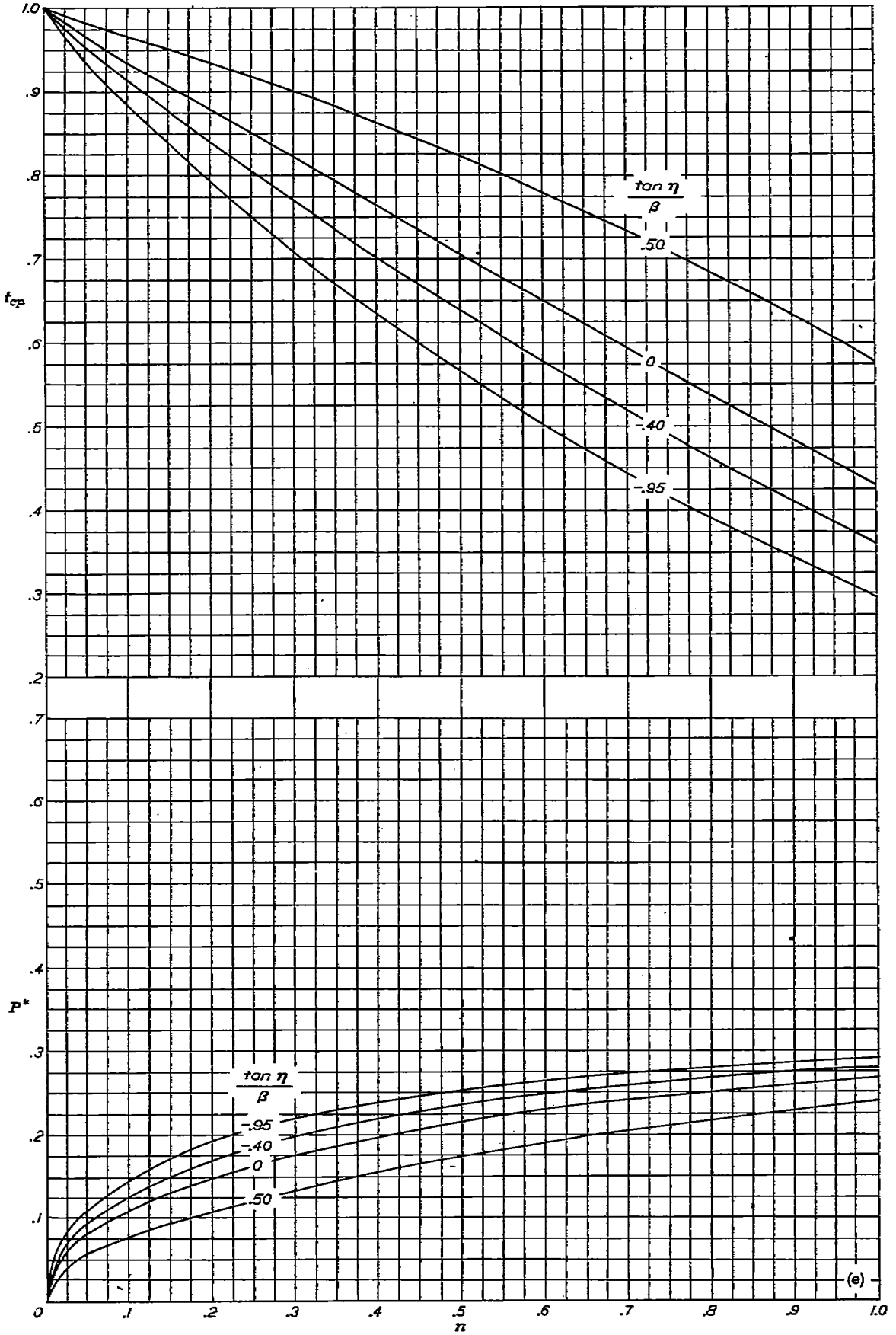

(e) $\frac{\tan \Lambda}{\beta}=0.50$.

FIGURE 7.—Continued.

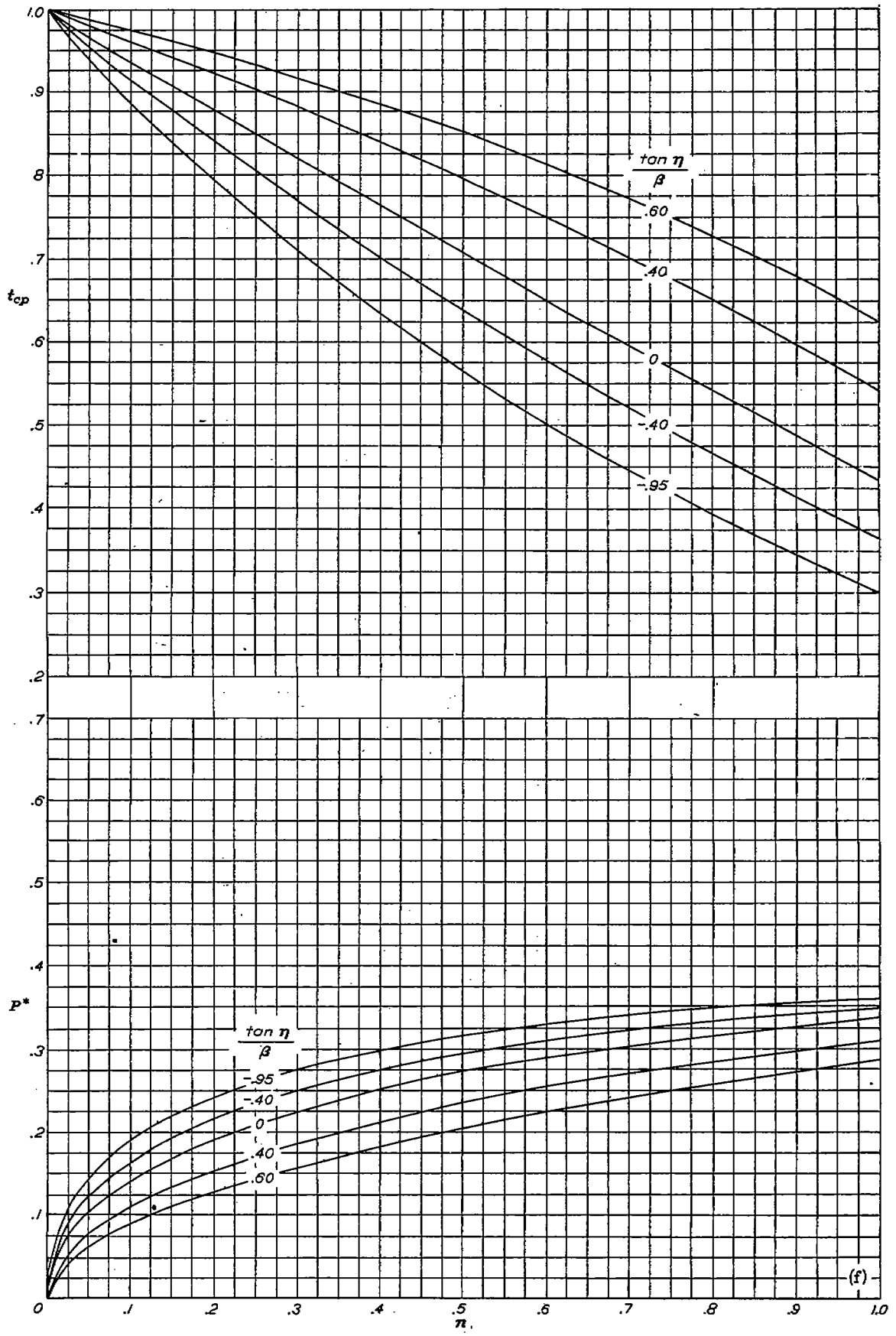

(f) $\frac{\tan \Lambda}{\beta}$=0.60.

FIGURE 7—Continued

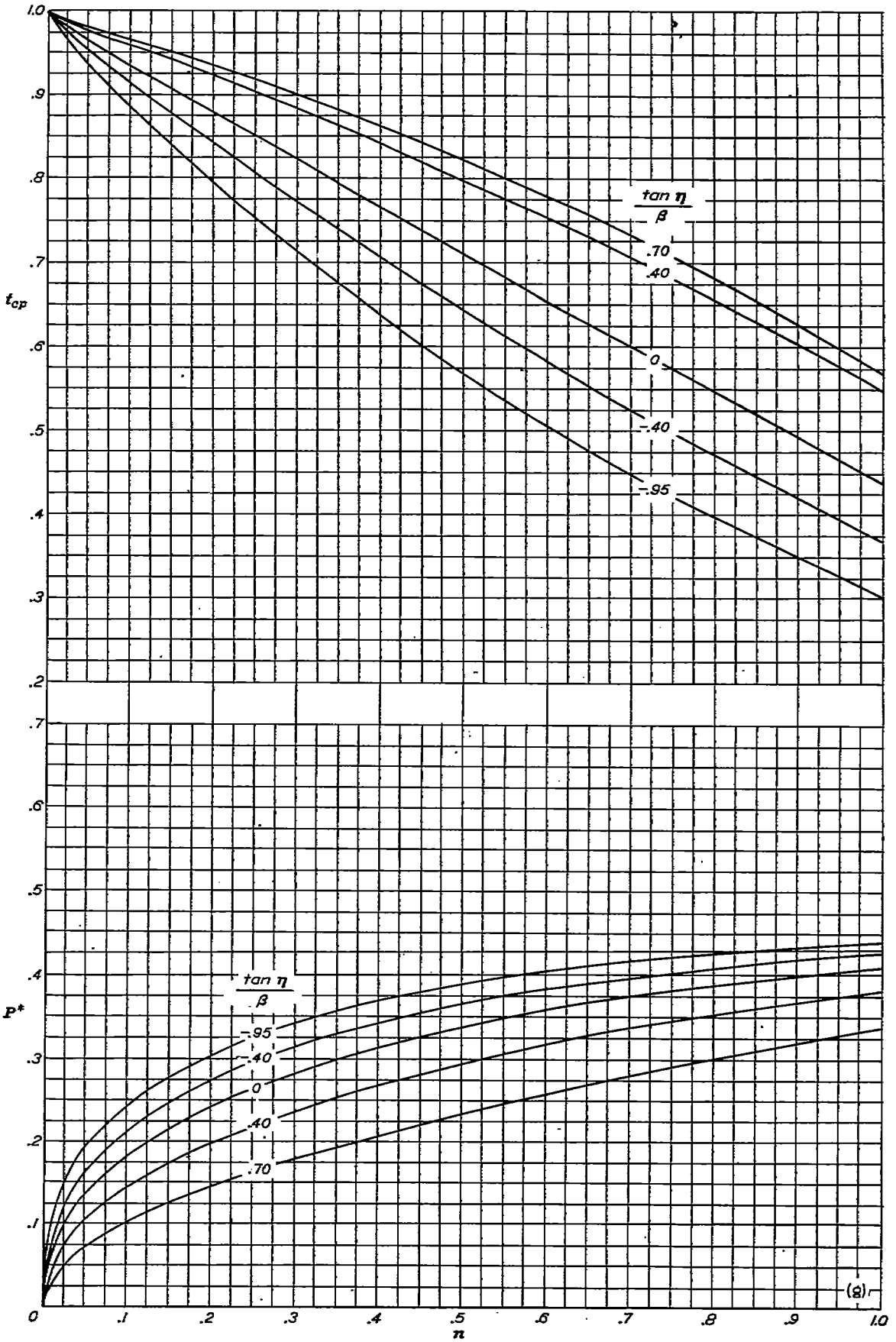

(g) $\frac{\tan \Lambda}{\beta}=0.70$.

FIGURE 7.—Continued.

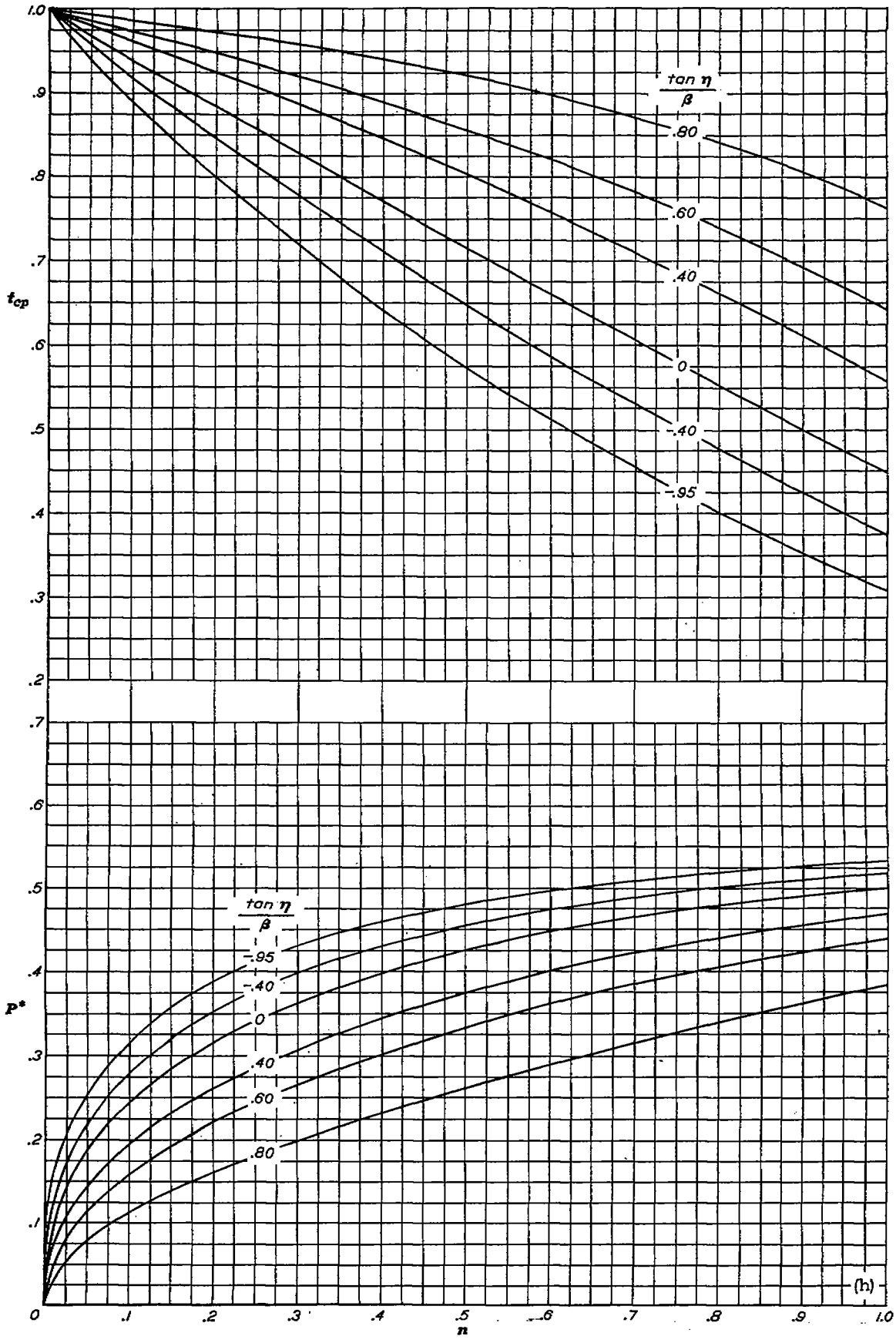

(h) $\frac{\tan \Lambda}{\beta}=0.80$;

FIGURE 7.—Continued.

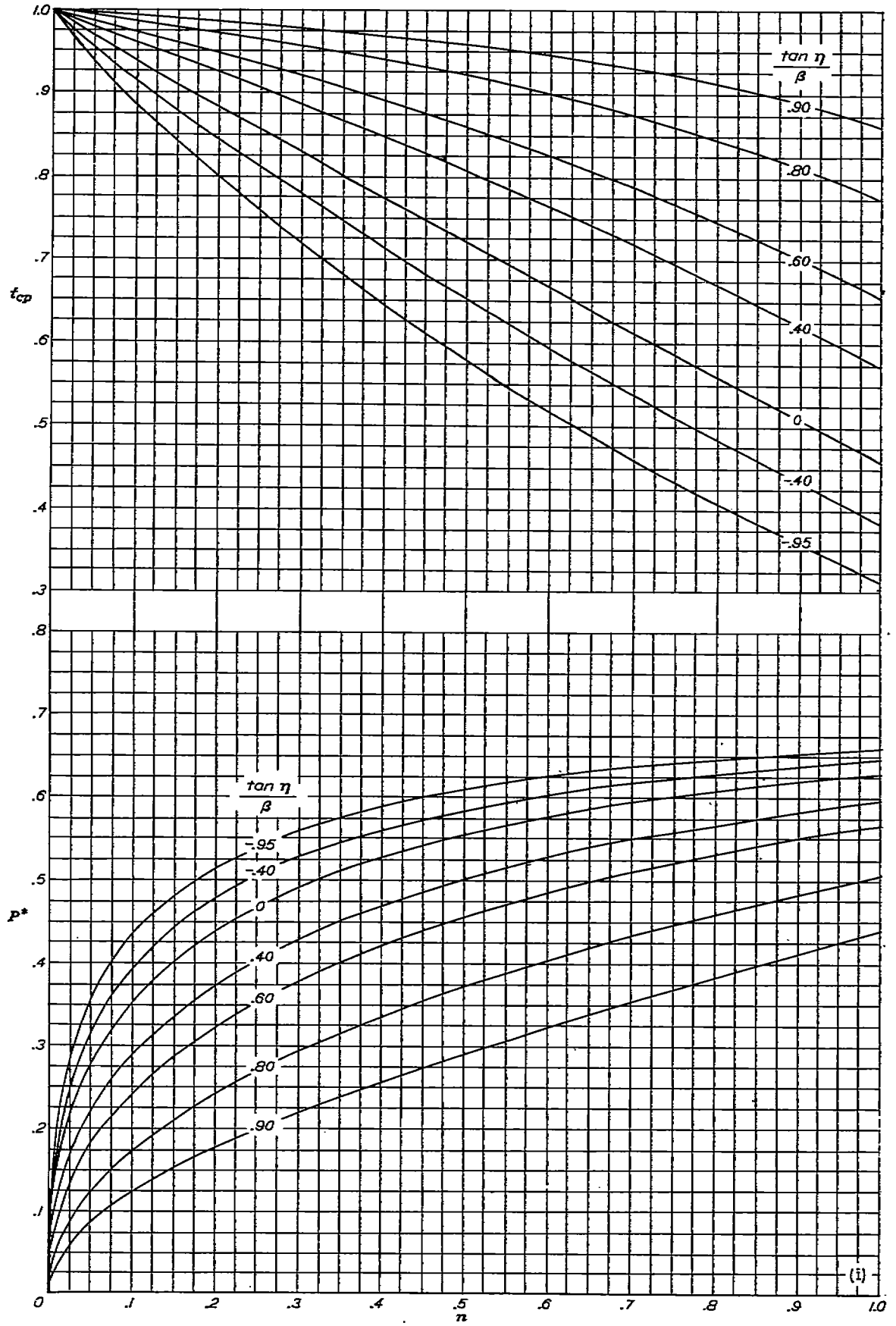

(i) $\frac{\tan \Lambda}{\beta}$=0.90.

FIGURE 7.—Continued.

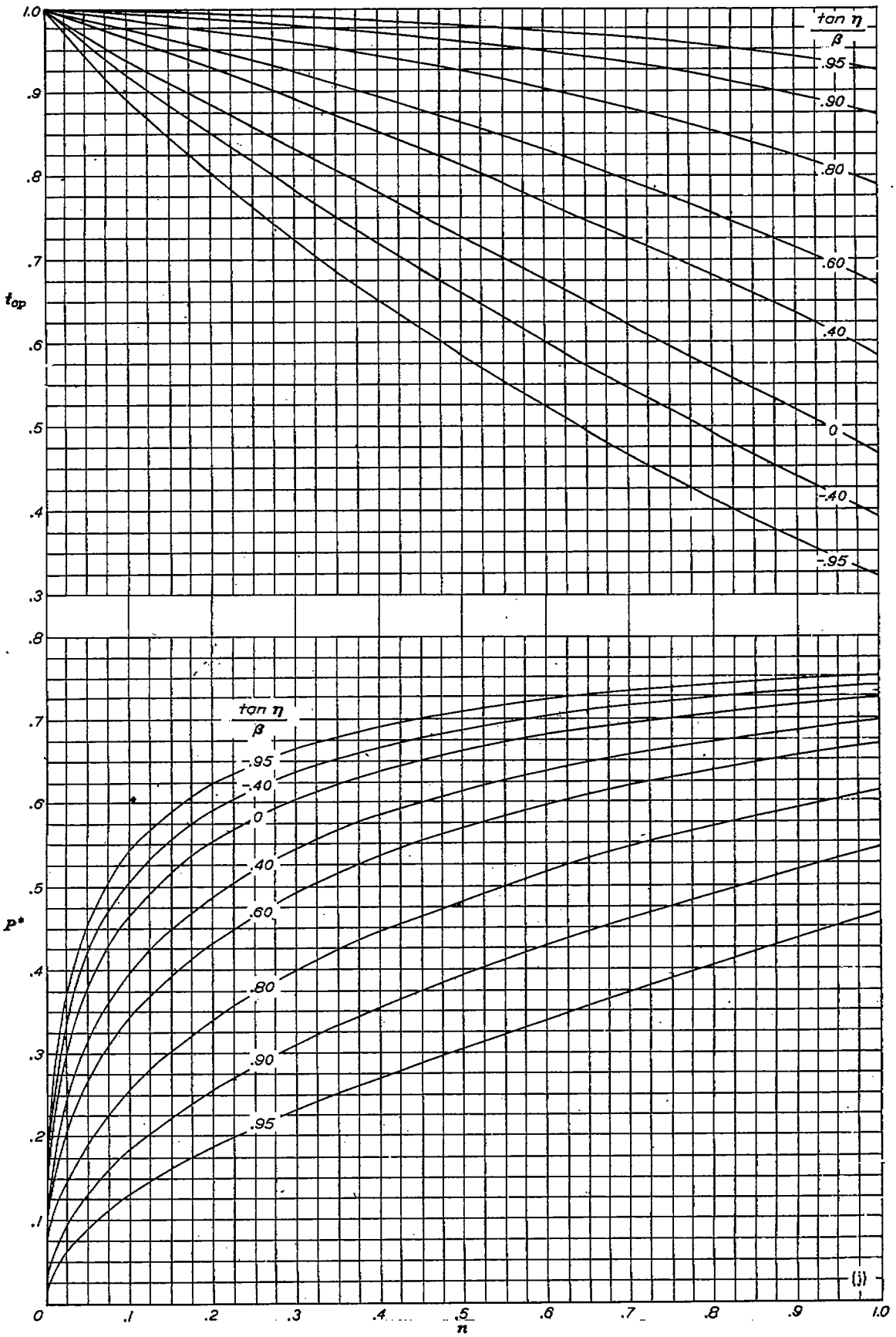

(j) $\frac{\tan \Lambda}{\beta}=0.95$.

FIGURE 7.—Concluded.

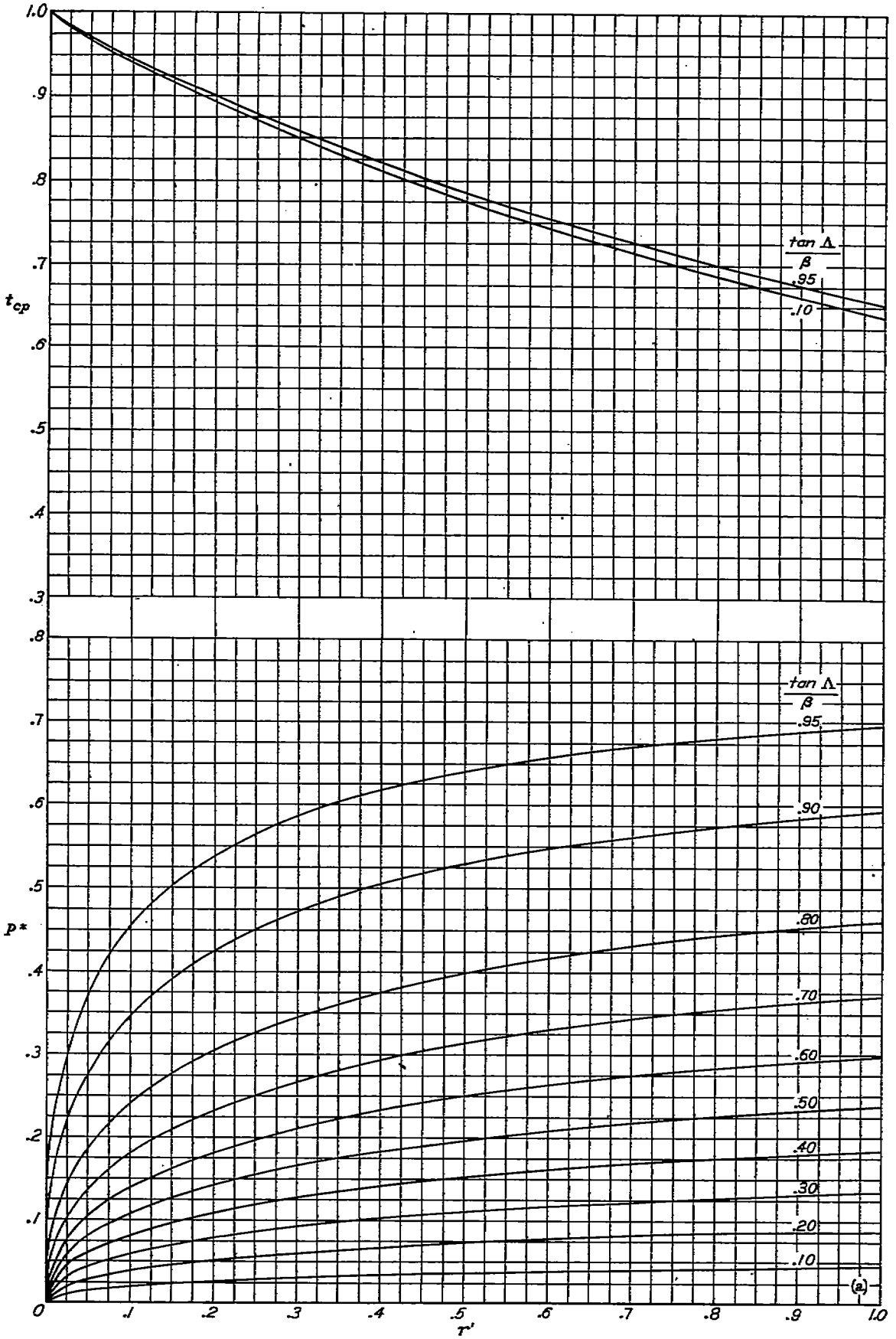

(a) $r'=0$ to 1.0.

FIGURE 8.—Loading distribution along streamwise sections intersecting wing-root Mach cone.

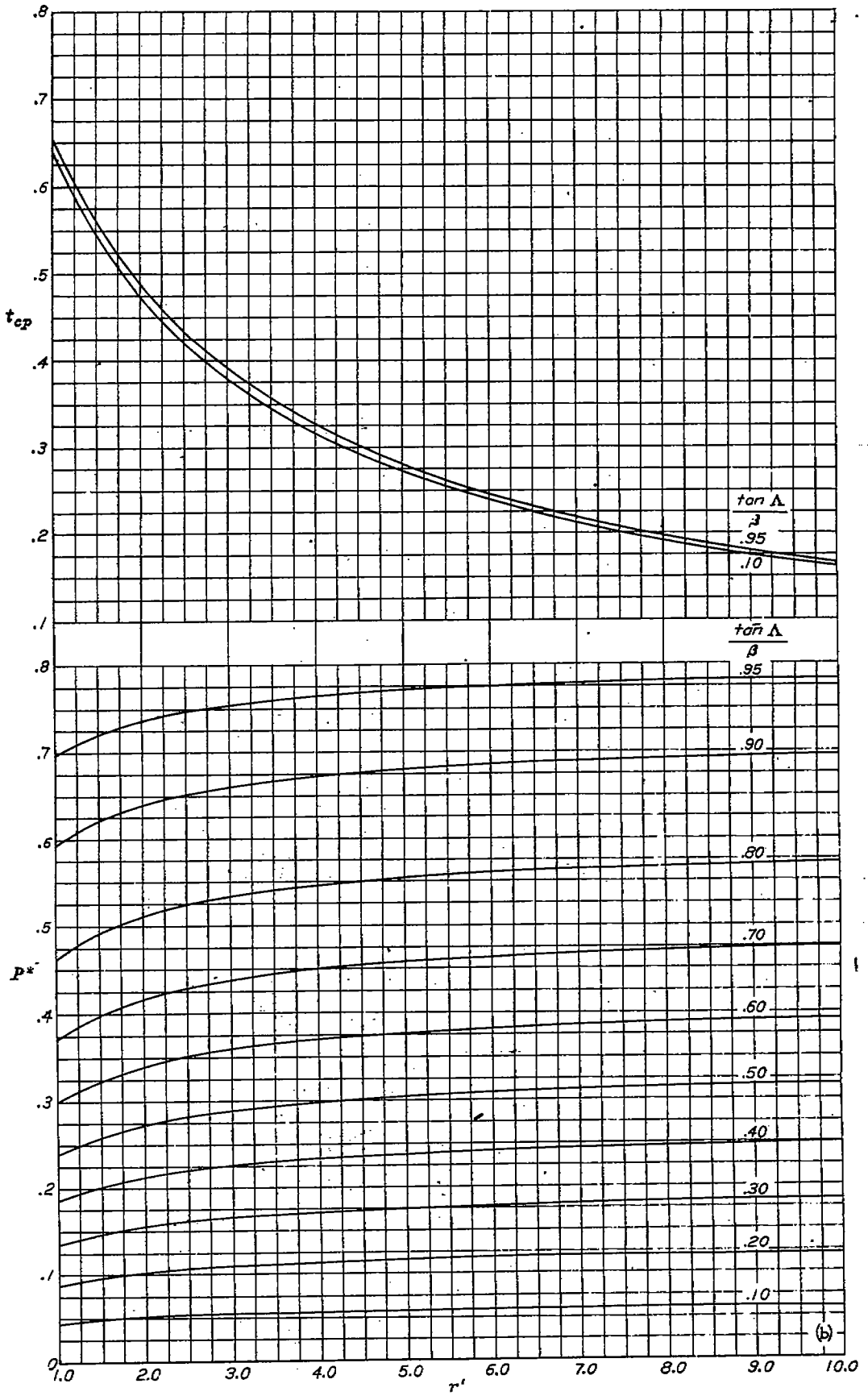

(b) $r'=1.0$ to 10.0.

FIGURE 8.—Concluded.

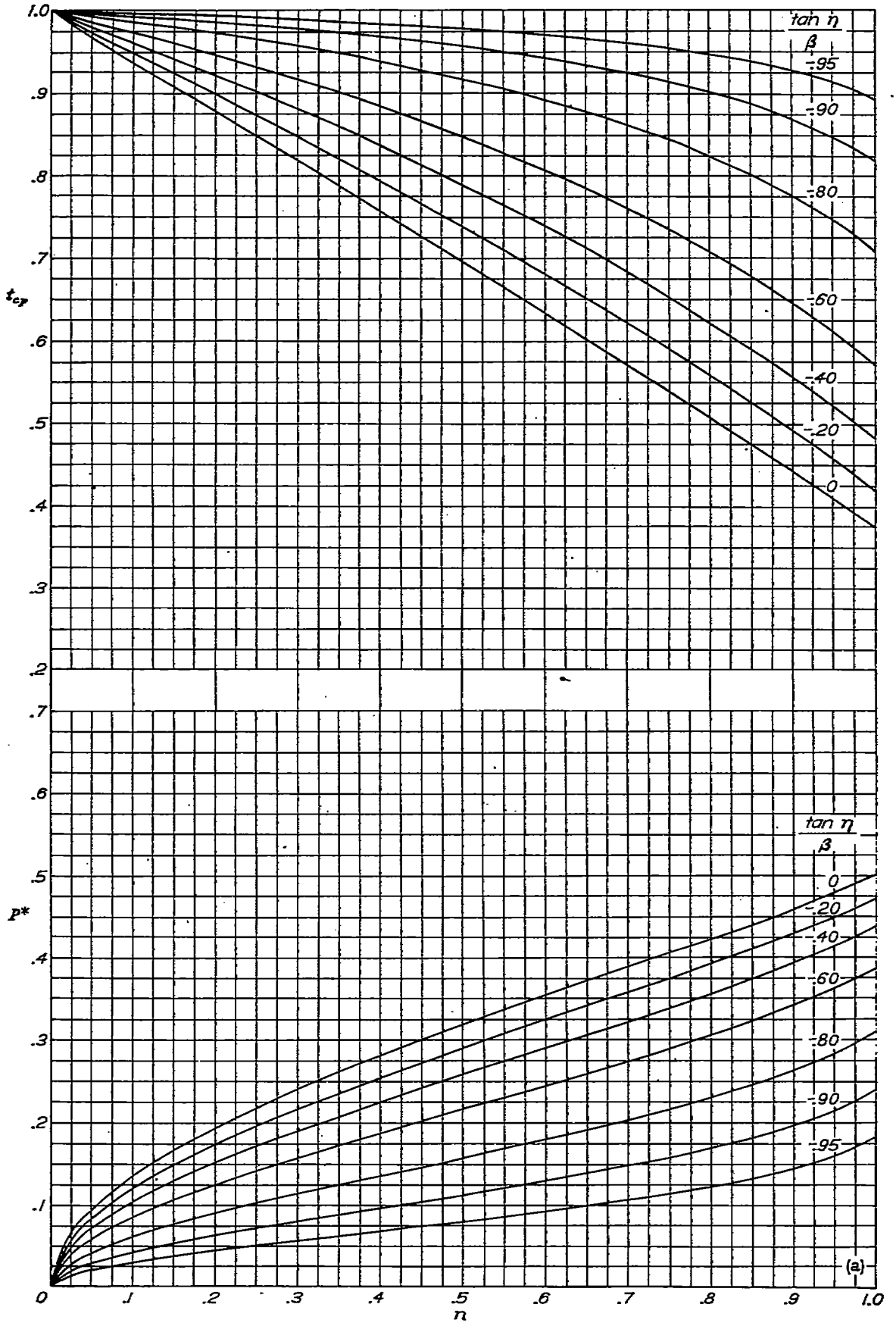

(a) $\frac{\tan \Lambda}{\beta} = 0$.

FIGURE 9.—Loading distribution along inclined sections intersecting wing-tip Mach cone.

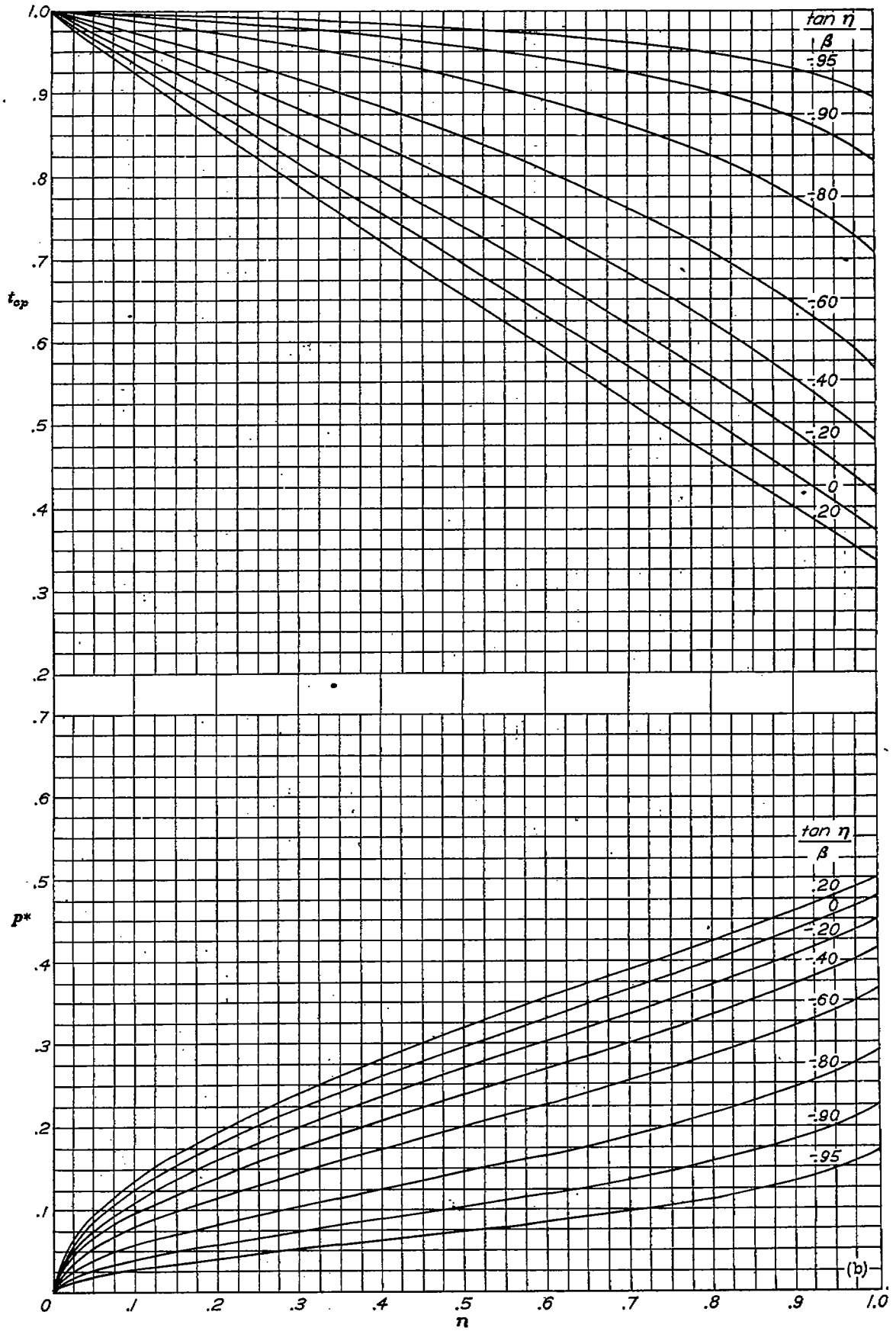

(b) $\frac{\tan \Lambda}{\beta}=0.20$.

FIGURE 9.—Continued.

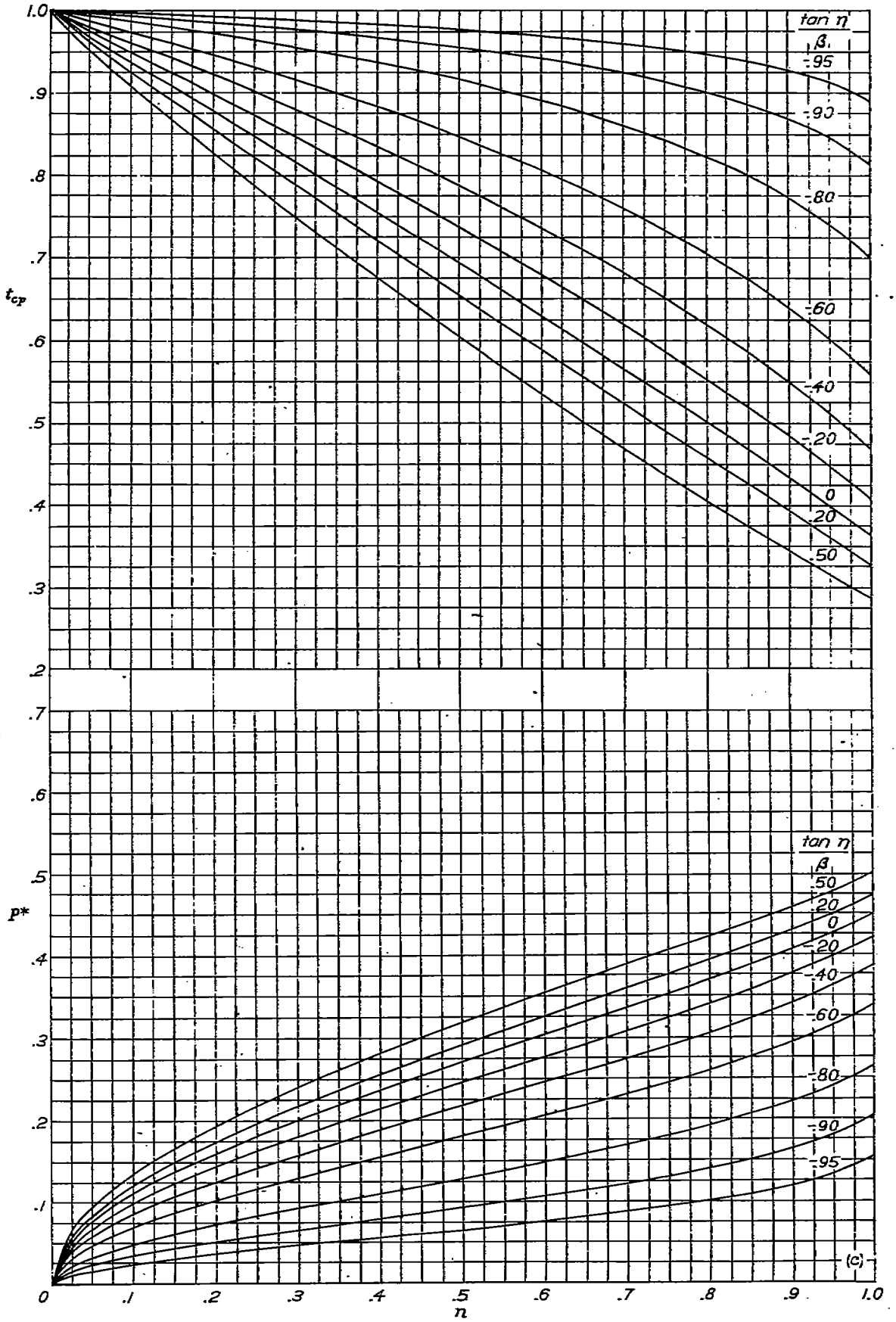

(c) $\frac{\tan \Lambda}{\beta}=0.50$.

FIGURE 9.—Continued.

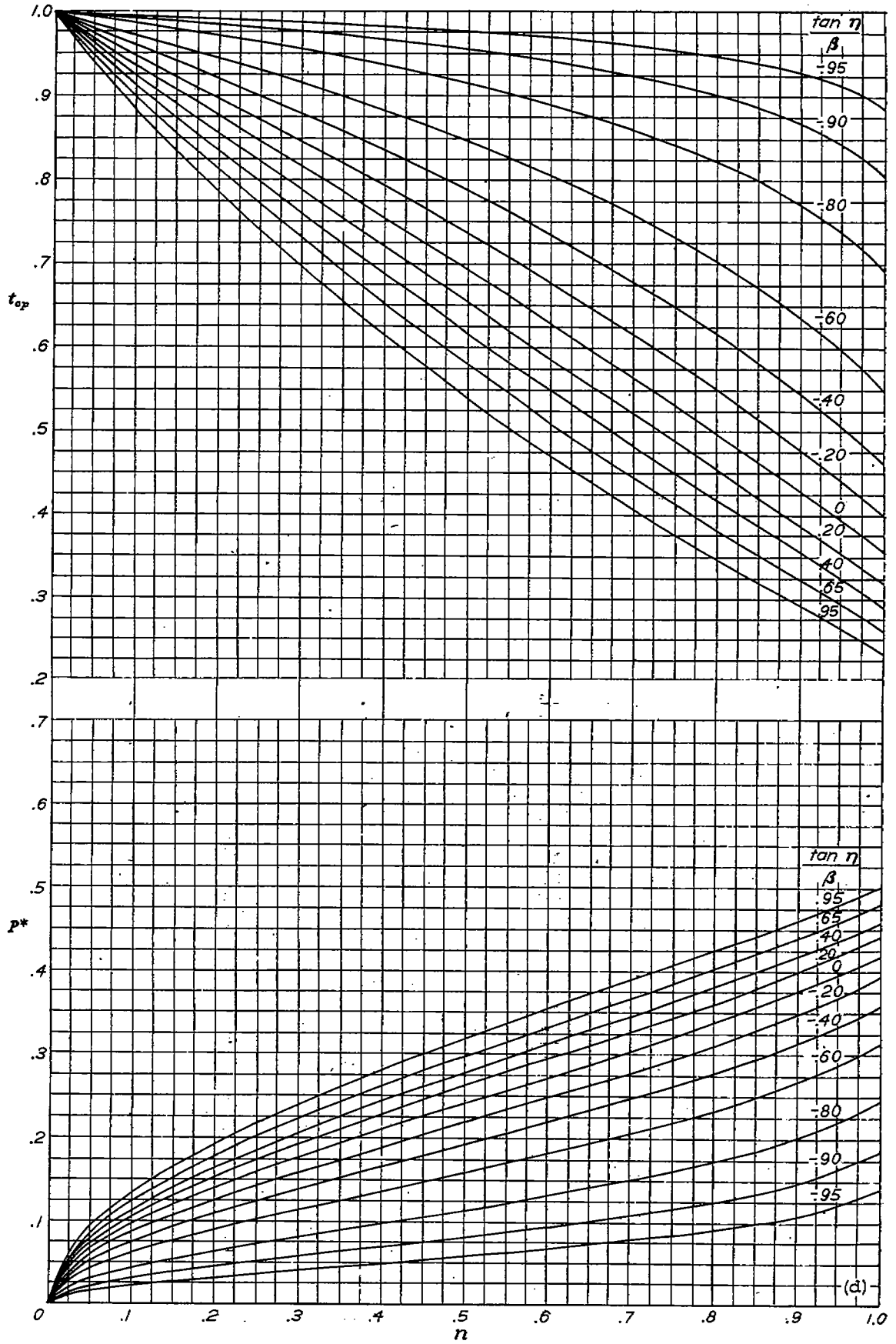

(d) $\frac{\tan \Lambda}{\beta} = 0.95$.

FIGURE 9.—Concluded

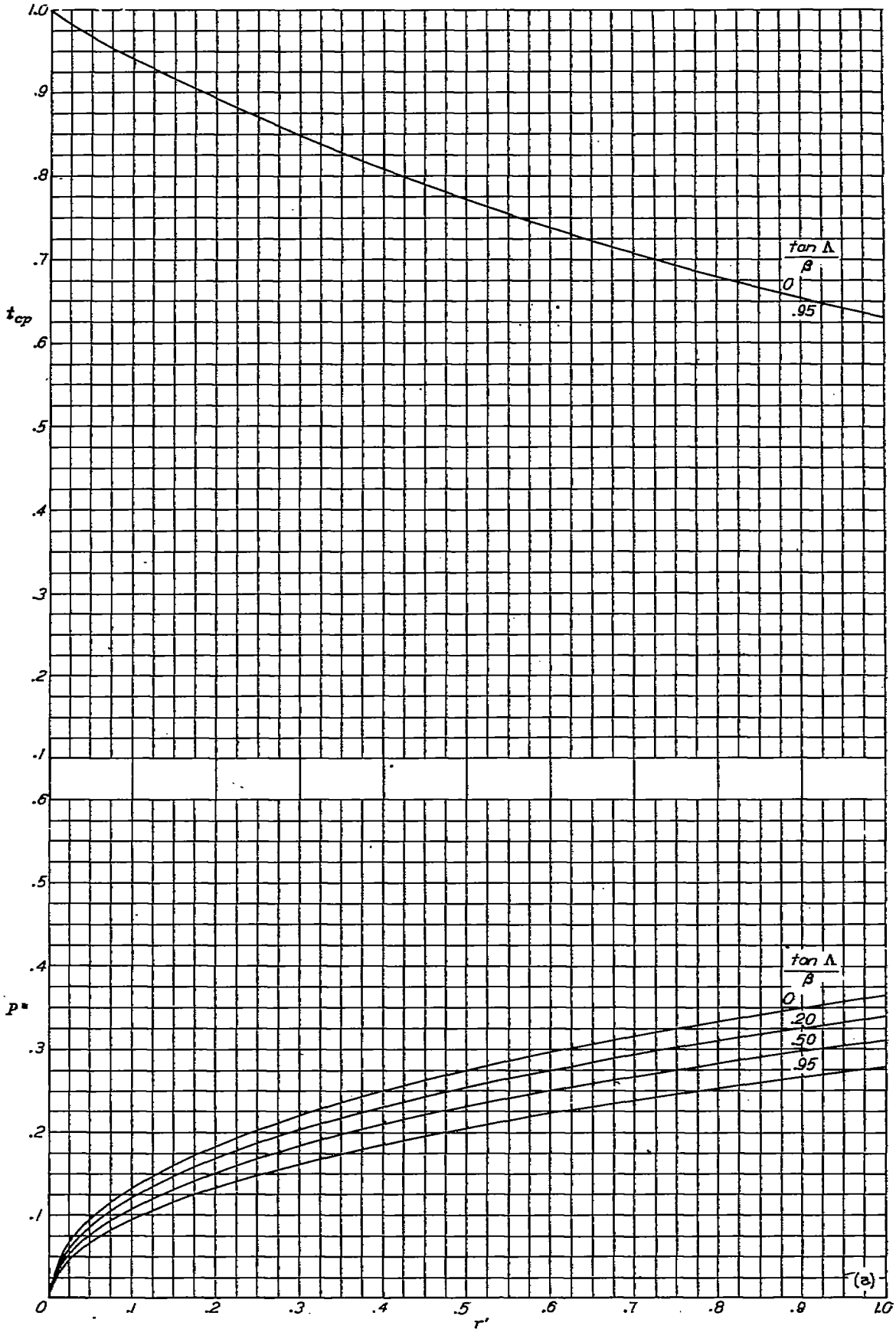

(a) $r'=0$ to 1.0.

FIGURE 10.—Loading distribution along streamwise sections intersecting wing-tip Mach cone.

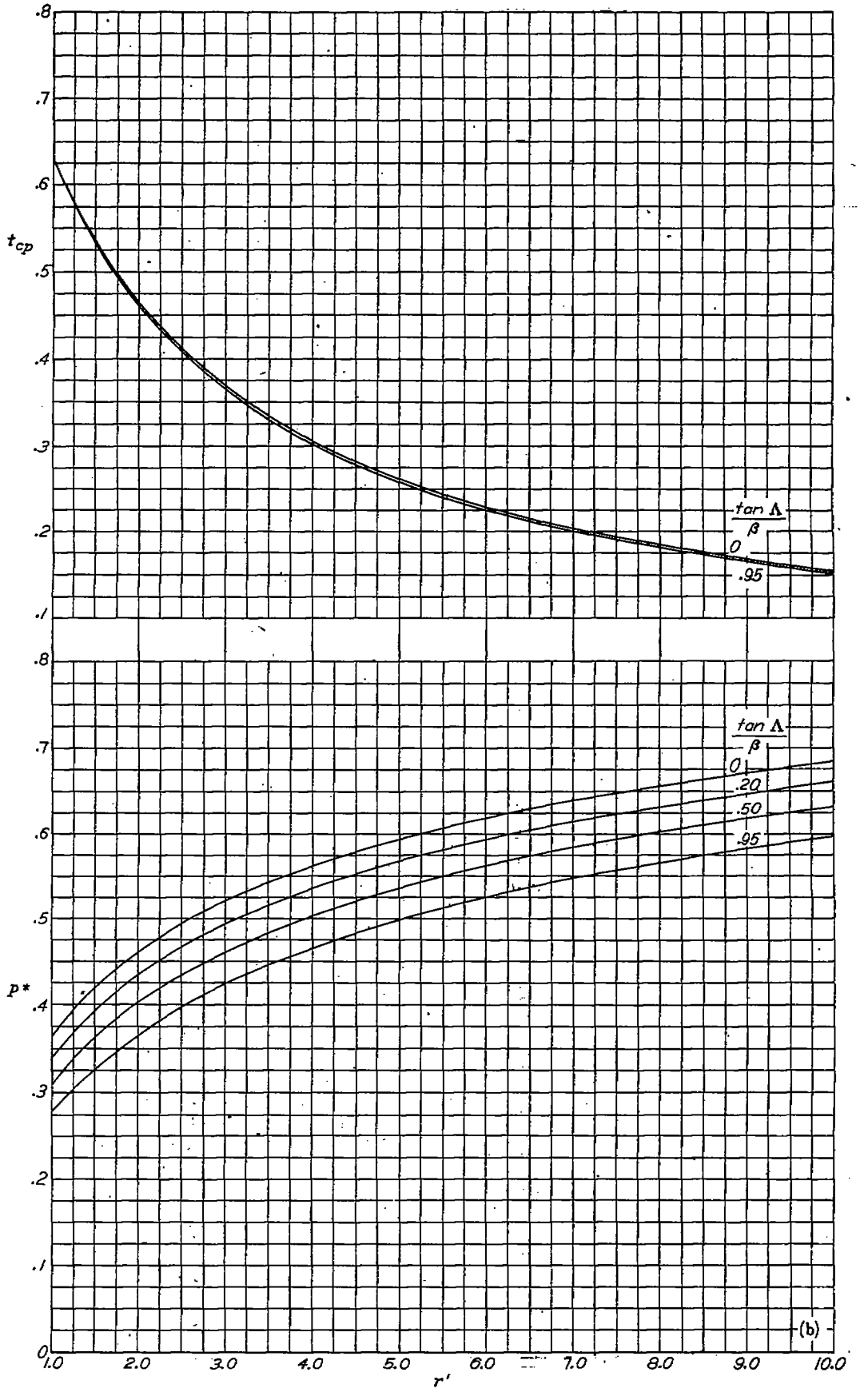

(b) $r'=1.0$ to 10.0.

FIGURE 10.—Concluded.

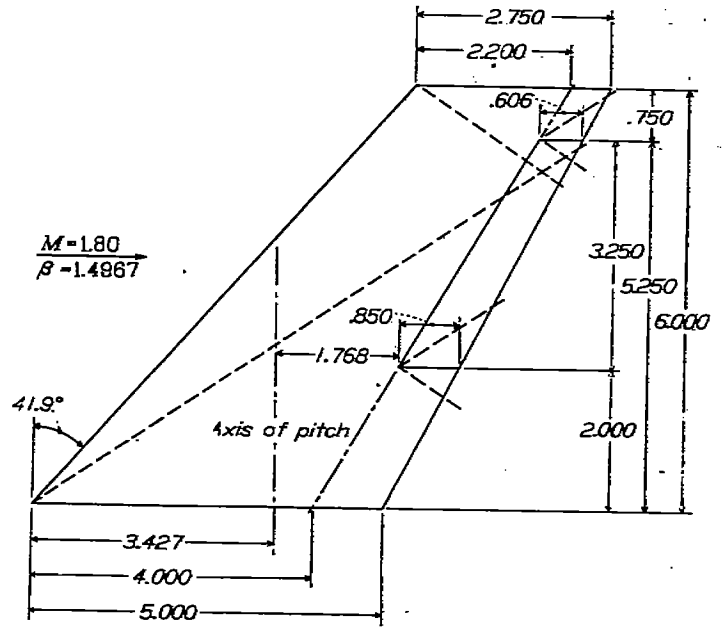

FIGURE 11.—Configuration used in sample calculation. $\left(\frac{\tan\Lambda}{\beta}=0.5995;\ \frac{\tan\Lambda_{HL}}{\beta}=0.3990;\ \frac{\tan\Lambda_{TE}}{\beta}=0.3489;\ S=23.250\ \ \bar{c}=3.984;\ \lambda_f=0.713;\ S_f=2.366;\ 2M_c=1.490.\right)$

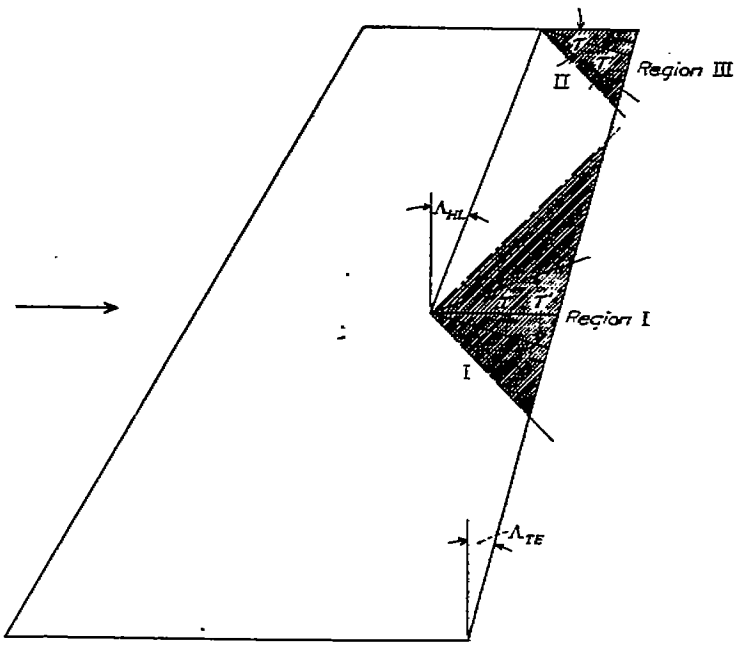

FIGURE 12.—Illustration of ordinates used in integrating pressures over conical regions of deflected controls.

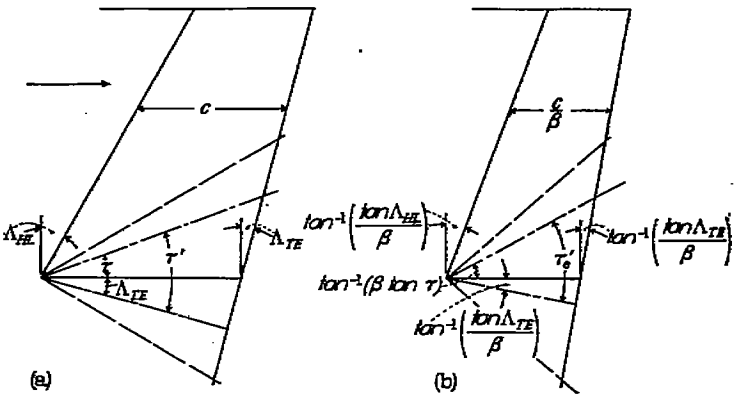

(a) Initial plan form ($M=\sqrt{3.25}$; $\beta=1.5$).

(b) Equivalent plan form ($M_e=\sqrt{2}$; $\beta_e=1.0$).

FIGURE 13.—Example transformation from one plan-form Mach number configuration to an equivalent plan form at a Mach number of $\sqrt{2}$.

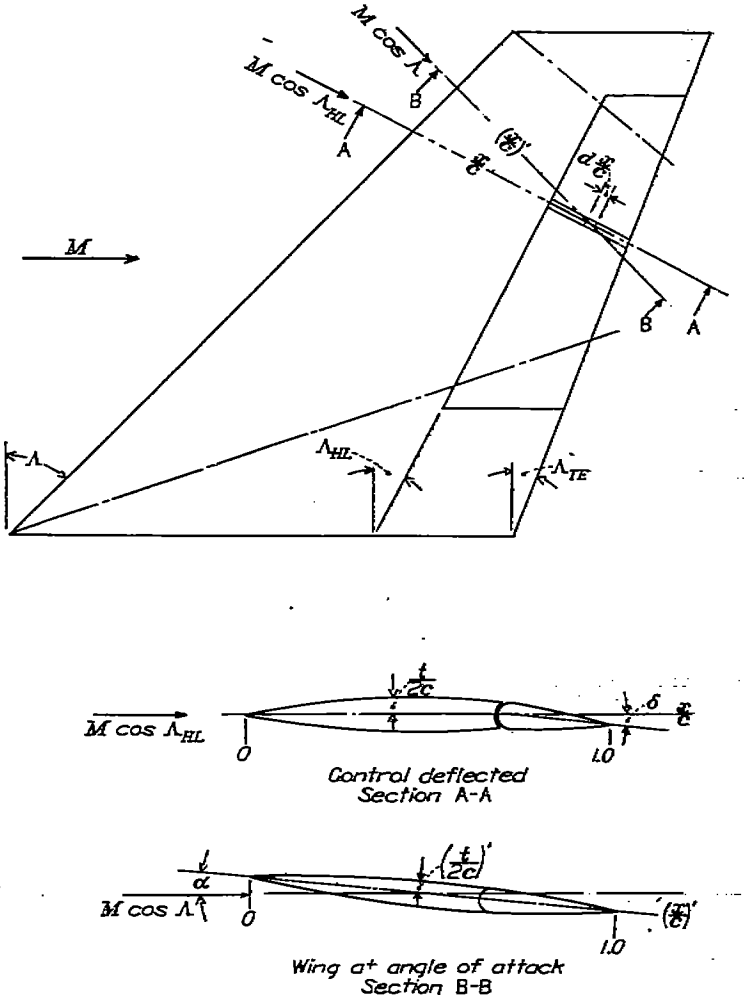

FIGURE 14.—Illustration of parameters used in determining the two-dimensional characteristics of trailing-edge controls having thickness.

TABLE I.—GENERAL EQUATIONS USED FOR DETERMINING CHARACTERISTICS OF DEFLECTED CONTROLS

[Subscripts I, I_a, I_b, I_c, II, II_a, II_b, II_c, III, III_a, and III_b refer to regions defined in fig. 1]

(a) Configuration Having Control Located Inboard from the Wing Tip

Parameter	Formula
C_{L_δ}'	$\frac{2C_{p_0}}{\delta}\left[\frac{S_{L_0}}{S_f}+\left(P\frac{S_L}{S_f}\right)_{\mathrm{I}}+\left(P\frac{S_L}{S_f}\right)_{\mathrm{II}}\right]$
C_{m_δ}'	$\frac{-2C_{p_0}}{\delta}\left[\frac{m_0}{2M_a}+\left(P\frac{S_L\bar{x}}{2M_a}\right)_{\mathrm{I}}+\left(P\frac{S_L\bar{x}}{2M_a}\right)_{\mathrm{II}}\right]$
C_{l_δ}'	$\frac{2C_{p_0}}{\delta}\left[\frac{l_0}{b_fS_f}+\left(P\frac{S_L\bar{y}}{b_fS_f}\right)_{\mathrm{I}}+\left(P\frac{S_L\bar{y}}{b_fS_f}\right)_{\mathrm{II}}\right]$
C_{h_δ}	$\frac{-2C_{p_0}}{\delta}\left[\frac{m_0}{2M_a}+\left(P\frac{S_L\bar{x}}{2M_a}\right)_{\mathrm{I}_c}+\left(P\frac{S_L\bar{x}}{2M_a}\right)_{\mathrm{I}_a}^{*}-\left(P\frac{S_L\bar{x}}{2M_a}\right)_{\mathrm{I}_b}^{*}+\left(P\frac{S_L\bar{x}}{2M_a}\right)_{\mathrm{II}_c}+\left(P\frac{S_L\bar{x}}{2M_a}\right)_{\mathrm{II}_a}^{*}-\left(P\frac{S_L\bar{x}}{2M_a}\right)_{\mathrm{II}_b}^{*}\right]$

(b) Configuration Having Control Located at the Wing Tip

Parameter	Formula
C_{L_δ}'	$\frac{2C_{p_0}}{\delta}\left[\frac{S_{L_0}}{S_f}+\left(P\frac{S_L}{S_f}\right)_{\mathrm{I}}+\left(P\frac{S_L}{S_f}\right)_{\mathrm{I}_a}^{*}-\left(P\frac{S_L}{S_f}\right)_{\mathrm{I}_b}^{*}+\left(P\frac{S_L}{S_f}\right)_{\mathrm{III}}\right]$
C_{m_δ}'	$\frac{-2C_{p_0}}{\delta}\left[\frac{m_0}{2M_a}+\left(P\frac{S_L\bar{x}}{2M_a}\right)_{\mathrm{I}}+\left(P\frac{S_L\bar{x}}{2M_a}\right)_{\mathrm{I}_a}^{*}-\left(P\frac{S_L\bar{x}}{2M_a}\right)_{\mathrm{I}_b}^{*}+\left(P\frac{S_L\bar{x}}{2M_a}\right)_{\mathrm{III}}\right]$
C_{l_δ}'	$\frac{2C_{p_0}}{\delta}\left[\frac{l_0}{b_fS_f}+\left(P\frac{S_L\bar{y}}{b_fS_f}\right)_{\mathrm{I}}+\left(P\frac{S_L\bar{y}}{b_fS_f}\right)_{\mathrm{I}_a}^{*}-\left(P\frac{S_L\bar{y}}{b_fS_f}\right)_{\mathrm{I}_b}^{*}+\left(P\frac{S_L\bar{y}}{b_fS_f}\right)_{\mathrm{III}}\right]$
C_{h_δ}	$\frac{-2C_{p_0}}{\delta}\left[\frac{m_0}{2M_a}+\left(P\frac{S_L\bar{x}}{2M_a}\right)_{\mathrm{I}_c}+\left(P\frac{S_L\bar{x}}{2M_a}\right)_{\mathrm{I}_a}^{*}-\left(P\frac{S_L\bar{x}}{2M_a}\right)_{\mathrm{I}_b}^{*}+\left(P\frac{S_L\bar{x}}{2M_a}\right)_{\mathrm{III}}+\left(P\frac{S_L\bar{x}}{2M_a}\right)_{\mathrm{III}_a}^{*}-\left(P\frac{S_L\bar{x}}{2M_a}\right)_{\mathrm{III}_b}^{*}\right]$

TABLE II.—COMPONENT PARTS OF EQUATIONS USED IN CALCULATING CHARACTERISTICS OF DEFLECTED CONTROLS HAVING TAPERED PLAN FORMS

(a) Average Pressure Ratio

Values of P for regions II, II_a, II_b, and II_c are obtained by substituting $-a$, $-d$, and $1/\lambda_f$ for a, d, and λ_f in equations for regions I, I_a, I_b, and I_c, respectively. In cases where plus and minus signs are together ($\pm$), the upper sign must be used when values of a and d substituted are such that $a-d$ is negative and the lower sign must be used when values of a and d substituted are such that $a-d$ is positive.

Region (fig. 1)	Average pressure ratio
I	$P=\frac{\sqrt{(1-a^2)(1-d^2)}-(1-a)(1+d)}{2(a-d)}$
I_a	$P^*=\frac{1-d}{\lambda_f(1-d)-(1-a)}\left\{\frac{\lambda_f}{\pi}\cos^{-1}\left[\frac{(1-a^2)-\lambda_f(1-ad)}{\lambda_f(a-d)}\right]-\frac{1}{\pi}\sqrt{\frac{1-a^2}{1-d^2}}\cos^{-1}\left[\frac{(1-ad)-\lambda_f(1-d^2)}{(a-d)}\right]\right\}$
I_b	$P^*=\frac{1}{\lambda_f(1-d)-(1-a)}\left\{\frac{\lambda_f}{\pi}(a-d)\cos^{-1}\left[\frac{(1-a^2)-\lambda_f(1-ad)}{\lambda_f(a-d)}\right]+\frac{(1-\lambda_f)\sqrt{1-a^2}}{\pi}\log_e\left\lvert\frac{(a-\lambda_f d)\pm\sqrt{2\lambda_f(1-ad)-\lambda_f^2(1-d^2)-(1-a^2)}}{1-\lambda_f}\right\rvert\right\}$
I_c	$P=\frac{1-d}{a-d}\left[\sqrt{\frac{1-a^2}{1-d^2}}\left(1-\frac{1}{\pi}\cos^{-1}d\right)+\frac{1}{\pi}\cos^{-1}a-\frac{1-a}{1-d}\right]$
III	$P=\frac{(1+a)-\sqrt{(1+a)(1+d)}}{a-d}$
III_a	$P^*=\frac{1}{(1+d)-\lambda_f(1+a)}\left\{\frac{1+d}{\pi}\cos^{-1}\left[\frac{(2+a+d)-2\lambda_f(1+a)}{(a-d)}\right]-\frac{\lambda_f\sqrt{(1+a)(1+d)}}{\pi}\cos^{-1}\left[\frac{2(1+d)-\lambda_f(2+a+d)}{\lambda_f(a-d)}\right]\right\}$
III_b	$P^*=\frac{1}{\lambda_f(1+a)-(1+d)}\left\{\frac{a-d}{\pi}\cos^{-1}\left[\frac{(2+a+d)-2\lambda_f(1+a)}{(a-d)}\right]\mp\frac{2}{\pi}\sqrt{(1+a)(1-\lambda_f)[\lambda_f(1+a)-(1+d)]}\right\}$

TABLE II.—COMPONENT PARTS OF EQUATIONS USED IN CALCULATING CHARACTERISTICS OF DEFLECTED CONTROLS HAVING TAPERED PLAN FORMS—Continued

(b) Center-of-Pressure Ray Location

[Values of t_{cp}' (or r_{cp}) for regions II, II_a, II_b, and II_c are obtained by substituting $-a$, $-d$, and $1/\lambda_f$ for a, d, and λ_f in equations for regions I, I_a, I_b, and I_c, respectively. In cases where plus and minus signs are together ($\pm$), the upper sign must be used when values of a and d substituted are such that $a-d$ is negative and the lower sign must be used when values of a and d substituted are such that $a-d$ is positive.]

Region (fig. 1)	Center-of-pressure ray location (t_{cp}' or r_{cp})
I	$t_{cp}'=\frac{1}{4P(a-d)^2}\left\{\sqrt{\frac{1-a^2}{1-d^2}}\,(1+3ad-3d^2-ad^3)-\frac{1+d}{1-d}\,[(1-a^2)(1-d^2)-2d(1-a)^2]\right\}$
I_a	$t_{cp}'^*=\frac{1}{2P^*(a-d)(1+d)[\lambda_f(1-d)-(1-a)]}\left\{\left(\frac{1-d^2}{\pi}\right)[2\lambda_f(1+ad)-\lambda_f^2(1+d^2)]\cos^{-1}\left[\frac{(1-a^2)-\lambda_f(1-ad)}{\lambda_f(a-d)}\right]-\right.$ $\left.\frac{1}{\pi}\sqrt{\frac{1-a^2}{1-d^2}}\,(1+3ad-3d^2-ad^3)\cos^{-1}\left[\frac{(1-ad)-\lambda_f(1-d^2)}{a-d}\right]\pm\frac{(1+d^2)}{\pi}\sqrt{(1-a^2)[2\lambda_f(1-ad)-\lambda_f^2(1-d^2)-(1-a^2)]}\right\}$
I_b	$r_{cp}^*=\frac{1}{2P^*[\lambda_f(1-d)-(1-a)]}\left\{\frac{\lambda_f(a-d)[2a-\lambda_f(a+d)]}{\pi(1-\lambda_f)}\cos^{-1}\left[\frac{(1-a^2)-\lambda_f(1-ad)}{\lambda_f(a-d)}\right]\pm\right.$ $\left.\frac{\sqrt{(1-a^2)[2\lambda_f(1-ad)-\lambda_f^2(1-d^2)-(1-a^2)]}}{\pi}+\frac{a(1-\lambda_f)\sqrt{1-a^2}}{\pi}\log_e\left|\frac{(a-\lambda_f d)\pm\sqrt{2\lambda_f(1-ad)-\lambda_f^2(1-d^2)-(1-a^2)}}{1-\lambda_f}\right|\right\}$
I_c	$t_{cp}'=\frac{1}{2P(1+d)(a-d)^2}\left\{\sqrt{\frac{1-a^2}{1-d^2}}\,(1+3ad-3d^2-ad^3)\left(1-\frac{1}{\pi}\cos^{-1}d\right)+\frac{(a-d)(1+d^2)\sqrt{1-a^2}}{\pi}-\right.$ $\left.\frac{1+d}{1-d}\,[(1-a^2)(1-d^2)-2d(1-a)^2]+\frac{(1-d^2)(1+2ad-d^2)}{\pi}\cos^{-1}a\right\}$
III	$t_{cp}'=\frac{1}{4P(1+d)(a-d)^2}\left\{\sqrt{(1+a)(1+d)}[(2-a+d)(1-d^2)+2ad(1+d)+2d(1+a)]-2[(1-a^2)(1-d^2)+2d(1+a)^2]\right\}$
III_a	$t_{cp}'^*=\frac{1}{4P^*(a-d)[\lambda_f(1+a)-(1+d)]}\left\{\frac{2(1+d)}{\pi\lambda_f}[2\lambda_f(1+ad)-(1+d^2)]\cos^{-1}\left[\frac{(2+a+d)-2\lambda_f(1+a)}{a-d}\right]\pm\right.$ $\frac{2(1+d^2)}{\pi}\sqrt{(1+a)[\lambda_f(2+a+d)-\lambda_f^2(1+a)-(1+d)]}-$ $\left.\frac{\lambda_f}{\pi}\sqrt{\frac{1+a}{1+d}}\,[(2-a+d)(1-d^2)+2ad(1+d)+2d(1+a)]\cos^{-1}\left[\frac{2(1+d)-\lambda_f(2+a+d)}{\lambda_f(a-d)}\right]\right\}$
III_b	$r_{cp}^*=\frac{1}{6P^*(1-\lambda_f)[\lambda_f(1+a)-(1+d)]}\left\{\frac{3(a-d)[2a\lambda_f-(a+d)]}{\pi}\cos^{-1}\left[\frac{(2+a+d)-2\lambda_f(1+a)}{a-d}\right]\pm\right.$ $\left.\frac{2[2\lambda_f(1-2a)-(2-3a-d)]}{\pi}\sqrt{(1+a)[\lambda_f(2+a+d)-\lambda_f^2(1+a)-(1+d)]}\right\}$

TABLE II.—COMPONENT PARTS OF EQUATIONS USED IN CALCULATING CHARACTERISTICS OF DEFLECTED CONTROLS HAVING TAPERED PLAN FORMS—Concluded

(c) Geometric Parameters $S_f=\frac{\beta b_f^2(a-d)(1+\lambda_f)}{2(1-\lambda_f)}$ and $2M_a=\frac{\beta^2 b_f^2(a-d)^2(1-\lambda_f^3)}{3(1-\lambda_f)^2\sqrt{1+\beta^2a^2}}$

Region (fig. 1)	S_L/S_f	$S_L\bar{y}/b_fS_f$	$S_L\bar{x}/2M_a$
I	$\frac{2(a-d)}{(1-\lambda_f^2)(1-d^2)}$	$\frac{S_L}{S_f}\frac{2(a-d)(t_{cp}'-d)}{3(1-\lambda_f)(1+d^2)}$	$\frac{S_L}{S_f}\frac{1-\lambda_f^3}{1-\lambda_f^2}\left[\frac{(1+ad)-(a-d)t_{cp}'}{1+d^2}\right]$
I_a	$\frac{\lambda_f(1-d)-(1-a)}{(1-\lambda_f^2)(1-d)}$	$\frac{S_L}{S_f}\frac{2(a-d)(t_{cp}'-d)}{3(1-\lambda_f)(1+d^2)}$	$\frac{S_L}{S_f}\frac{1-\lambda_f^3}{1-\lambda_f^2}\left[\frac{(1+ad)-(a-d)t_{cp}'}{1+d^2}\right]$
I_b	$\frac{\lambda_f(1-d)-(1-a)}{(1+\lambda_f)(a-d)}$	$\frac{2}{3}\frac{S_L}{S_f}$	$\frac{S_L}{S_f}\frac{1-\lambda_f^3}{1-\lambda_f^2}\left[\frac{(1-\lambda_f)(r_{cp}-a)}{a-d}\right]$
I_c	----------	----------	$\frac{(a-d)[(1+ad)-(a-d)t_{cp}']}{(1-\lambda_f^2)(1-d)(1+d^2)}$
II	$\frac{2\lambda_f^2(a-d)}{(1-\lambda_f^2)(1-d^2)}$	$\frac{S_L}{S_f}\left[1-\frac{2\lambda_f(a-d)(t_{cp}'+d)}{3(1-\lambda_f)(1+d^2)}\right]$	$\frac{S_L}{S_f}\lambda_f\frac{1-\lambda_f^3}{1-\lambda_f^2}\left[\frac{(1+ad)+(a-d)t_{cp}'}{1+d^2}\right]$
II_a	----------	----------	$\frac{\lambda_f^2[\lambda_f(1+a)-(1+d)][(1+ad)+(a-d)t_{cp}']}{(1-\lambda_f^2)(1+d)(1+d^2)}$
II_b	----------	----------	$\frac{(1-\lambda_f)^2[\lambda_f(1+a)-(1+d)](r_{cp}+a)}{(1-\lambda_f^2)(a-d)^2}$
II_c	----------	----------	$\frac{\lambda_f^2(a-d)[(1+ad)+(a-d)t_{cp}']}{(1-\lambda_f^2)(1+d)(1+d^2)}$
III	$\frac{\lambda_f^2(a-d)}{(1-\lambda_f^2)(1+d)}$	$\frac{S_L}{S_f}\left[1-\frac{2\lambda_f(a-d)(t_{cp}'+d)}{3(1-\lambda_f)(1+d^2)}\right]$	$\frac{\lambda_f^2(a-d)[(1+ad)+(a-d)t_{cp}']}{(1-\lambda_f^2)(1+d)(1+d^2)}$
III_a	----------	----------	$\frac{\lambda_f^2[\lambda_f(1+a)-(1+d)][(1+ad)+(a-d)t_{cp}']}{(1-\lambda_f^2)(1+d)(1+d^2)}$
III_b	----------	----------	$\frac{(1-\lambda_f)^2[\lambda_f(1+a)-(1+d)](r_{cp}+a)}{(1-\lambda_f^2)(a-d)^2}$
Two-dimensional	$\frac{\left(\frac{1-a}{1-d}\right)-\lambda_f^2\left(\frac{1+a}{1+d}\right)}{(1-\lambda_f^2)}$	$\frac{\left\{(1+a)(1-\lambda_f)-\frac{(a-d)^2}{(1-\lambda_f)^2(1-d)^2}-\frac{[(1+d)-\lambda_f(1+a)]^2}{(1-\lambda_f)^2(1+d)^2}\right\}}{3(a-d)(1+\lambda_f)}$	$\frac{\left(\frac{1-a}{1-d}\right)^2-\lambda_f^2\left(\frac{1+a}{1+d}\right)^2}{2(1-\lambda_f^2)}$

TABLE III.—COMPONENT PARTS OF EQUATIONS USED IN CALCULATING CHARACTERISTICS OF DEFLECTED CONTROLS HAVING UNTAPERED PLAN FORMS

(a) Average Pressure Ratio and Center-Of-Pressure Ray Location

[Values of P and t_{cp}' (or r_{cp}) for regions II, II_a, II_b, and II_c are obtained by substituting $-a$ for a in equations for regions I, I_a, I_b, and I_c, respectively]

Region (fig. 1)	Average pressure ratio	Center-of-pressure ray location (t_{cp}' or r_{cp})
I	$P=\frac{1}{2}$	$t_{cp}'=\frac{8a+(1+a^2)}{4(1-a^2)}$
I_a	$P^a=\frac{1}{(1+a)[1-(1-a)A_f']}\left\{\frac{\sqrt{(1-a^2)[1+2aA_f'-(1-a^2)A_f'^2]}}{\pi}-\frac{(1-a^2)A_f'-a}{\pi}\cos^{-1}[(1-a^2)A_f'-a]\right\}$	$t_{cp}'^a=\frac{1}{4P^a(1+a)(1-a^2)[1-(1-a)A_f']}\left\{\frac{(7a^2-2a^4+1)-2A_f'(1-a^2)^2[2a+(1+a^2)A_f']}{\pi}\cos^{-1}[(1-a^2)A_f'-a]+\frac{[a(7-a^2)+(1-a^4)A_f']\sqrt{(1-a^2)[1+2aA_f'-(1-a^2)A_f'^2]}}{\pi}\right\}$
I_b	$P^b=\frac{1}{1-(1-a)A_f'}\left\{\frac{1}{\pi}\cos^{-1}[(1-a^2)A_f'-a]+\frac{A_f'\sqrt{1-a^2}}{\pi}\log_e\left\lvert\frac{1+aA_f'-\sqrt{1+2aA_f'-(1-a^2)A_f'^2}}{A_f'}\right\rvert\right\}$	$r_{cp}^b=\frac{1}{2P^b[1-(1-a)A_f']}\left\{\frac{1+2aA_f'}{\pi A_f'}\cos^{-1}[(1-a^2)A_f'-a]-\frac{\sqrt{(1-a^2)[1+2aA_f'-(1-a^2)A_f'^2]}}{\pi}+\frac{aA_f'\sqrt{1-a^2}}{\pi}\log_e\left\lvert\frac{1+aA_f'-\sqrt{1+2aA_f'-(1-a^2)A_f'^2}}{A_f'}\right\rvert\right\}$
I_c	$P=\frac{1}{(1+a)}\left(1+\frac{a}{\pi}\cos^{-1}a-\frac{\sqrt{1-a^2}}{\pi}\right)$	$t_{cp}'=\frac{1}{4P(1+a)(1-a^2)}\left[8a+(1+a^2)+\frac{7a^2-2a^4+1}{\pi}\cos^{-1}a-\frac{a(7-a^2)\sqrt{1-a^2}}{\pi}\right]$
III	$P=\frac{1}{2}$	$t_{cp}'=\frac{5-8a-3a^2}{8(1+a)}$
III_a	$P^a=\frac{1}{2[1-(1+a)A_f']}\left\{\frac{2\sqrt{A_f'(1+a)[1-A_f'(1+a)]}}{\pi}-\frac{2A_f'(1+a)-1}{\pi}\cos^{-1}[2A_f'(1+a)-1]\right\}$	$t_{cp}'^a=\frac{1}{16P^a(1+a)[1-(1+a)A_f']}\left\{\frac{3-8a-5a^2-8A_f'(1+a)^2[A_f'(1+a^2)-2a]}{\pi}\cos^{-1}[2A_f'(1+a)-1]-2\left[\frac{5a^2+8a-3-2A_f'(1+a)(1+a^2)}{\pi}\right]\sqrt{A_f'(1+a)[1-A_f'(1+a)]}\right\}$
III_b	$P^b=\frac{1}{1-(1+a)A_f'}\left\{\frac{1}{\pi}\cos^{-1}[2A_f'(1+a)-1]-\frac{2\sqrt{A_f'(1+a)[1-(1+a)A_f']}}{\pi}\right\}$	$r_{cp}^b=\frac{1}{6P^bA_f'[1-(1+a)A_f']}\left\{\frac{3(1-2aA_f')}{\pi}\cos^{-1}[2A_f'(1+a)-1]-\frac{2[1+2A_f'(1-2a)]}{\pi}\sqrt{A_f'(1+a)[1-(1+a)A_f']}\right\}$

(b) Geometric Parameters $S_f=\frac{\beta b_f^2}{A_f'}$ and $2M_a=\frac{\beta^2 b_f^3}{A_f'^2\sqrt{1+\beta^2a^2}}$

Region (fig. 1)	S_L/S_f	$S_L\bar{y}/b_fS_f$	$S_L\bar{x}/2M_a$
I	$\frac{1}{A_f'(1-a^2)}$	$\frac{S_L}{S_f}\frac{(1+4a)}{6A_f'(1-a^2)}$	$\frac{2}{3}\frac{S_L}{S_f}$
I_a	$\frac{1-A_f'(1-a)}{2A_f'(1-a)}$	$\frac{S_L}{S_f}\frac{2(t_{cp}'-a)}{3A_f'(1+a^2)}$	$\frac{2}{3}\frac{S_L}{S_f}$
I_b	$\frac{1-A_f'(1-a)}{2}$	$\frac{2}{3}\frac{S_L}{S_f}$	$\frac{2}{3}\frac{S_L}{S_f}A_f'(r_{cp}-a)$
I_c	----------	----------	$\frac{1}{3A_f'(1-a)}$
II	$\frac{1}{A_f'(1-a^2)}$	$\frac{S_L}{S_f}\left[1-\frac{(1-4a)}{6A_f'(1-a^2)}\right]$	$\frac{2}{3}\frac{S_L}{S_f}$
II_a	----------	----------	$\frac{1-A_f'(1+a)}{3A_f'(1+a)}$
II_b	----------	----------	$\frac{A_f'(r_{cp}+a)[1-A_f'(1+a)]}{3}$
II_c	----------	----------	$\frac{1}{3A_f'(1+a)}$
III	$\frac{1}{2A_f'(1+a)}$	$\frac{S_L}{S_f}\left[1-\frac{5}{12A_f'(1+a)}\right]$	$\frac{2}{3}\frac{S_L}{S_f}$
III_a	----------	----------	$\frac{1-A_f'(1+a)}{3A_f'(1+a)}$
III_b	----------	----------	$\frac{A_f'(r_{cp}+a)[1-A_f'(1+a)]}{3}$
Two-dimensional	$\frac{A_f'(1-a^2)-1}{A_f'(1-a^2)}$	$\frac{3A_f'(1-a)(1-a^2)[A_f'(1+a)-1]-4a}{6A_f'^2(1-a^2)^2}$	$\frac{3A_f'(1-a^2)-4}{6A_f'(1-a^2)}$

TABLE IV.—EXAMPLE OF NUMERICAL INTEGRATION OF PRESSURES ALONG AN INCLINED SECTION INTERSECTING WING-ROOT MACH CONE

$1-P'$

(1)	(2)	(3)	(4)	(5)	(6)	(7)	(8)
n	1−(1)	$\frac{1}{K_1\times(1)}$	$\left[\frac{(2)}{(3)}\right]^2$	$\frac{1}{\beta^2\times(4)}$	$\frac{K_2}{(5)}$	(6)−1	$\frac{\cos^{-1}(7)}{\pi}$
0.1	0.9	0.98	0.8434	0.7892	1.9007	0.9007	0.1431
.2	.8	.96	.6944	.8264	1.8151	.8151	.1967
.3	.7	.94	.5545	.8614	1.7414	.7414	.2842
.4	.6	.92	.4253	.8937	1.6784	.6784	.2627
.5	.5	.90	.3086	.9229	1.6258	.6253	.2850
.6	.4	.88	.2066	.9484	1.5816	.5816	.3024
.7	.3	.86	.1217	.9690	1.5470	.5470	.3158
.8	.2	.84	.0567	.9858	1.5216	.5216	.3258
.9	.1	.82	.0149	.9963	1.5056	.5056	.3318
1.0	0	.80	0	1.0000	1.5000	.5000	.3333

$\beta=0.80$

$K_1=\frac{\tan\eta}{\beta}=0.20$

$\beta^2=0.25$

$K_2=2(1-\beta^2)=1.50$

t_{ep} P^*

			(1)	(2)	(3)	(4)	(5)	(6)	(7)	(8)	(9)	(10)	(11)	(12)	(13)	(14)	(15)	(16)	(17)	(18)
			MULTIPLIERS																	
	n	$1-P'$	$n=0.1$	0.2	0.3	0.4	0.5	0.6	0.7	0.8	0.9	1.0	$\Sigma(1-P')\times$ (1) to (10)	Incr. Σ (11) $_{area}$	Incr. Σ (11) $_{mom.}$	(12)−(13)	(12)−$K_1\times$(13)	$\frac{(14)}{(15)}$	$\frac{1}{n}$	(12)×(17)
AREA	0.1	0.1431	0.130786	0.037500	−0.004167	0.004167	0	0	0	0	0	0	0.009797	0.009797	0.000626	0.009171	0.009672	0.9482	10.0000	0.0980
	.2	.1967	−.045340	.079167	.054167	−.020833	0	0	0	0	0	0	.017154	.026951	.003219	.023732	.026807	.9021	5.0000	.1348
	.3	.2842	0	−.020833	.054167	.079167	0	0	0	0	0	0	.021650	.048601	.008661	.039940	.046869	.8522	3.3333	.1620
	.4	.2627	0	.004167	−.004167	.037500	.037500	−.004167	.004167	0	0	0	.024891	.073492	.017401	.056091	.070012	.8012	2.5000	.1887
	.5	.2850	0	0	0	0	.079167	.054167	−.020833	0	0	0	.027480	.100922	.029764	.071158	.094969	.7493	2.0000	.2018
	.6	.3024	0	0	0	0	−.020833	.054167	.079167	0	0	0	.029407	.130329	.045951	.084378	.121139	.6965	1.6667	.2171
	.7	.3158	0	0	0	0	.004167	−.004167	.037500	.037500	−.004167	.004167	.030940	.161269	.066075	.095194	.148054	.6430	1.4286	.2205
	.8	.3258	0	0	0	0	0	0	0	.079167	.054167	−.020833	.032682	.193951	.090148	.103203	.175821	.5867	1.2500	.2417
	.9	.3318	0	0	0	0	0	0	0	−.020833	.054167	.079167	.032861	.226212	.113092	.108120	.202694	.5337	1.1111	.2518
	1.0	.3333	0	0	0	0	0	0	0	.004167	−.004167	.037500	.033266	.259478	.149689	.109789	.229540	.4783	1.0000	.2595
MOMENT	0.1	0.1431	0.008667	0.008667	0	0	0	0	0	0	0	0	0.000620							
	.2	.1967	−.001667	.008333	.037500	−.008333	0.000833	0	0	0	0	0	.002598							
	.3	.2842	0	0	.023750	.016250	−.006250	0	0	0	0	0	.005442							
	.4	.2627	0	0	−.008333	.021667	.031667	0	0	0	0	0	.008740							
	.5	.2850	0	0	.002083	−.002083	.018750	.018750	−.002083	.002083	0	0	.012383							
	.6	.3024	0	0	0	0	0	.047500	.032500	−.012500	0	0	.016187							
	.7	.3158	0	0	0	0	0	−.014583	.037917	.055417	0	0	.021034							
	.8	.3258	0	0	0	0	0	.003333	−.003333	.030000	.033333	−.008667	.024078							
	.9	.3318	0	0	0	0	0	0	0	0	.060000	.060000	.027944							
	1.0	.3333	0	0	0	0	0	0	0	0	−.008333	.041667	.031597							

TABLE V.—EXAMPLE OF NUMERICAL INTEGRATION OF PRESSURES ALONG A STREAMWISE SECTION INTERSECTING WING-ROOT MACH CONE

$1-P'$

(1) r'	(2) $[1+(1)]^2$	(3) $\frac{g^2+}{K_1\times(2)}$	(4) $(2)-g^2$	(5) $\frac{(3)}{(4)}$	(6) $\frac{\cos^{-1}(5)}{\pi}$
0.1	1.21	0.855	0.96	0.8906	0.1503
.2	1.44	.970	1.19	.8151	.1967
.3	1.69	1.095	1.44	.7604	.2250
.4	1.96	1.230	1.71	.7193	.2445
.5	2.25	1.375	2.00	.6875	.2587
.6	2.56	1.530	2.31	.6623	.2696
.7	2.89	1.695	2.64	.6420	.2781
.8	3.24	1.870	2.99	.6254	.2849
.9	3.61	2.055	3.36	.6116	.2905
1.0	4.00	2.250	3.75	.6000	.2952

$g=0.50$

$g^2=0.25$

$K_1=(1-2g^2)=0.50$

t_{cp} P^*

	r'	$1-P'$	(1) MULTIPLIERS $r'=0.1$	(2) 0.2	(3) 0.3	(4) 0.4	(5) 0.5	(6) 0.6	(7) 0.7	(8) 0.8	(9) 0.9	(10) 1.0	(11) $\Sigma(1-P')\times$ (1) to (10)	(12) Incr. Σ $(11)_{area}$	(13) Incr. Σ $(11)_{mom.}$	(14) (12)+(13)	(15) $\frac{(12)}{(14)}$	(16) $\frac{1}{r'}$	(17) (12)×(16)
AREA	0.1	0.1503	0.130786	0.037500	−0.004167	0.004167	0	0	0	0	0	0	0.010739	0.010739	0.000674	0.111413	0.9409	10.0000	0.1074
	.2	.1967	−.045340	.079167	.054167	−.020833	0	0	0	0	0	0	.017540	.028279	.003315	.031594	.8951	5.0000	.1414
	.3	.2250	0	−.020833	.054167	.079167	0	0	0	0	0	0	.021197	.049476	.008635	.058111	.8514	3.3333	.1649
	.4	.2445	0	.004167	−.004167	.037500	.037500	−.004167	.004167	0	0	0	.023510	.072986	.016886	.089872	.8121	2.5000	.1825
	.5	.2587	0	0	0	0	.079167	.054167	−.020833	0	0	0	.025192	.098178	.028287	.126415	.7766	2.0000	.1964
	.6	.2696	0	0	0	0	−.020833	.054167	.079167	0	0	0	.026439	.124617	.042788	.167405	.7444	1.6667	.2077
	.7	.2781	0	0	0	0	.004167	−.004167	.037500	.037500	−.004167	.004167	.027402	.152019	.060606	.212625	.7150	1.4286	.2172
	.8	.2849	0	0	0	0	0	0	0	.079167	.054167	−.020833	.028162	.180181	.081733	.261914	.6879	1.2500	.2252
	.9	.2905	0	0	0	0	0	0	0	−.020833	.054167	.079167	.028779	.208960	.106200	.315160	.6630	1.1111	.2322
	1.0	.2952	0	0	0	0	0	0	0	.004167	−.004167	.037500	.029292	.238252	.134031	.372283	.6400	1.0000	.2383

MOMENT	0.1	0.1503	0.006667	0.006667	0	0	0	0	0	0	0	0	0.000674
	.2	.1967	−.001667	.008333	.007500	−.000833	.000833	0	0	0	0	0	.002641
	.3	.2250	0	0	.023750	.016250	−.006250	0	0	0	0	0	.005320
	.4	.2445	0	0	−.008333	.021667	.031667	0	0	0	0	0	.008251
	.5	.2587	0	0	.002083	−.002083	.018750	.018750	−.002083	.002083	0	0	.011351
	.6	.2696	0	0	0	0	0	.047500	.032500	−.012500	0	0	.014561
	.7	.2781	0	0	0	0	0	−.014583	.037917	.055417	0	0	.017818
	.8	.2849	0	0	0	0	0	.003333	−.003333	.030000	.033333	−.006667	.021127
	.9	.2905	0	0	0	0	0	0	0	0	.060000	.060000	.024467
	1.0	.2952	0	0	0	0	0	0	0	0	−.008333	.041667	.027831

TABLE V.—EXAMPLE OF NUMERICAL INTEGRATION OF PRESSURES ALONG A STREAMWISE SECTION INTERSECTING WING-ROOT MACH CONE—Concluded

(1)	(2)	(3)	(4)	(5)	(6)
r'	$[1+(1)]^2$	$g^2+K_1\times(2)$	$(2)-g^2$	$\frac{(3)}{(4)}$	$\frac{\cos^{-1}(5)}{\pi}$
2.0	9.00	4.750	8.75	0.5429	0.3173
3.0	16.00	8.250	15.75	.5238	.3245
4.0	25.00	12.750	24.75	.5152	.3277
5.0	36.00	18.250	35.75	.5105	.3295
6.0	49.00	24.750	48.75	.5077	.3305
7.0	64.00	32.250	63.75	.5059	.3312
8.0	81.00	40.750	80.75	.5046	.3316
9.0	100.00	50.250	99.75	.5038	.3319
10.0	121.00	60.750	120.75	.5031	.3322

$g=0.50$

$g^2=0.25$

$K_1=(1-2g^2)=0.50$

$1-P'$

t_{cp} P'

			(1)	(2)	(3)	(4)	(5)	(6)	(7)	(8)	(9)	(10)	(11)	(12)	(13)	(14)	(15)	(16)
			MULTIPLIERS															
	r'	$1-P'$	$r'=2.0$	3.0	4.0	5.0	6.0	7.0	8.0	9.0	10.0	$\Sigma(1-P')\times$ (1) to (9)	Incr. Σ $(10)_{area}$	Incr. Σ $(10)_{mom.}$	(11)+(12)	$\frac{(11)}{(13)}$	$\frac{1}{r'}$	(11)×(15)
AREA	1.0	0.2052	0.375000	−0.041667	0.041667	0	0	0	0	0	0	0.23825	0.23825	0.13408				
	2.0	.3173	.791667	.541667	−.208333	0	0	0	0	0	0	.30795	.54620	.59888	1.14513	0.4770	0.50000	0.2731
	3.0	.3245	−.208333	.541667	.791667	0	0	0	0	0	0	.32169	.86789	1.40307	2.27096	.3823	.33333	.2888
	4.0	.3277	.041667	−.041667	.375000	.375000	−.041667	.041667	0	0	0	.32598	1.19387	2.54540	3.73927	.3193	.25000	.2985
	5.0	.3295	0	0	0	.791667	.541667	−.208333	0	0	0	.32869	1.52256	4.02470	5.54726	.2745	.20000	.3045
	6.0	.3305	0	0	0	−.208333	.541667	.791667	0	0	0	.33005	1.85261	5.84000	7.69261	.2408	.16667	.3088
	7.0	.3312	0	0	0	.041667	−.041667	.375000	.375000	−.041667	.041667	.33085	2.18346	7.99066	10.17412	.2146	.14286	.3119
	8.0	.3316	0	0	0	0	0	0	.791667	.541667	−.208333	.33141	2.51487	10.47680	12.99117	.1936	.12500	.3144
	9.0	.3319	0	0	0	0	0	0	−.208333	.541667	.791667	.33175	2.84662	13.29623	16.14285	.1763	.11111	.3163
	10.0	.3322	0	0	0	0	0	0	.041667	−.041667	.375000	.33205	3.17867	16.45070	19.62937	.1619	.10000	.3179
MOMENT	1.0	0.2052	0.375000	−0.041667	0.041667	0	0	0	0	0	0	0.13408						
	2.0	.3173	1.583333	1.083333	−.416667	0	0	0	0	0	0	.46490						
	3.0	.3245	−.625000	1.625000	2.375000	0	0	0	0	0	0	.80414						
	4.0	.3277	.166667	−.166667	1.500000	1.500000	−.166667	.166667	0	0	0	1.14233						
	5.0	.3295	0	0	0	8.958333	2.708333	−1.041667	0	0	0	1.47930						
	6.0	.3305	0	0	0	−1.250000	3.250000	4.750000	0	0	0	1.81530						
	7.0	.3312	0	0	0	.291667	−.291667	2.625000	2.625000	−.291667	.291667	2.15066						
	8.0	.3316	0	0	0	0	0	0	6.333333	4.333333	−1.666667	2.48564						
	9.0	.3319	0	0	0	0	0	0	−1.875000	4.875000	7.125000	2.81993						
	10.0	.3322	0	0	0	0	0	0	.416667	−.416667	3.750000	3.15447						

TABLE VI.—EXAMPLE OF NUMERICAL INTEGRATION OF PRESSURES ALONG AN INCLINED SECTION INTERSECTING WING-TIP MACH CONE

(1)	(2)	(3)	(4)	(5)	(6)	(7)
n	$K_2\times(1)$	$K_4-(2)$	$K_3\times(1)$	$K_1-(4)$	$\frac{(3)}{(5)}$	$\frac{\cos^{-1}(6)}{\pi}$
0.1	0.27	1.23	0.03	1.47	0.8367	0.1844
.2	.54	.96	.06	1.44	.6667	.2677
.3	.81	.69	.09	1.41	.4894	.3372
.4	1.08	.42	.12	1.38	.3044	.4016
.5	1.35	.15	.15	1.35	.1111	.4646
.6	1.62	−.12	.18	1.32	−.0909	.5290
.7	1.89	−.39	.21	1.29	−.3023	.5978
.8	2.16	−.66	.24	1.26	−.5238	.6755
.9	2.43	−.93	.27	1.23	−.7561	.7729
1.0	2.70	−1.20	.30	1.20	−1.0000	1.0000

$g=0.50$

$K_1=\frac{\tan\eta}{\beta}=0.20$

$K_2=(2+g+K_1)=2.70$

$K_3=(g-K_1)=0.30$

$K_4=(1+g)=1.50$

	n	$1-P'$	(1) MULTIPLIERS n=0.1	(2) 0.2	(3) 0.3	(4) 0.4	(5) 0.5	(6) 0.6	(7) 0.7	(8) 0.8	(9) 0.9	(10) 1.0	(11) $\Sigma(1-P')\times(1)$ to (10)	(12) Incr. Σ (11)$_{area}$	(13) Incr. Σ (11)$_{mom.}$	(14) (12)−(13)	(15) (12)+$K_1\times$(13)	(16) l_{cp} (14)/(15)	(17) P' $\frac{1}{n}$	(18) (12)×(17)
AREA	0.1	0.1844	0.113301	0.037500	−0.004167	0.004167	0	0	0	0	0	0	0.012065	0.012065	0.000766	0.011299	0.012218	0.9248	10.0000	0.1207
	.2	.2667	−.032975	.079167	.054167	−.020833	0	0	0	0	0	0	.022757	.034822	.004348	.030579	.035671	.8573	5.0000	.1741
	.3	.3372	0	−.020833	.054167	.079167	0	0	0	0	0	0	.030324	.065146	.011891	.053255	.067524	.7887	3.3333	.2172
	.4	.4016	0	.004167	−.004167	.037500	.041667	−.008333	0	0	0	0	.036946	.102092	.024885	.077207	.107069	.7211	2.5000	.2552
	.5	.4646	0	0	0	0	.066667	.066667	0	0	0	0	.043299	.145391	.044436	.100955	.154276	.6544	2.0000	.2908
	.6	.5290	0	0	0	0	−.008333	.041667	.037500	−.004167	.004167	0	.049669	.195060	.071793	.123267	.209419	.5886	1.6667	.3251
	.7	.5978	0	0	0	0	0	0	.079167	.054167	−.020833	0	.056311	.251871	.108464	.142907	.273064	.5233	1.4286	.3591
	.8	.6755	0	0	0	0	0	0	−.020833	.054167	.079167	−.033494	.063546	.314917	.156182	.158735	.346163	.4586	1.2500	.3936
	.9	.7729	0	0	0	0	0	0	.004167	−.004167	.037500	.121105	.072212	.387129	.217654	.169475	.430660	.3935	1.1111	.4301
	1.0	1.0000	0	0	0	0	0	0	0	0	0	.017389	.084988	.472117	.298483	.173634	.531814	.3265	1.0000	.4721
MOMENT	0.1	0.1844	0.007917	0.005417	−0.002083	0	0	0	0	0	0	0	0.000766							
	.2	.2677	−.004167	.010833	.015833	0	0	0	0	0	0	0	.008477							
	.3	.3372	.001250	−.001250	.011250	.011250	−.001250	.001250	0	0	0	0	.007648							
	.4	.4016	0	0	0	.031667	.021667	−.008333	0	0	0	0	.012994							
	.5	.4646	0	0	0	−.010416	.027083	.039583	0	0	0	0	.019541							
	.6	.5290	0	0	0	.002500	−.002500	.022500	.022500	−.002500	.002500	0	.027367							
	.7	.5978	0	0	0	0	0	0	.035417	.037917	−.014583	0	.036671							
	.8	.6755	0	0	0	0	0	0	−.016667	.043334	.063334	−.030795	.047718							
	.9	.7729	0	0	0	0	0	0	.003750	−.003750	.033750	.108995	.061472							
	1.0	1.0000	0	0	0	0	0	0	0	0	0	.017389	.080829							

TABLE VII.—EXAMPLE OF NUMERICAL INTEGRATION OF PRESSURES ALONG A SPANWISE SECTION INTERSECTING WING-TIP MAC CONE

(1)	(2)	(3)	(4)	(5)
r'	$K_1-(1)$	$K_1+(1)$	$\frac{(2)}{(3)}$	$\frac{\cos^{-1}(4)}{\pi}$
0.1	1.40	1.60	0.8750	0.1609
.2	1.30	1.70	.7647	.2229
.3	1.20	1.80	.6667	.2677
.4	1.10	1.90	.5789	.3035
.5	1.00	2.00	.5000	.3333
.6	.90	2.10	.4286	.3590
.7	.80	2.20	.3636	.3815
.8	.70	2.30	.3043	.4016
.9	.60	2.40	.2500	.4196
1.0	.50	2.50	.2000	.4359

$g=0.50$

$K_1=(1+g)=1.50$

			(1)	(2)	(3)	(4)	(5)	(6)	(7)	(8)	(9)	(10)	(11)	(12)	(13)	(14)	(15)	(16)	(17)
			MULTIPLIERS																
	r'	$1-P'$	$r'=0.1$	0.2	0.3	0.4	0.5	0.6	0.7	0.8	0.9	1.0	$\Sigma(1-P')\times$ (1) to (10)	Incr. Σ $(11)_{area}$	Incr. Σ $(11)_{mom.}$	(12)+(13)	$\frac{(12)}{(14)}$	$\frac{1}{r'}$	(12)×(16)
AREA	0.1	0.1609	0.118301	0.037500	−0.004167	0.004167	0	0	0	0	0	0	0.010880	0.010880	0.000701	0.011581	0.9395	10.0000	0.1088
	.2	.2229	−.032975	.079167	.054167	−.020833	0	0	0	0	0	0	.019368	.030248	.003681	.033870	.8928	5.0000	.1512
	.3	.2677	0	−.020833	.054167	.079167	0	0	0	0	0	0	.024639	.054887	.009826	.064713	.8482	3.3333	.1880
	.4	.3035	0	.004167	−.004167	.037500	.037500	−.004167	.004167	0	0	0	.028501	.083488	.019872	.103360	.8077	2.5000	.2087
	.5	.3333	0	0	0	0	.079167	−.054167	−.020833	0	0	0	.031878	.115866	.034245	.149611	.7711	2.0000	.2307
	.6	.3590	0	0	0	0	−.020833	.054167	.079167	0	0	0	.034645	.150011	.053322	.203333	.7378	1.6667	.2500
	.7	.3815	0	0	0	0	.004167	−.004167	.037500	.037500	−.004167	.004167	.037048	.187059	.077422	.264481	.7073	1.4286	.2672
	.8	.4016	0	0	0	0	0	0	0	.079167	.054167	−.020833	.039175	.226234	.106818	.333052	.6793	1.2500	.2828
	.9	.4196	0	0	0	0	0	0	0	−.020833	.054167	.079167	.041076	.267310	.141748	.409058	.6535	1.1111	.2970
	1.0	.4359	0	0	0	0	0	0	0	.004167	−.004167	.037500	.042788	.310098	.182409	.492507	.6296	1.0000	.3101
MOMENT	0.1	0.1609	0.006667	0.006667	0	0	0	0	0	0	0	0	0.000701						
	.2	.2229	−.001667	.008333	.007500	−.000833	.000833	0	0	0	0	0	.002930						
	.3	.2677	0	0	.023750	.016250	−.006250	0	0	0	0	0	.006195						
	.4	.3035	0	0	−.008333	.021667	.031667	0	0	0	0	0	.010046						
	.5	.3333	0	0	.002083	−.002083	.018750	.018750	−.002083	.002083	0	0	.014273						
	.6	.3590	0	0	0	0	0	.047500	.032500	−.012500	0	0	.019077						
	.7	.3815	0	0	0	0	0	−.014583	.037917	.055417	0	0	.024100						
	.8	.4016	0	0	0	0	0	.003333	−.003333	.030000	.033333	−.006667	.029306						
	.9	.4196	0	0	0	0	0	0	0	0	.060000	.060000	.034930						
	1.0	.4359	0	0	0	0	0	0	0	0	−.008333	.041667	.040661						

TABLE VII.—EXAMPLE OF NUMERICAL INTEGRATION OF PRESSURES ALONG A STREAMWISE SECTION INTERSECTING WING-TIP MACH CONE—Concluded

$1-P'$

(1) r'	(2) $K_1-(1)$	(3) $K_1+(1)$	(4) $\frac{(2)}{(3)}$	(5) $\frac{\cos^{-1}(4)}{\pi}$
2.0	−0.50	3.50	−0.1429	0.5456
3.0	−1.50	4.50	−.3333	.6082
4.0	−2.50	5.50	−.4545	.6502
5.0	−3.50	6.50	−.5385	.6810
6.0	−4.50	7.50	−.6000	.7048
7.0	−5.50	8.50	−.6471	.7240
8.0	−6.50	9.50	−.6842	.7398
9.0	−7.50	10.50	−.7143	.7533
10.0	−8.50	11.50	−.7391	.7647

$g=0.50$

$K_1=(1+g)=1.50$

t_{cp} P^*

	r'	$1-P'$	(1) MULTIPLIERS $r'=2.0$	(2) 3.0	(3) 4.0	(4) 5.0	(5) 6.0	(6) 7.0	(7) 8.0	(8) 9.0	(9) 10.0	(10) $\Sigma(1-P)\times$ (1) to (9)	(11) Incr. Σ $(10)_{area}$	(12) Incr. Σ $(10)_{mom.}$	(13) (11)+(12)	(14) $\frac{(11)}{(13)}$	(15) $\frac{1}{r'}$	(16) (11)×(15)
AREA	1.0	0.4359	0.375000	−0.041667	0.041667	0	0	0	0	0	0		0.31010	0.18241				
	2.0	.5456	.791667	.541667	−.208333	0	0	0	0	0	0	0.49578	.80588	.93798	1.74386	0.4621	0.50000	0.4029
	3.0	.6082	−.208333	.541667	.791667	0	0	0	0	0	0	.57972	1.38560	2.39084	3.77644	.3669	.33333	.4619
	4.0	.6502	.041667	−.041667	.375000	.375000	−.041667	.041667	0	0	0	.62981	2.01541	4.60144	6.61685	.3046	.25000	.5039
	5.0	.6810	0	0	0	.791667	.541667	−.208333	0	0	0	.66628	2.68169	7.60253	10.28422	.2608	.20000	.5363
	6.0	.7048	0	0	0	−.208333	.541667	.791667	0	0	0	.69338	3.37507	11.41797	14.79304	.2282	.16667	.5625
	7.0	.7240	0	0	0	.041667	−.041667	.375000	.375000	−.041667	.041667	.71468	4.08975	16.06526	20.15501	.2029	.14286	.5843
	8.0	.7398	0	0	0	0	0	0	.791667	.541667	−.208333	.73210	4.82185	21.55735	26.37920	.1828	.12500	.6027
	9.0	.7533	0	0	0	0	0	0	−.208333	.541667	.791667	.74673	5.56858	27.90570	33.47428	.1664	.11111	.6187
	10.0	.7647	0	0	0	0	0	0	.041667	−.041667	.375000	.75917	6.32775	35.11875	41.44650	.1527	.10000	.6328
MOMENT	1.0	0.4359	0.375000	−0.041667	0.041667	0	0	0	0	0	0	0.18241						
	2.0	.5456	1.583333	1.083333	−.416667	0	0	0	0	0	0	.75557						
	3.0	.6082	−.625000	1.625000	2.375000	0	0	0	0	0	0	1.45286						
	4.0	.6502	.166667	−.166667	1.500000	1.500000	−.166667	.166667	0	0	0	2.21060						
	5.0	.6810	0	0	0	3.958333	2.708333	−1.041667	0	0	0	3.00109						
	6.0	.7048	0	0	0	−1.250000	3.250000	4.750000	0	0	0	3.81544						
	7.0	.7240	0	0	0	.291667	−.291667	2.625000	2.625000	−.291667	.291667	4.64729						
	8.0	.7398	0	0	0	0	0	0	6.333333	4.333333	−1.666667	5.49209						
	9.0	.7533	0	0	0	0	0	0	−1.875000	4.375000	7.125000	6.34835						
	10.0	.7647	0	0	0	0	0	0	.416667	−.416667	3.750000	7.21305						

TABLE VIII.—CONTROL-SURFACE CHARACTERISTICS NOT INCLUDED IN FIGURES

(a) Tapered Controls

α	δ	λ_f	$1/\lambda_f$	Wing-tip controls			Inboard controls	α	δ	λ_f	Wing-tip controls			Inboard controls
				$\beta C_{l_2}'$	$\beta C_{L_2}'$	$\beta C_{m_2}'$	$\beta C_{l_2}'$				$\beta C_{l_2}'$	$\beta C_{L_2}'$	$\beta C_{m_2}'$	$\beta C_{l_2}'$
−0.95	−0.80	----	0.95	−0.2678	------	--------	--------	0.20	−0.80	0	−0.0474	0.1164	−0.1875	−0.0474
	−.90	----	.95	−.2778	------	--------	--------		−.80	.20	−.0680	.1139	−.1865	−.0661
−.80	−.60	----	.95	−.2162	------	--------	--------		−.80	.40	−.1162	.1053	−.1794	−.1102
	−.85	0.95	----	−.1335	------	--------	--------		−.80	.60	−.2096	.0848	−.1555	−.2106
	−.95	0	----	--------	0.2236	−0.2751	--------		−.95	0	−.7606	.2236	−1.3644	−.7606
	−.95	.20	----	--------	.2232	−.2751	--------		−.95	.20	−.9021	.2184	−1.3578	−.9917
	−.95	.40	----	−.1076	.2218	−.2741	--------		−.95	.40	−1.4204	.1997	−1.3085	−1.4551
	−.95	.60	----	−.2325	.2184	−.2709	−0.2311	.40	−.80	0	--------	.1164	−.2133	--------
	−.95	.80	----	−.6156	.2074	−.2587	−.6306		−.80	.20	--------	.1128	−.2118	--------
	−.95	.95	----	−2.3878	.1399	−.1814	−2.0759		−.80	.40	−.1389	.1002	−.2004	−.1422
−.60	−.80	.95	----	−.3349	------	--------	−.4466		−.95	0	−.9058	.2236	−1.5823	−.9058
	−.95	0	----	−.1796	.2236	−.4930	−.1796		−.95	.20	−1.1787	.2161	−1.5715	−1.1793
	−.95	.20	----	−.2420	.2226	−.4925	−.2413		−.95	.40	−1.6805	.1896	−1.4907	−1.7248
	−.95	.40	----	−.3773	.2192	−.4888	−.3762	.60	−.60	0	--------	------	−.0927	--------
	−.95	.60	----	−.6670	.2105	−.4758	−.6759		−.60	.20	--------	------	−.0917	--------
	−.95	.80	----	−1.4710	.1823	−.4276	−1.6150		−.60	.40	--------	------	−.0845	--------
−.40	−.80	0	----	--------	------	−.1099	--------		−.80	0	−.0819	.1164	−.2392	−.0819
	−.80	.20	----	--------	------	−.1097	--------		−.80	.20	−.1148	.1109	−.2366	−.1106
	−.80	.40	----	--------	------	−.1084	--------		−.80	.40	−.1820	.0927	−.2180	−.1742
	−.80	.60	----	--------	------	−.1038	--------		−.95	0	−1.0510	.2236	−1.8001	−1.0510
	−.80	.80	----	−.1747	------	−.0868	−.1776		−.95	.20	−1.3642	.2123	−1.7818	−1.3569
	−.95	0	----	−.3249	.2236	−.7109	−.3249		−.95	.40	−1.8747	.1737	−1.6453	−1.9945
	−.95	.20	----	−.4299	.2219	−.7097	−.4289	.80	.75	.95	--------	------	--------	.1405
	−.95	.40	----	−.6446	.2159	−.7008	−.6459		.60	.95	--------	------	--------	.2229
	−.95	.60	----	−1.0835	.2009	−.6705	−1.1206		−.60	0	--------	------	−.1009	--------
	−.95	.80	----	−2.1657	.1526	−.5574	−2.5993		−.60	.20	--------	------	−.0990	--------
−.20	−.80	0	----	--------	------	−.1357	--------		−.60	.40	--------	------	−.0861	--------
	−.80	.20	----	--------	------	−.1354	--------		−.80	0	−.0991	------	−.2650	--------
	−.80	.40	----	--------	------	−.1328	--------		−.80	.20	−.1397	------	−.2602	--------
	−.80	.60	----	−.1106	------	−.1241	−.1050		−.80	.40	−.2121	------	−.2352	--------
	−.80	.80	----	−.2618	------	−.0926	−.2945		−.95	0	−1.1963	.2236	−2.0180	--------
	−.95	0	----	−.4701	.2236	−.9287	−.4701		−.95	.20	−1.5463	.2042	−1.9822	--------
	−.95	.20	----	−.6175	.2210	−.9264	−.6165		−.95	.40	−2.0117	.1395	−1.7162	--------
	−.95	.40	----	−.9086	.2119	−.9094	−.9156	.95	.90	.96	--------	------	--------	.4493
	−.95	.60	----	−1.4756	.1890	−.8509	−1.5654		.80	.95	--------	------	--------	.4359
0	−.80	0	----	--------	------	−.1616	--------		−.60	0	--------	------	−.1070	−.0132
	−.80	.20	----	--------	------	−.1610	--------		−.60	.20	--------	------	−.1026	−.0207
	−.80	.40	----	--------	------	−.1566	--------		−.60	.40	--------	------	−.0703	−.0411
	−.80	.60	----	−.1617	------	−.1416	−.1578		−.80	0	--------	------	−.2844	−.1121
	−.95	0	----	−.6153	.2236	−1.1466	−.6153		−.80	.20	−.1625	------	−.2721	−.1496
	−.95	.20	----	−.8050	.2199	−1.1426	−.8041		−.80	.40	−.2250	------	−.1812	−.2302
	−.95	.40	----	−1.1680	.2067	−1.1129	−1.1853		−.95	0	−1.3052	.2236	−2.1813	−1.3052
	−.95	.60	----	−1.8326	.1740	−1.0110	−2.0102		−.95	.20	−1.6659	.1789	−2.0869	−1.6952
									−.95	.40	−1.7604	.0264	−1.3815	−2.4665

(b) Untapered Controls

α	A_f'	Wing-tip controls			Inboard controls	α	A_f'	Wing-tip controls			Inboard controls
		$\beta C_{l_2}'$	$\beta C_{L_2}'$	$\beta C_{m_2}'$	$\beta C_{l_2}'$			$\beta C_{l_2}'$	$\beta C_{L_2}'$	$\beta C_{m_2}'$	$\beta C_{l_2}'$
−0.95	0.8	−1.1421	0.1878	−0.0379	−1.2498	0	6.0	0.0320	0.0669	−0.0330	0.0349
	2.0	−.4242	.2093	−.1022	−.4328		8.0	.0327	.0676	−.0335	.0349
	4.0	−.1619	.2164	−.1070	−.1605		10.0	.0331	.0681	−.0337	.0349
	6.0	−.0720	.2188	−.1086	−.0698	.20	.8	.0125	.0446	−.0182	.0449
	8.0	−.0265	.2200	−.1094	−.0244		2.0	.0272	.0601	−.0282	.0393
	10.0	.0009	.2207	−.1099	.0029		4.0	.0317	.0657	−.0319	.0375
−.80	.8	−.1061	.0962	−.0447	−.1034		6.0	.0330	.0676	−.0332	.0369
	2.0	−.0117	.1063	−.0528	.0065		8.0	.0337	.0685	−.0338	.0366
	4.0	.0225	.1123	−.0556	.0259		10.0	.0341	.0690	−.0341	.0364
	6.0	.0342	.1137	−.0564	.0366	.40	.8	.0128	.0415	−.0158	.0608
	8.0	.0402	.1143	−.0568	.0420		2.0	.0289	.0603	−.0275	.0472
	10.0	.0437	.1147	−.0571	.0452		4.0	.0341	.0682	−.0328	.0426
−.60	.8	−.0190	.0702	−.0323	−.0075		6.0	.0356	.0709	−.0346	.0411
	2.0	.0173	.0804	−.0391	.0232		8.0	.0362	.0722	−.0354	.0404
	4.0	.0302	.0839	−.0414	.0334		10.0	.0366	.0730	−.0360	.0399
	6.0	.0346	.0850	−.0421	.0368	.60	.8	.0120	.0379	−.0131	.0948
	8.0	.0369	.0856	−.0425	.0385		2.0	.0300	.0603	−.0257	.0641
	10.0	.0382	.0859	−.0427	.0395		4.0	.0334	.0726	−.0345	.0539
−.40	.8	.0005	.0592	−.0268	.0154		6.0	.0406	.0782	−.0376	.0506
	2.0	.0226	.0694	−.0338	.0290		8.0	.0415	.0804	−.0391	.0487
	4.0	.0302	.0728	−.0358	.0336		10.0	.0420	.0818	−.0400	.0477
	6.0	.0328	.0739	−.0366	.0351	.80	.8	.0087	.0321	−.0087	.2198
	8.0	.0341	.0745	−.0370	.0358		2.0	.0296	.0589	−.0222	.1228
	10.0	.0349	.0748	−.0372	.0363		4.0	.0441	.0804	−.0343	.0905
−.20	.8	.0078	.0527	−.0233	.0263		6.0	.0503	.0921	−.0420	.0797
	2.0	.0245	.0633	−.0307	.0319		8.0	.0535	.0982	−.0461	.0743
	4.0	.0301	.0675	−.0332	.0338		10.0	.0549	.1018	−.0485	.0711
	6.0	.0319	.0688	−.0340	.0344	.95	.8	−.0048	.0149	.0032	1.4733
	8.0	.0328	.0694	−.0344	.0347		2.0	.0242	.0526	−.0157	.6564
	10.0	.0334	.0698	−.0346	.0349		4.0	.0440	.0809	−.0282	.3841
0	.8	.0110	.0482	−.0205	.0349		6.0	.0564	.0998	−.0368	.2933
	2.0	.0258	.0611	−.0291	.0349		8.0	.0657	.1145	−.0438	.2479
	4.0	.0305	.0655	−.0320	.0349		10.0	.0732	.1269	−.0501	.2207

TABLE IX.—COMPUTING FORM FOR C_{l_α}

(a) Dimensions and Preliminary Computing Form

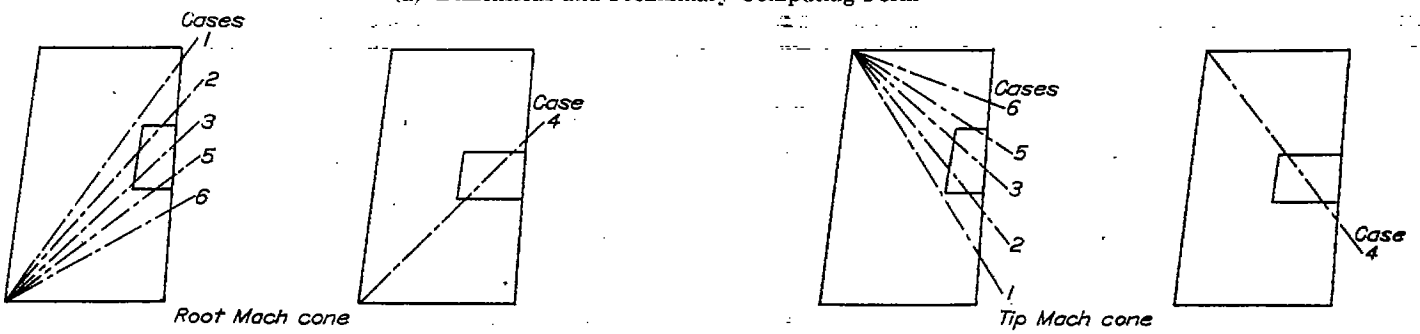

$M = \underline{1.80}$

$\beta = \sqrt{M^2-1} = \underline{1.4967}$

Root case 3

Tip case 3

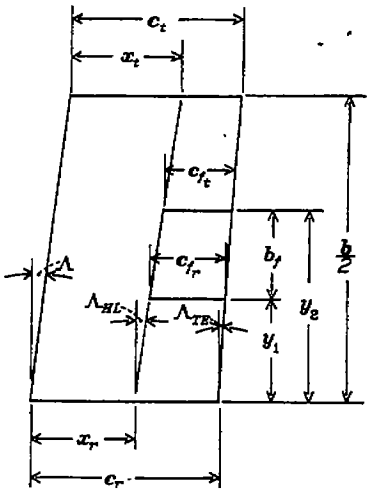

$g = \frac{\tan \Lambda}{\beta} = \underline{0.5995}$

$a = \frac{\tan \Lambda_{HL}}{\beta} = \underline{0.3990}$

$d = \frac{\tan \Lambda_{TE}}{\beta} = \underline{0.3489}$

$K_1 = \beta y_2 = \underline{7.8577}$

$K_2 = \beta y_1 = \underline{2.9934}$

$K_3 = \beta\left(\frac{b}{2} - y_1\right) = \underline{5.9868}$

$K_4 = \beta\left(\frac{b}{2} - y_2\right) = \underline{1.1225}$

$K_5 = \beta y_2^2 = \underline{41.2528}$

$K_6 = \frac{1}{\beta(1-d)} = \underline{1.0262}$

$K_7 = \frac{1}{\beta(1-a)} = \underline{1.1117}$

$K_8 = \beta y_1^2 = \underline{5.9868}$

$K_9 = \beta\left(\frac{b}{2} - y_1\right)^2 = \underline{23.9472}$

$K_{10} = \frac{1}{\beta(1+d)} = \underline{0.4953}$

$K_{11} = \frac{1}{\beta(1+a)} = \underline{0.4776}$

$K_{12} = \beta\left(\frac{b}{2} - y_2\right)^2 = \underline{0.8419}$

Tapered flap:

$2M_a 3\sqrt{1+\beta^2 a^2} = b_f \frac{c_{f_r}^3 - c_{f_t}^3}{c_{f_r} - c_{f_t}} = \underline{5.2159}$

Untapered flap:

$2M_a 3\sqrt{1+\beta^2 a^2} = 3 b_f c_{f_r}^2 = \underline{\quad\quad}$

TABLE IX.—COMPUTING FORM FOR C_{h_α}—Concluded

(b) Form for summing $(PS_L\bar{x})^*$ of triangular segments of conical-flow region

	Figures for determining columns (2) and (3)	Region	Column (6)=0 for cases in table IX(a)	(1) Enter curve at following value of n or r'	(2) P^*	(3) t_{cp}	(4) $3\bar{x}\sqrt{1+\beta^2a^2}$	(5) $2S_L$	(6) (2)×(4)×(5)
Root Mach cone	Figure 8	1	3, 5, 6	$\frac{c_r}{K_1}-(1-d)=$ ____	____	____	$\frac{2K_1(1-at_{cp})}{t_{cp}}-3x_r=$ ____	(1)×K_3=____	0
		2	2, 3, 4, 5, 6	$\frac{x_r}{K_1}-(1-a)=$ ____	____	____	$3x_r-\frac{2K_1(1-at_{cp})}{t_{cp}}=$ ____	(1)×K_5=____	0
	Figure 7 $\frac{\tan\eta}{\beta}=d$	3	6	$1-\frac{K_2}{c_r}(1-d)=0.6102$	0.258	0.736	$\frac{2c_r(1-at_{cp})}{(1-dt_{cp})}-3x_r=-2.4965$	(1)×$c_r^2K_6$=15.6547	−10.0832
		4	3, 5, 6	$1-\frac{K_1}{c_r}(1-d)=$ ____	____	____	$3x_r-\frac{2c_r(1-at_{cp})}{(1-dt_{cp})}=$ ____	(1)×$c_r^2K_4$=____	0
	Figure 7 $\frac{\tan\eta}{\beta}=a$	5	4, 5, 6	$1-\frac{K_2}{x_r}(1-a)=0.5502$	.245	____	$x_r=4.0000$	(1)×$x_r^2K_7$=9.7865	9.5908
		6	2, 3, 4, 5, 6	$1-\frac{K_1}{x_r}(1-a)=$ ____	____	____	$-x_r=$ ____	(1)×$x_r^2K_7$=____	0
	Figure 8	7	6	$\frac{c_r}{K_2}-(1-d)=1.0192$	.300	.645	$3x_r-\frac{2K_2(1-at_{cp})}{t_{cp}}=5.1074$	(1)×K_8=6.1017	9.3941
		8	4, 5, 6	$\frac{x_r}{K_2}-(1-a)=0.7333$	.277	.711	$\frac{2K_2(1-at_{cp})}{t_{cp}}-3x_r=-5.9688$	(1)×K_8=4.4021	−7.2778
Tip Mach cone	Figure 10	1	3, 5, 6	$\frac{c_t}{K_3}-(1+d)=$ ____	____	____	$\frac{2K_3(1+at_{cp})}{t_{cp}}-3x_t=$ ____	(1)×K_9=____	0
		2	2, 3, 4, 5, 6	$\frac{x_t}{K_3}-(1+a)=$ ____	____	____	$3x_t-\frac{2K_3(1+at_{cp})}{t_{cp}}=$ ____	(1)×K_9=____	0
	Figure 9 $\frac{\tan\eta}{\beta}=d$	3	6	$1-\frac{K_4(1+d)}{c_t}=0.4494$	.280	.662	$\frac{2c_t(1+at_{cp})}{(1+dt_{cp})}-3x_t=-0.9520$	(1)×$c_t^2K_{10}$=1.6833	−.4487
		4	3, 5, 6	$1-\frac{K_3(1+d)}{c_t}=$ ____	____	____	$3x_t-\frac{2c_t(1+at_{cp})}{(1+dt_{cp})}=$ ____	(1)×$c_t^2K_{10}$=____	0
	Figure 9 $\frac{\tan\eta}{\beta}=a$	5	4, 5, 6	$1-\frac{K_4(1+a)}{x_t}=0.2862$	.224	____	$x_t=2.2000$	(1)×$x_t^2K_{11}$=0.6616	.3260
		6	2, 3, 4, 5, 6	$1-\frac{K_3(1+a)}{x_t}=$ ____	____	____	$-x_t=$ ____	(1)×$x_t^2K_{11}$=____	0
	Figure 10	7	6	$\frac{c_t}{K_4}-(1+d)=1.1010$	.314	.609	$3x_t-\frac{2K_4(1+at_{cp})}{t_{cp}}=2.0179$	(1)×K_{12}=0.9185	.5820
		8	4, 5, 6	$\frac{x_t}{K_4}-(1+a)=0.5609$	.236	.751	$\frac{2K_4(1+at_{cp})}{t_{cp}}-3x_t=-2.7150$	(1)×K_{12}=0.4722	−.3025
									$\sum$ (6)=1.7358

$$C_{h_\alpha}=\frac{-2}{57.3\beta\sqrt{1-\beta^2}}\left(1-\frac{\sum(6)}{2.3M_a3\sqrt{1+\beta^2a^2}}\right)=-0.0194$$